

Western Australian School of Mines

**Fundamentals of Chalcopyrite Dissolution in Alkaline Glycine
Solutions**

Gregory Michael O'Connor


**This thesis is presented for the Degree of
Doctor of Philosophy
of
Curtin University**

October 2018

Author's Declaration

To the best of my knowledge and belief this thesis contains no material previously published by any other person except where due acknowledgment has been made.

This thesis contains no material which has been accepted for the award of any other degree or diploma in any university.



[Author]



[Date]

List of Publications

O'Connor, G.M., Lepkova, K., Eksteen, J.J. and Oraby, E.A., 2018. Electrochemical Behaviour of Copper in Alkaline glycine solutions. *Hydrometallurgy*, 181: 221-229.

O'Connor, G.M., Lepkova, K., Eksteen, J.J. and Oraby, E.A., 2018. Electrochemical Behaviour and Surface Analysis of Chalcopyrite in Alkaline Glycine Solutions. *Hydrometallurgy*, 182: 32-43.

Abstract

It is well known that copper dissolution from chalcopyrite is slow compared to other copper minerals. The literature is inconsistent in defining why this is so, but it is often thought to be due to "passivation". This is said to be an inhibiting surface layer generated by an initial oxidation reaction. If this passive layer were not present, chalcopyrite should dissolve freely as would a metal under similar conditions where thermodynamics favour soluble species. Chalcopyrite is not a metal but a natural semiconductor. Metal-like properties are speculated to be induced due to natural impurities in the mineral which increase the conductivity and result in what is known as a degenerate semiconductor.

The passive layer is often speculated to be a metal deficient sulfide or polysulfide, such as $\text{Cu}_{1-x}\text{Fe}_{1-y}\text{S}_2$. This mineral phase has never been directly measured and does not exist as a discrete mineral in nature. At best it has been inferred from X-ray Photoelectron Spectroscopy by a broadening of the sulfur peak which can be deconvoluted into disulfide and monosulfide components. The disulfide is said to be indicative of a passive species. The difficulty in directly observing this passive layer is in contrast to other well-known metal deficient layers on minerals, such as covellite on chalcocite that is readily observed visually.

An alternative proposal to passivation is that the electronic structure of chalcopyrite is of primary importance in copper leaching. Atomic and molecular orbital theories are well established and lead to the band theory of solids. The closely spaced molecular orbitals in a solid crystal form a continuum of energy bands. In chalcopyrite, like all semiconductors and insulators there exists a gap in these energy bands. This is a region of energies in the band structure that has no population of electrons. Electron transfer from the solid is forbidden in this region of energies, which coincides with the redox potential of common oxidants such as the ferric/ferrous couple. For an oxidant to exchange electrons with a semiconductor it should have a standard potential outside the range of the band gap. This is consistent with observations of higher leach rates using controlled potential leaching at low potentials, or with strong oxidants such as dichromate or hypochlorous acid with high standard potentials.

Slow leach rates have also been observed in several studies using alkaline solutions with ammonia or cyanide as a complexing agent. Recent research at Curtin University has shown this is also the case with glycine as a complexing agent in

alkaline media. The reasoning is also often attributed to passivation, implying that copper should freely leach from chalcopyrite if not for this layer.

In this project the electrochemical behaviour of metallic copper and semiconducting chalcopyrite were measured. The behaviour was compared to gain an insight into factors that affect the leaching behaviour of metals and semiconductors in this medium and to determine if chalcopyrite does indeed behave like a metal with a passive layer.

For metallic copper, potentiodynamic polarisation measurements were carried out over the pH range 9.0 to 11.5, at temperatures of 22°C and 60°C and glycine concentrations 0.1 M and 0.3 M. An optimal window for corrosion current, a proxy for leaching rates, was determined to be between pH 10.0 and 10.5 with a maximum at 60°C and 0.3 M glycine. Passivation was only observed at pH values greater than 10.5, and then only at potentials above 0.200 V (versus Ag/AgCl) for quiescent solutions. This passivation potential increased with the rotation rate of the electrode, meaning passivation was less easily achieved with rotation. The passive layer broke down after a short rest at the open circuit potential, which allowed reactivation of the surface and high initial currents to briefly flow until the layer re-formed. Potential-step and capacitance measurements are consistent with the formation of a duplex oxide layer of CuO and Cu₂O that thickens with increasing potential. The copper glycinate complex itself also acts as an oxidising agent, the effectiveness is increased with its concentration and the concentration of free glycine. Free glycine oxidised irreversibly above 1.0 V (vs Ag/AgCl).

Electrochemical experiments with a chalcopyrite rotating disk electrode showed no behaviour that resembled metal passivation or the speculated chalcopyrite passivation in acid solutions. The current increased with applied potential from the open circuit potential with no resemblance to the low current passivation region seen in acid solutions. A loosely held porous layer developed on the surface consisting largely of iron oxyhydroxides that had a limited effect on the anodic current. Elemental sulfur and a disulfide species were detected using XPS and Raman spectroscopy but did not passivate the surface as has been proposed for acid solutions. The disulfide species is sometimes used to infer a metal deficient sulfide or polysulfide that is responsible for passivation but in this study it had no passivating influence. Current-potential curves showed features of a non-ideal semiconductor that were explained by charge transfer via surface states.

Leaching experiments showed a greatly enhanced leach rate using oxidants that have an energy at or near the conduction band edge of chalcopyrite. Ferricyanide (0.35 V vs SHE) and triiodide (0.54 V vs SHE) were used at varying concentrations to show that leaching proceeds without passivation. At high oxidant dosages, up to 85% copper was extracted in 48 hours, with leaching still proceeding. The use of oxidants with standard potentials within the band gap such as ferric ion in acid solutions or chlorate in alkaline solutions extracted less than 5% copper in 48 hours. These results confirm the electrochemical results that copper leaching from chalcopyrite is not hindered by passivation, and that the semiconducting properties of the mineral should be considered.

Acknowledgements

I am extremely grateful to my three supervisors: Prof Jacques Eksteen, Dr Katerina Lepkova and Dr Elsayed Oraby. Their guidance, encouragement and faith in my work kept me motivated over the last four years. I acknowledge the financial support from Curtin University through the Research Training Scheme

I thank the staff and students of the Curtin Corrosion Centre. In particular Professor Brian Kinsella for organising a place for me to carry out my work and Hoda Ehsani and Yu Long for everyday help in the laboratory. I am also grateful to the staff and students of the WASM Gold Technology Group for helpful discussions and encouragement.

I would also like to acknowledge the scientists and engineers I have cited in this thesis. Without their hard work and dedication, my work would not have been possible.

Lastly I thank my parents Geoffrey and Jeanne, for demonstrating the healthy scepticism that is essential for scientific study.

Dedication

I dedicate this work to my wife Louisa and children Penelope and Michael. Your love and humour have helped me keep perspective throughout the years of writing this work. I would not have done this without you.

Table of Contents

Author's Declaration	iii
List of Publications	v
Abstract	vii
Acknowledgements.....	xi
Dedication	xiii
Table of Contents	xv
List of Figures	xxi
List of Tables	xxvii
List of Abbreviations	xxix
Chapter 1 Introduction	1
1.1 Background	1
1.2 Objectives	4
1.3 Thesis Structure	5
Chapter 2 Literature Review.....	7
2.1 Occurrence and Processing of Chalcopyrite	7
2.2 Hydrometallurgical attempts.....	8
2.3 Electronic structure	11
2.3.1 Atomic orbitals.....	12
2.3.2 Molecular orbitals and band theory	13
2.3.3 Band structure of semiconductors	17
2.3.4 Electron transfer	18
2.3.5 Expected electrochemical current-potential behaviour for ideal semiconductors.....	21
2.3.6 Implications for leaching and electrochemical behaviour.....	22
2.4 Arguments against the electronic band structure/semiconductor theory.....	23
2.4.1 Early arguments against passivation	23
2.4.2 Recent criticisms	25
2.4.2.1 Photo-effects on the chalcopyrite surface.....	26
2.4.2.2 The redox potential of Cu(II) complexes compared to hydrated ions.....	30

2.4.2.3	Limiting current	31
2.4.2.4	Capacitance Measurements	32
2.4.3	Summary	34
2.5	The passive layer	34
2.5.1	Passivation as understood in corrosion science	34
2.5.2	Early theories- elemental sulfur	36
2.5.3	Metal deficient models	37
2.5.4	“Passivation” by metal deficient layers.....	37
2.5.5	The metal deficient polysulfide.....	38
2.5.6	Surface analyses of the passive layer.....	40
2.5.7	Other layer proposals.....	44
2.5.8	The Burkin model for metal deficient layers.....	45
2.5.9	Passivation in alkaline pH.....	45
2.5.10	Arguments against passivation	48
2.5.11	Summary of the passivation proposals	48
2.6	Glycine leaching systems.....	49
2.6.1	Introduction – alkaline leaching systems	49
2.6.2	Glycine leaching	50
2.6.3	Properties of glycine	51
2.6.4	Glycine reactions with copper.....	52
2.6.5	Passivation of Copper Metal	54
2.6.6	Glycine reactions with Chalcopyrite.....	54
2.6.7	Oxidation of glycine.....	56
2.7	Oxidants for chalcopyrite-glycine system	56
2.8	Conclusion	57
Chapter 3	Electrochemical Behaviour of Copper in Alkaline Glycine Solutions	59
3.1	Introduction	59
3.2	Experimental	60
3.2.1	Potentiodynamic polarisation	60
3.2.2	Evans diagrams and diffusion study.....	61
3.2.3	Staircase Potential Step and Capacitance	62
3.2.4	Raman spectroscopy	62
3.2.5	Cyclic voltammetry.....	62
3.3	Results and Discussion	62

3.3.1	Conditions for optimal copper dissolution	62
3.3.2	Evans Diagrams	64
3.3.3	Passivation	66
3.3.4	Staircase Potential Step and capacitance measurements	69
3.3.5	Surface analysis.....	70
3.3.6	Oxidation of glycine	71
3.4	Conclusions	71
Chapter 4	Electrochemical Behaviour and Surface Analysis of Chalcopyrite in Alkaline Glycine Solutions.....	73
4.1	Introduction	73
4.2	Experimental.....	74
4.2.1	Sample details.....	74
4.2.2	Electrochemical Experiments	74
4.2.3	Surface Analysis	75
4.3	Results.....	76
4.3.1	General features of current-voltage behaviour.....	76
4.3.2	Effect of pH	76
4.3.3	Effect of glycine concentration	77
4.3.4	Effect of rotation speed	78
4.3.5	Effect of Temperature.....	79
4.3.6	Effect of a pre-oxidised surface layer	80
4.3.7	Effect of potential step duration	81
4.3.8	Capacitance.....	82
4.3.9	Chronoamperometry	83
4.3.10	XPS and Raman Spectroscopy Analysis.....	86
4.3.10.1	Samples oxidised in air, at the OCP and at 0.15 V (vs Ag/AgCl).....	86
4.3.10.2	Sample stepped to 0.4 V (vs Ag/AgCl).....	88
4.3.10.3	Sample stepped to 0.65 V (vs Ag/AgCl).....	89
4.3.10.4	Sample stepped to 0.85 V (vs Ag/AgCl).....	90
4.3.10.5	Sample stepped to 1 V (vs Ag/AgCl).....	91
4.3.10.6	Summary of XPS Results.....	92
4.4	Discussion	93
4.5	Conclusion.....	96

Chapter 5	Comparison of Electrochemical Dissolution of Metallic Copper and Semiconducting Chalcopyrite.....	99
5.1	Background	99
5.2	Current potential curves	99
5.3	Disk rotation	100
5.4	Capacitance	101
5.5	Surface analyses	102
5.6	Summary	102
Chapter 6	Chalcopyrite Leaching in Alkaline Glycine Solutions.....	103
6.1	Experimental	103
6.1.1	Sample details	103
6.1.2	Leaching process	104
6.2	Results and discussion.....	104
6.2.1	Oxidant requirements	104
6.2.2	Effect of oxidant concentration	105
6.2.3	Effect of staged oxidant addition	107
6.2.4	Comparison with stronger oxidants.....	108
6.2.5	Leaching with Grinding Media	110
6.2.6	Images of Leach Residue	112
6.2.7	Summary	114
Chapter 7	Conclusions and Recommendations	115
7.1	Metallic copper	115
7.2	Chalcopyrite	116
7.3	Further study.....	117
Appendix A	Electrochemical measurements.....	127
A.1	Potentiodynamic polarisation.....	127
A.2	Linear sweep voltammetry and Evans diagrams.....	133
A.3	Chronomaperometry	135
A.4	Potential step-capacitance methods.....	135
Appendix B	XPS and Raman spectra interpretation.....	137
B.1	XPS.....	137
B.2	Raman Spectroscopy.....	138

Appendix C	Chalcopyrite Characterisation	138
C.1	Microprobe data	138
Appendix D	Co-author Attribution Statement	142

List of Figures

Figure 1.1: Annual World Mine Production of Copper (U.S. Geological Survey, 2016).....	1
Figure 1.2: Average copper prices for each calendar year from 1998 to 2015 in 1998 US dollars. (U.S. Geological Survey 2016).....	2
Figure 2.1: Early studies of extraction of copper from chalcopyrite in acidic solutions under various reagent schemes (Sullivan, 1933). Concentrations of ferric salts 2%, acid concentration not specified.....	8
Figure 2.2: Extraction of copper from copper sulfides in ammonia at 25 ° C. Pressure 690 kPa, free NH ₃ added 2:1 weight ratio for copper. (NH ₃) ₂ SO ₄ added at 1.5:1 weight ratio to copper.	9
Figure 2.3: Extraction of copper from copper sulfides in ammonia at 75° C. Pressure 690 kPa, free NH ₃ added 2:1 weight ratio for copper. (NH ₃) ₂ SO ₄ added at 1.5:1 weight ratio to copper.	10
Figure 2.4: Electron configuration of the constituent atoms of chalcopyrite, showing high and low spin iron 3d orbitals	13
Figure 2.5: Molecular orbitals of a ZnS ₄ cluster and the corresponding band model. (Osseo-Asare, 1992).....	14
Figure 2.6: Molecular orbital diagrams for CuS ₄ ⁷⁻ and FeS ₄ ⁵⁻ that comprise chalcopyrite. The “crystal field” orbitals caused by iron d orbital splitting are also shown (Tossell et al., 1982).	16
Figure 2.7: n-type, p-type, and degenerate semiconductors.	18
Figure 2.8: Energy levels of a typical semiconductor and redox couple (Memming, 2007).	19
Figure 2.9: Schematic of the energy levels in chalcopyrite and redox couples (Crundwell, 1988)	20
Figure 2.10: Energy levels of a semiconductor and redox couple with a lower concentration of reduced species (Memming, 2007).....	21
Figure 2.11: Schematic of a current potential curve for a typical n-type semiconductor (Schmickler, 2010).	21
Figure 2.12: Comparison of the Tafel slopes of chalcopyrite and pyrite (Springer, 1970).	24
Figure 2.13: Apparent correlation of current density and temperature for a chalcopyrite electrode held at 0.577 V (vs SHE) (Nicol, 2016).....	27
Figure 2.14: The effect of red, violet and green lasers on current density and temperature.....	28
Figure 2.15: Voltamogram for the reduction of iron (III) on chalcopyrite with periodic illumination by a violet laser.....	29

Figure 2.16: Current density of chalcopyrite held at 550 V (vs Ag/AgCl) with pulsed light from a light chopper.....	30
Figure 2.17: The effect of scan rate on observation of a possible limiting current. (Crundwell et al., 2015; Ghahremaninezhad et al., 2010).	32
Figure 2.18: General Eh-pH diagram showing passivation and corrosion (Brett and Brett, 1993)	34
Figure 2.19: Typical current potential curve showing a passivation and passive breakdown.	35
Figure 2.20: Comparison of natural and synthetic dissolution of chalcopyrite (Dutrizac et al., 1969).	36
Figure 2.21: Model of passive layer by Ammou – Chokroum (1977).....	37
Figure 2.22: Chronoamperometry curves with rests at the OCP for times indicated (Parker et al., 1981).....	38
Figure 2.23: Sulfur peak for chalcopyrite exposed to air for three days (Buckley and Woods, 1984)	40
Figure 2.24: Leach curves at 110°C and 1.38 MPa oxygen pressure (Hackl et al., 1995).....	41
Figure 2.25: Comparison of sulfur peak for leached and unleached chalcopyrite (Hackl et al., 1995)	41
Figure 2.26: Proportion of various sulfur species as a percentage of total sulfur (Ghahremaninezhad et al., 2013).....	42
Figure 2.27: Effect of agitation on leach rates in alkaline ammonia solutions (Beckstead and Miller, 1977).	46
Figure 2.28: Comparison of alkaline (A) and acid (B) current potential curves. Scan rate 30 mV/minute (Warren and Wadsworth, 1984; Warren et al., 1982).	47
Figure 2.29 Variation of the glycinate ion mole fraction with pH at 25°C and 60°C.....	52
Figure 2.30: Eh-pH diagrams for the copper-glycine system at 25°C (left) and 60°C (right).....	54
Figure 2.31: Eh-pH diagrams for chalcopyrite at 25°C, left and 60°C, right. The relative positions of the valence and conduction bands are labelled “VB” and “CB” respectively.....	55
Figure 2.32: Comparison of alkaline iodide-ammonia leaching with ferric sulfate acid leaching. Study 1: 0.1 M Fe ³⁺ , pH 1, 25°C (Ammou-Chokroum et al., 1977); Study 2: 0.1 M Fe ³⁺ , 0.1 M H ₂ SO ₄ 75°C (Dutrizac et al., 1969); Study 3: 2M NH ₃ , pH 9.8, I ₂ 0.005 M, 25°C (Guan and Han, 1997).	57
Figure 3.1: Potentiodynamic polarisation curves: (a) effect of pH at 22°C and 0.1 M glycine. (b) Effect of temperature and concentration of glycine at pH 10.....	63
Figure 3.2: (a) Variation of i_{corr} with pH. (b) Variation of E_{corr} with pH.....	63

Figure 3.3: Effect of rotation speed (rpm) on anodic and cathodic scans in solutions of 0.3 M glycine at 25°C at pH 10.....	64
Figure 3.4: Effect of glycine concentration on the anodic curves at 22°C, left and 60°C, right, with a superimposed cathodic curve in a glycine-free solution. Rotation rate 1000 rpm and pH 10.....	65
Figure 3.5: Cathodic reduction of aerated pH 10 glycine/copper sulfate mixture at (a) 22°C, (b) 60°C. Solutions of 0.3 M glycine with: 1) 0 M CuSO ₄ ; 2) 0.001 M CuSO ₄ ; 3) 0.002 M CuSO ₄ ; 4) 0.004 M CuSO ₄ . The anodic scan was obtained from a de-aerated solution.	66
Figure 3.6: Static electrode showing passivation of copper at pH 11 and 12 in 0.1 M glycine.	67
Figure 3.7: Passivation of RDE at pH 12 and 0.1 M glycine showing the effect of rotation speed.....	67
Figure 3.8: Current decay curves in solutions of 0.1 M glycine at pH 12 held at 0.5 V (vs SHE).	68
Figure 3.9: Current vs time and corresponding capacitance V potential. (a) Non passivating conditions with 0.3 M glycine at pH 10.5 and 1000 rpm. (b) Passivating conditions with 0.1 M glycine at pH 12 and 0 rpm.	69
Figure 3.10: Raman spectra of copper that has been oxidised at 0.6 V (vs SHE) held at the OCP, and a fresh sample exposed to air showing a poorly crystalline cuprite layer.	70
Figure 3.11: Cyclic voltammograms of 0.3 M glycine at pH 12 and 25°C and 60°C with scan rates of 10, 20, 50 and 100 mV/s.....	71
Figure 4.1: Current-potential transients at different pH values in 0.3 M glycine compared to 0.3 M H ₂ SO ₄ solution.	77
Figure 4.2: Effect of glycine concentration on current potential transient at pH 10.5. Glycine concentration is 0.3 M and temperature is 25°C.....	78
Figure 4.3: Effect of rotation speed on the current potential transients at pH 10.5 and 0.3 M glycine concentration at 25°C.....	79
Figure 4.4: Effect of temperature at 25°C and 60°C. Glycine concentration 0.3 M and pH 10.5.....	80
Figure 4.5: Effect of a surface layer generated at 0.65 V (vs Ag/AgCl). Glycine concentration is 0.3 M and pH 10.5	81
Figure 4.6: Effect of different potential step duration at pH 10.5 and 0.3 M glycine.	81
Figure 4.7: Comparison of current and capacitance at 1 kHz in 30g/l H ₂ SO ₄ , left, and 0.3 M glycine at pH 10.5, right.....	83
Figure 4.8: Chronoamperometry at 0.65 V (vs Ag/AgCl) in solutions of 0.3 M glycine at pH 10.5.....	84
Figure 4.9: Chronoamperometry at 0.65 V (vs Ag/AgCl). Close-up view of the initial and second current transients of Figure 4.8.....	84

Figure 4.10: Current vs time for a potential step experiment at pH 10.5 with 0.3 M glycine at 25°C.....	85
Figure 4.11: Copper, iron and sulfur XPS peaks of chalcopyrite. From top to bottom: (a) air oxidised, (b) oxidised at OCP, (c) stepped to 0.15 V (vs Ag/AgCl). Solution was 0.3 M glycine at pH 10.5.	86
Figure 4.12: Raman spectrum of oxidised chalcopyrite. From top to bottom: (a) Air oxidised, (b) Oxidised at OCP, (c) oxidised at 0.15 V (vs Ag/AgCl). Solution was 0.3 M glycine at pH 10.5.	87
Figure 4.13: Copper, iron and sulfur XPS peaks for chalcopyrite stepped to 0.4 V (vs Ag/AgCl) in 0.3 M glycine at pH 10.5. From top to bottom: (a) overlayer, (b) underlayer	88
Figure 4.14: Left: Raman spectrum of overlayer showing mixed spectra of chalcopyrite, sulfur and oxyhydroxides. Right: elemental sulfur with minor chalcopyrite in oxide layer cracks. Sample stepped to 0.4 V (vs Ag/AgCl) in 0.3 M glycine at pH 10.5.....	89
Figure 4.15: Copper, iron and sulfur XPS peaks of chalcopyrite stepped to 0.65 V (vs Ag/AgCl). "S*" denotes an unidentified species- possibly sulfite in 0.3 M glycine at pH 10.5. From top to bottom: (a) overlayer, (b) underlayer.	89
Figure 4.16: Left: Raman spectrum of mixed sulfur and oxyhydroxide in the surface overlayer. Right Elemental sulfur in cracks in the overlayer in 0.3 M glycine at pH 10.5.....	90
Figure 4.17: Copper, iron and sulfur XPS peaks of chalcopyrite stepped to 0.85 V (vs Ag/AgCl) in 0.3 M glycine at pH 10.5. From top to bottom: (a) overlayer, (b) underlayer.	90
Figure 4.18: Raman spectrum of mixed sulfur, oxyhydroxide and chalcopyrite in overlayer at 0.85 V (vs Ag/AgCl) in 0.3 M glycine at pH 10.5.....	91
Figure 4.19: Copper, iron and sulfur XPS peaks of chalcopyrite stepped to 1.0 V (vs Ag/AgCl) in 0.3 M glycine at pH 10.5. From top to bottom: (a) overlayer, (b) underlayer.	91
Figure 4.20: Left: Raman spectrum of mixed oxide/sulfur in overlayer; right: elemental sulfur in overlayer crack in 0.3 M glycine at pH 10.5.....	92
Figure 4.21: Band diagram for chalcopyrite in alkaline glycine solutions at different applied potentials (vs Ag/AgCl).	95
Figure 5.1: Comparison of copper metal undergoing passivation and semiconducting chalcopyrite. Conditions pH 10.5, 0.1 M glycine.....	100
Figure 5.2: Comparison of current versus time graphs for copper metal (left) and chalcopyrite (right) with disk rotation of 0 rpm and 1000 rpm. Glycine concentration 0.1 M, pH 10.5.	101

Figure 6.1: Comparison of alkaline glycine leaches at pH 10 with 0.3 M glycine and 0.15 M ferric leach. All were carried out at 55°C. Reagent dosages are specified in Table 6.3	106
Figure 6.2: ORP and pH for the comparative leach tests in Figure 6.1	106
Figure 6.3: Effect of staged additions of ferricyanide and triiodide. All were carried out at 55°C	107
Figure 6.4: ORP and pH for the staged oxidant addition tests	108
Figure 6.5: Comparison of chlorate leach to a ferricyanide and ferricyanide/chlorate blend in 0.3 M glycine at 25°C at pH 10.....	109
Figure 6.6: ORP and pH for chlorate and ferricyanide. pH 10, 0.3 M glycine.....	109
Figure 6.7: Leaching with grinding media at 25°C, pH 10, 0.3 M glycine. 25 g of ferricyanide added at 0 and 4 hours.....	111
Figure 6.8: ORP and pH for tests with and without grinding media in the bottle.....	112
Figure 6.9: Fresh chalcopyrite (left) compared with acid leached residue (right).....	112
Figure 6.10: Chalcopyrite partially leached with low oxidant dosages. On the left is the ferricyanide leach, on the right is the triiodide leach	113
Figure 6.11: Chalcopyrite leached to about 50% to 55% copper extraction using high oxidant dosage. Ferricyanide (left); triiodide (right).	113
Figure 6.12 Chalcopyrite leached with a staged addition of a large excess of oxidant. Ferricyanide (left); triiodide (right).....	114
Figure App A.1. Typical current potential polarisation resistance plots for different corroding systems (Kelly, 2002) p 128.....	128
Figure App A.2: Example of Resistance polarisation calculation with Biologic software.	129
Figure App A.3. Example of how an Evans diagram for the commonly studied gold-cyanide system (Heath and Rumball, 1998)	133

List of Tables

Table 4.1 Surface elemental distribution from survey scans.....	92
Table 4.2: Sulfur species on the friable overlayer and the exposed surface beneath.....	93
Table 6.1: Elemental assay sample used for leach tests.....	103
Table 6.2: Oxidant requirements for 1 gram of chalcopyrite.	104
Table 6.3: Mass of oxidants added for each test.....	105
Table App A-1: Resistance polarisation and calculated i_{corr} values for copper metal.....	130

List of Abbreviations

E°	Standard redox potential
E_{corr}	Corrosion potential
E_{ox}	Potential of oxidising species in a couple
E_{red}	Potential of reducing species in a couple
Gly	Glycine
i_{corr}	Corrosion current
OCP	Open Circuit Potential
ORP	Oxidation Reduction Potential
SEM	Scanning Electron Microscope
SHE	Standard Hydrogen Electrode
XPS	X-ray Photo Electron Spectroscopy

Chapter 1 Introduction

1.1 Background

According to data from the US Geological Society, world production of copper has steadily increased since the start of the 20th century as can be seen in Figure 1.1. This is in line with the development of electrical goods and world population growth. The modernisation of China has contributed to the high production rates since the mid-1990s.

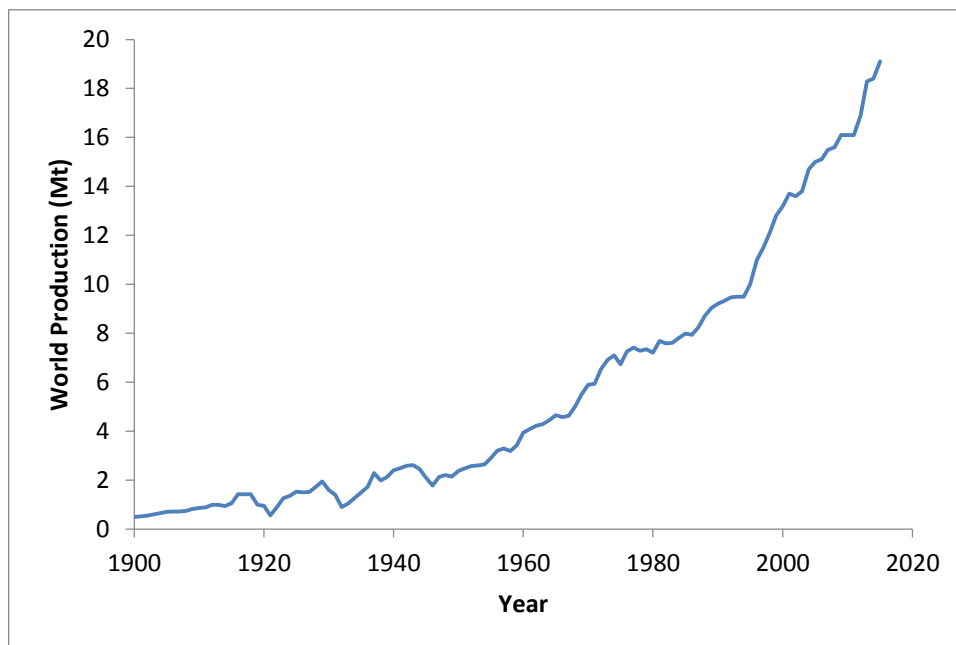


Figure 1.1: Annual World Mine Production of Copper (U.S. Geological Survey, 2016)

Being a finite resource, there has long been a concern that reserves will be exhausted followed by a significant decline in quality of life. As early as 1924, predictions were made that copper would be uneconomic within a decade and result in the end of electrical technology (Webb, 2012). These predictions didn't consider improvements in technology that allowed the exploitation of lower grade resources. Froth flotation was being developed around this time and in 1925 xanthate collectors were introduced, making more reserves economically viable to process (Fuerstenau, 2007).

These predictions of copper shortages were repeated in the 1970s, citing observations of declining ore grades and reserves coupled with strict environmental regulations. At this time it was suggested that an alternative to flotation such as a hydrometallurgical process was needed (Panlasigui, 1970; Paynter, 1973; Weiss, 1976). However, innovations with high intensity flotation such as the Jameson cell and with stirred grinding mills allowed much finer grain sizes to be recovered (Fuerstenau, 2007; Wills, 2015). Hydrometallurgical methods were restricted to heap leaching of low grade oxide and supergene sulfides.

Environmental regulations such as the US Clean Air Act of the 1970s also suggested that a hydrometallurgical route for copper would be required to curb SO₂ pollution. However, improvements in smelting technology through sulfur capture (such as flash smelting) has reduced this motivation (Habashi, 1978). These continued improvements in grinding, flotation and smelting are reflected in the fact copper prices generally decreased in the latter half of the 20th century. After this time high demand from China restored the price of copper to the levels seen in the 1970s, but it has been volatile, as seen in Figure 1.2. It remains to be seen if high prices are maintained and a hydrometallurgical route could be seriously considered for chalcopyrite. Today, hydrometallurgical recovery is restricted to about 20% of total copper production and is from easily leachable (relative to chalcopyrite) oxide and secondary sulfide sources (Watling, 2013).

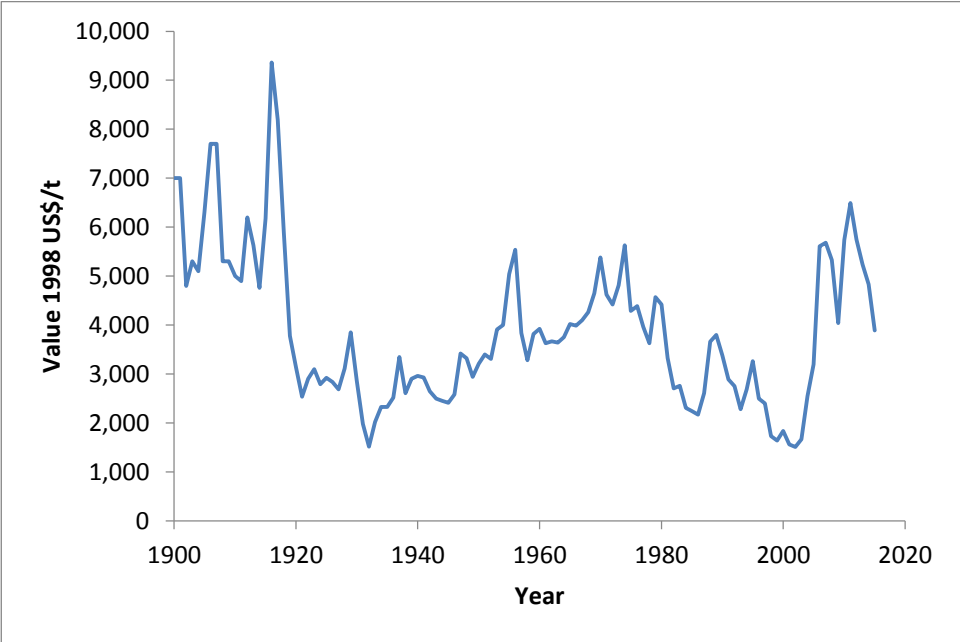


Figure 1.2: Average copper prices for each calendar year from 1998 to 2015 in 1998 US dollars. (U.S. Geological Survey 2016)

The global decline in copper grades and increasing ore complexity are still cited as motivations for finding a hydrometallurgical alternative to flotation/smelting and have prompted large research projects such as in situ mining (Córdoba et al., 2008; Robinson and Kuhar, 2018; Watling, 2013). However, it is obvious from Figure 1.2 that significantly higher and more stable prices would be required before chalcopyrite leaching would be feasible.

The biggest technical challenge for chalcopyrite leaching is the slow dissolution rate. This has been recognised since the early 20th century when the mineral was considered un-leachable (Greenawalt, 1912; Sullivan, 1933). The use of fine grinding and high temperatures were known to increase leach rates and these still form the basis of modern technologies such as the Activox and Albion processes (Schlesinger et al., 2011). These are capital intensive technologies with considerable costs that are applied to concentrate leaching.

In the 1970s, the idea that slow leach rates were caused by an inhibiting surface layer was proposed. Elemental sulfur was considered a candidate in early studies, but this was not widely accepted at the time (Dutrillac et al., 1969; Linge, 1976). A metal deficient sulfide or polysulfide was also proposed and seems to now be widely accepted by industry. The term “passivation” was introduced around 1977 and is now often used to describe the slow leach rate (Ammou-Chokroum et al., 1977).

The literature is however inconsistent when describing the fundamental properties of this layer, and some researchers have even questioned its existence (Klauber, 2008). The layer has never been directly observed but is inferred from surface measurements such as XPS (Buckley and Woods, 1984; Ghahremaninezhad et al., 2013; Hackl et al., 1995). To add to the uncertainty, recent work has proposed that the electronic structure of bulk chalcopyrite determines the leaching behaviour including the apparent “passivation” (Bryson et al., 2016; Crundwell et al., 2015). By using fundamental principles of inorganic chemistry, the electronic band structure of the mineral can explain the slow leach rates without the need to propose a passivating layer.

Recent research at Curtin University has shown that chalcopyrite leaching with the alternative lixiviant glycine in alkaline solutions is also slow compared to other copper minerals and is at a similar rate to acid systems (Tanda et al., 2017; Tanda, 2017; Watling, 2013). This is consistent with other alkaline lixiviants such as ammonia and cyanide (Adams, 2005; Stanczyk and Rampacek, 1966). The reasons for this have not yet been explored, but it is possible that a passivating species is present, or that the electronic structure of the mineral is responsible. Given the benign attributes of glycine, its insignificant dissolution of iron and its recyclability as a reagent, there is reason to consider it as a potential lixiviant for copper from chalcopyrite.

1.2 Objectives

The reason for the slow leach rate of chalcopyrite in glycine has not been researched in fundamental detail before. Based on the widely published studies of slow leach rates in both alkaline and acid solutions, two theories can be investigated: 1) Passivation by metal deficient sulfides or polysulfides, 2) restrictions imposed by the fundamental electronic band theory of solids and the semiconducting nature of chalcopyrite.

The objectives of this study are to:

- Critically review the literature on chalcopyrite leaching with particular attention to the evidence for passivation and the application of semiconductor theory based on the electronic structure of chalcopyrite.
- Investigate the electrochemical behaviour of copper metal in glycine solutions. This can serve as a baseline example for the behaviour of a metal in glycine. This can be compared to semiconducting chalcopyrite, which is often described as degenerate (or metal-like) with regards to leaching behaviour. Differences or similarities in leaching and passivation will be observed.
- Carry out electrochemical and surface analyses on chalcopyrite to determine any correlations of current density with possible passivating surface species.
- Perform leaching experiments on chalcopyrite with the mild oxidants ferricyanide and triiodide to confirm electrochemical results.

1.3 Thesis Structure

Chapter 2 critically reviews the literature on the passivation of chalcopyrite and the fundamental electronic structure and examines the evidence for claims made.

Chapter 3 describes the electrochemical behaviour of metallic copper under conditions expected in a metallurgical application. Passivation and surface reactivation are described and the surface examined with Raman spectroscopy.

Chapter 4 investigates the electrochemistry and surface species generated on chalcopyrite. The results are fitted to the behaviour expected by the band theory of solids for chalcopyrite.

Chapter 5 compares and summarises the electrochemical behaviour of metallic copper and semiconducting chalcopyrite

Chapter 6 describes the results of alkaline glycine leaching tests carried out on a chalcopyrite sample with ferricyanide and triiodide as oxidants in comparison to a ferric acid leach.

Chapter 7 summarises the results and discusses gaps in knowledge that could be investigated further with implications for processing.

Chapter 2 Literature Review

2.1 Occurrence and Processing of Chalcopyrite

Chalcopyrite is well known as the most abundant copper mineral on earth. It is present in sedimentary exhalative deposits, volcanic massive sulfides, porphyry and iron oxide copper gold deposits. The largest resources are in the porphyry deposits of South America, particularly Chile and Peru. The main Australian operations are the iron oxide copper gold deposits of Olympic Dam and Prominent Hill in South Australia and the lead/zinc/copper deposits of Mount Isa in Queensland. Other operations throughout NSW and Queensland include Cobar, Cadia and Selwyn. In Western Australia the main production is from the Golden Grove, Telfer and Nifty deposits with smaller quantities from Boddington (Geoscience Australia, 2012).

Copper production from chalcopyrite is usually by flotation and pyrometallurgy. This accounts for 80% of global copper production (Watling, 2013). The remaining 20% is from acid heap leaching of low grade secondary and oxide copper minerals. An alkaline alternative would be useful where acid consuming gangue is present, or if gold is also present in the oxide zone. The flotation and pyrometallurgical processes are well understood and likely to be the only method of production from chalcopyrite for the near future. Research in grinding, flotation and smelting have allowed finer grained ores to be processed and has improved environmental aspects of the process, particularly sulfur capture with smelting.

For several decades researchers have been suggesting that increasingly complex textures and low grades will dictate the need for a hydrometallurgical option (Panlasigui, 1970; Paynter, 1973; Weiss, 1976). This is still not a feasible process for chalcopyrite due to slow and incomplete leaching. As of 2018 copper leaching is limited to oxides and secondary (supergene) sulfides, usually low grade acid heap leaching in Chile. However, if recent high copper prices are maintained or increased in the coming years a hydrometallurgical alternative may be viable.

2.2 Hydrometallurgical attempts

Hydrometallurgical methods have been used for copper sulfide and oxide minerals since at least as far back as 1905 (Keith, 1905). These methods were used where smelting was unfavourable due to the low copper grades or the remoteness of the site to a smelter. It was recognised that chalcocite and metallic copper were readily leachable in ferric solutions, but some chalcopyrite rich ores required roasting before leaching (Sullivan, 1933).

The slow rate of copper leaching where chalcopyrite was specifically mentioned was noted at least as early as 1912 (Greenawalt, 1912; Morse and Tobelmann, 1916; Pike et al., 1930; Sullivan, 1933). Fine grinding to at least 45 μm , high temperatures, and the use of ferric chloride as an oxidant were all methods identified for increasing the leach rate. For high grade chalcopyrite specimens, extractions ranged from 2% in 40 days for a ferric sulfate solution at ambient temperature to 80% in 3 days for a boiling ferric chloride solution, as shown in Figure 2.1. Interestingly these studies specified that there was no selective leaching of any element such as iron, contrary to the current view that iron leaches preferentially to copper.

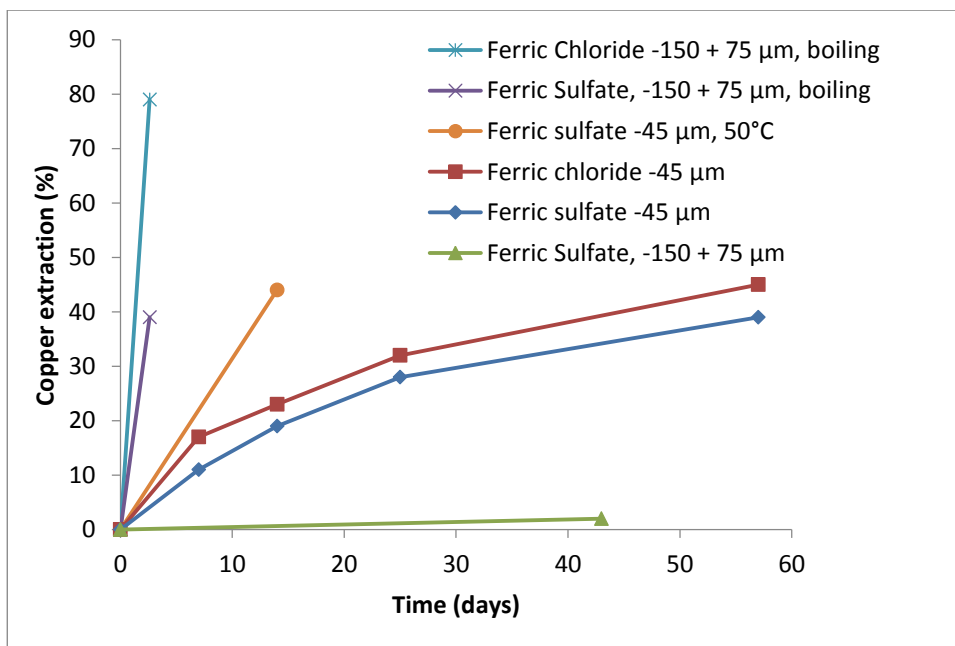


Figure 2.1: Early studies of extraction of copper from chalcopyrite in acidic solutions under various reagent schemes (Sullivan, 1933). Concentrations of ferric salts 2%, acid concentration not specified.

In the 1960s, ammoniacal leaching was tested at the US Bureau of Mines on a laboratory scale with a range of copper sulfide specimens ground to $-53\ \mu\text{m}$ (Stanczyk and Rampacek, 1966). Chalcopyrite was slower to leach than other sulfides at ambient temperature with a final recovery just under 85% after 8 hours of pressure leaching (Figure 2.2). However if the temperature was greater than 75°C and oxygen partial pressures greater than 690 kPa, leaching was complete within an hour, but still slower than other sulfides (Figure 2.3). The solution had to be highly agitated for mixing of the components and repeatability. The minimum weight ratio of ammonia to copper was about 3.5 to 1.

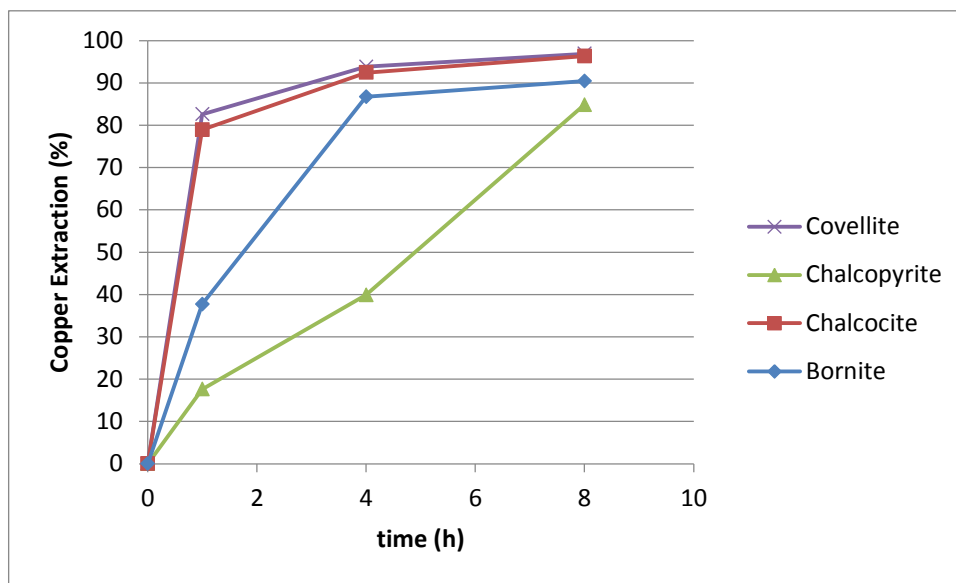


Figure 2.2: Extraction of copper from copper sulfides in ammonia at 25°C . Pressure 690 kPa, free NH_3 added 2:1 weight ratio for copper. $(\text{NH}_3)_2\text{SO}_4$ added at 1.5:1 weight ratio to copper.

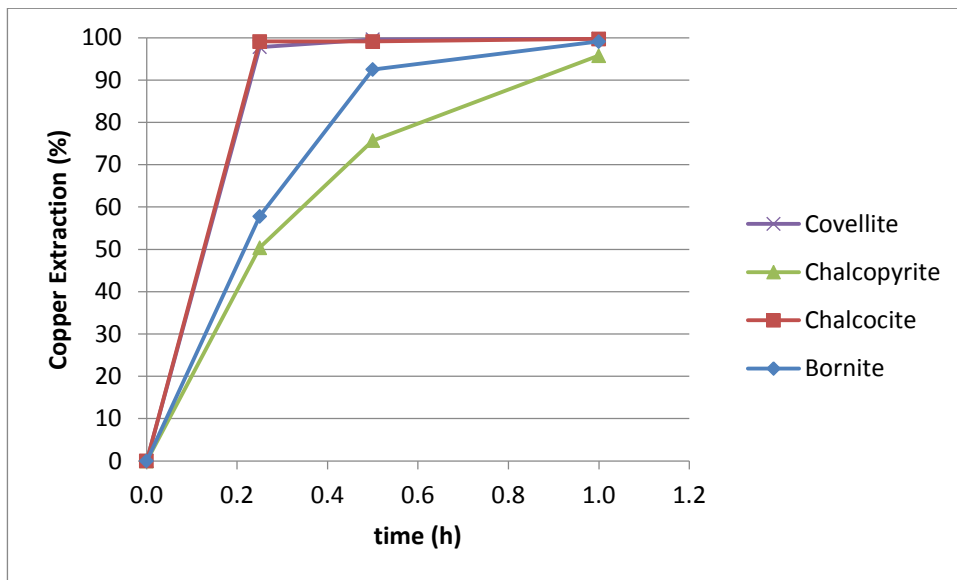


Figure 2.3: Extraction of copper from copper sulfides in ammonia at 75° C. Pressure 690 kPa, free NH₃ added 2:1 weight ratio for copper. (NH₃)₂SO₄ added at 1.5:1 weight ratio to copper.

This work was followed by the development of the industrial scale Arbiter process for flotation concentrates developed by Anaconda in Butte, Montana in 1974 (Arbiter and McNulty, 1999). This process used high agitation and oxygen for pressure leaching, but for practical considerations it was run at 138 kPa - much lower oxygen pressure than the Bureau of Mines Study of 690 kPa. The leach rates were consequently much slower than in the laboratory study. The plant closed in 1977, partly from slow kinetics but mainly due to maintenance costs incurred from harsh winters and because of no adequate means of disposal of ammonium sulfate. BHP attempted an ammonia leach at Escondida using ambient pressure and temperature in the 1990s. This also failed due to inadequate plant design and piloting (Arbiter and McNulty, 1999).

No other industrial scale attempts have been made due to slow or incomplete leaching, despite extensive lab and pilot scale studies. Around the late 1960s and early 1970s it was proposed that surface layers generated on the mineral surface through oxidation may inhibit leaching. In acid solutions this was at first thought to be elemental sulfur, but later studies showed that this was not likely, with a metal deficient polysulfide proposed instead (Dutrillac et al., 1969; Linge, 1976; Parker et al., 1981). In alkaline studies the inhibiting layer was thought to be iron oxides that could be removed with high agitation (Beckstead and Miller, 1977; Stanczyk and Rampacek, 1966).

The metal-deficient sulfides and metal-deficient polysulfides that were proposed as rate limiting through solid state diffusion in the 1970s have gained some level of general acceptance in the wider metallurgical community. However, among researchers who specifically investigate the chalcopyrite surface there is wide disagreement regarding the mechanism of passivation from these layers, their actual passivating ability and even the very existence of them (Crundwell, 2015; Ghahremaninezhad et al., 2013; Hackl et al., 1995; Klauber, 2008; Mikhlin et al., 2004). In any case, the nature, attributes and composition of the species remain loosely described and characterised.

Regardless of the mechanism involved, it is agreed that the dissolution reaction is an oxidation reaction with the transfer of electrons to an oxidising species in solution. It would therefore be expected that the electronic structure of chalcopyrite should play a primary role. Some authors have proposed that this dictates the leaching behaviour of chalcopyrite (Bryson et al., 2016; Crundwell, 2015; Crundwell et al., 2015). For this fundamental study, the literature on the electronic structure of chalcopyrite will first be reviewed, based on the well-known atomic and molecular orbital theories. An understanding of the fundamental reasons for slow leach rates may direct future research into finding a practical solution that can be implemented on an industrial scale.

2.3 Electronic structure

The electronic structure and bonding of any solid crystal or mineral such as chalcopyrite can be understood from atomic orbital and molecular orbital theories. A brief review of these is given here to illustrate the connection with the band theory of solids. It will be shown how the band theory may dictate the electron transfer from chalcopyrite with different redox couples. These orbital and band theories are widely accepted in the scientific community and are taught in high school and undergraduate chemistry courses.

2.3.1 Atomic orbitals

The atomic orbital theory is based on the wave functions that describe solutions to the Schrodinger wave equation (House, 2013; Vaughan, 1978). These wave functions define shapes of boundary surfaces where electrons can be found. They are expressed in terms of four quantum numbers, which arise out of mathematical restrictions on solutions to the equations. The Pauli Exclusion Principle states that no two electrons can have the same set of quantum numbers and these set up the basis for the electron configuration of atoms. The four quantum numbers are:

- n = The principle quantum number and is a positive integer (1, 2, 3,...). This defines the distance of an electron from the nucleus and hence it's energy.
- l = the orbital momentum quantum number less than $n = 0, 1, 2, \dots, (n-1)$. Designated s, p, d, and f. These describe the shape of the orbitals.
- m = magnetic quantum number = integers from -1 to $+1$. These describe the orientation the orbitals.
- s = spin quantum number = either $-1/2$, or $+1/2$.

The orbitals of interest for chalcopyrite are s, p and d. The atoms that make up chalcopyrite are generally agreed from fundamental studies to have the oxidation state Cu^+ , Fe^{3+} , S^{2-} (Shuey, 1975; Tossell et al., 1982). The electron configurations are:

- Cu^+ : $1s^2, 2s^2, 3s^2, 3p^6, 3d^{10}$
- Fe^{3+} : $1s^2, 2s^2, 3s^2, 3p^6, 3d^5$
- S^{2-} : $1s^2, 2s^2, 3s^2, 3p^6$

The d orbitals of copper and iron are split into two sub-groups. The dx^2-y^2 and dz^2 orbitals are oriented along the Cartesian axes, and d_{xy} , d_{yz} and d_{xz} orbitals are oriented between the axes. Due to interactions with ligands, these are split in energy in a process known as crystal field splitting. The dx^2-y^2 and dz^2 are denoted by their symmetry as the "e" orbitals, the d_{xy} , d_{yz} and d_{xz} are the " t_2 " orbitals as shown in Figure 2.4. This is important for the electronic and magnetic structure of chalcopyrite, particularly iron. This splitting results in high spin and low spin arrangements for iron that contribute to the antiferromagnetic character of the mineral. A thorough description of this theory as applied to sulfide minerals can be found in the literature (Vaughan, 1978).

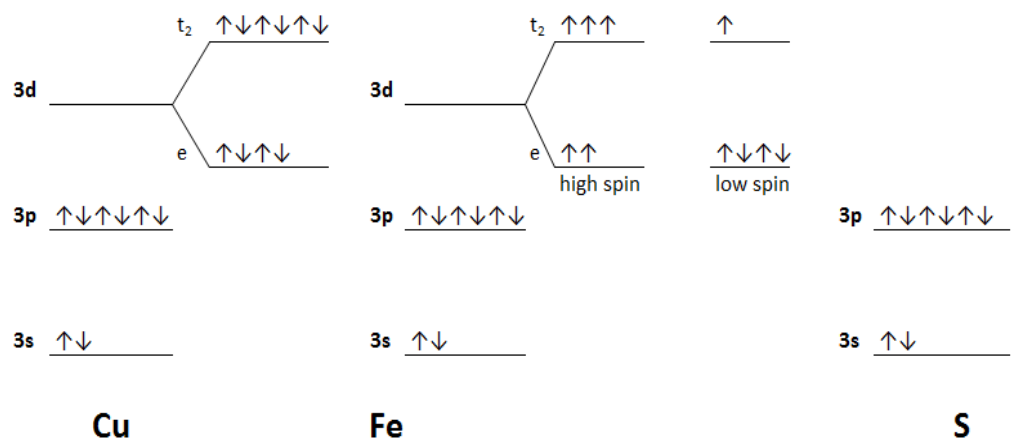


Figure 2.4: Electron configuration of the constituent atoms of chalcopyrite, showing high and low spin iron 3d orbitals .

2.3.2 Molecular orbitals and band theory

Following on from the atomic orbital model is the molecular orbital model. A simple example is shown in Figure 2.5 for the binary mineral sphalerite that illustrates the connection between molecular orbitals and energy bands. Here the overlap of atomic orbitals of the zinc metal and the sulfur ligand results in molecular orbitals of bonding and anti-bonding character. The bonding orbitals are more stable and lie at a lower energy than the constituent atomic orbitals of the bonding atoms. The antibonding orbitals are less stable, and lie at a higher energy as shown in the left image in Figure 2.5.

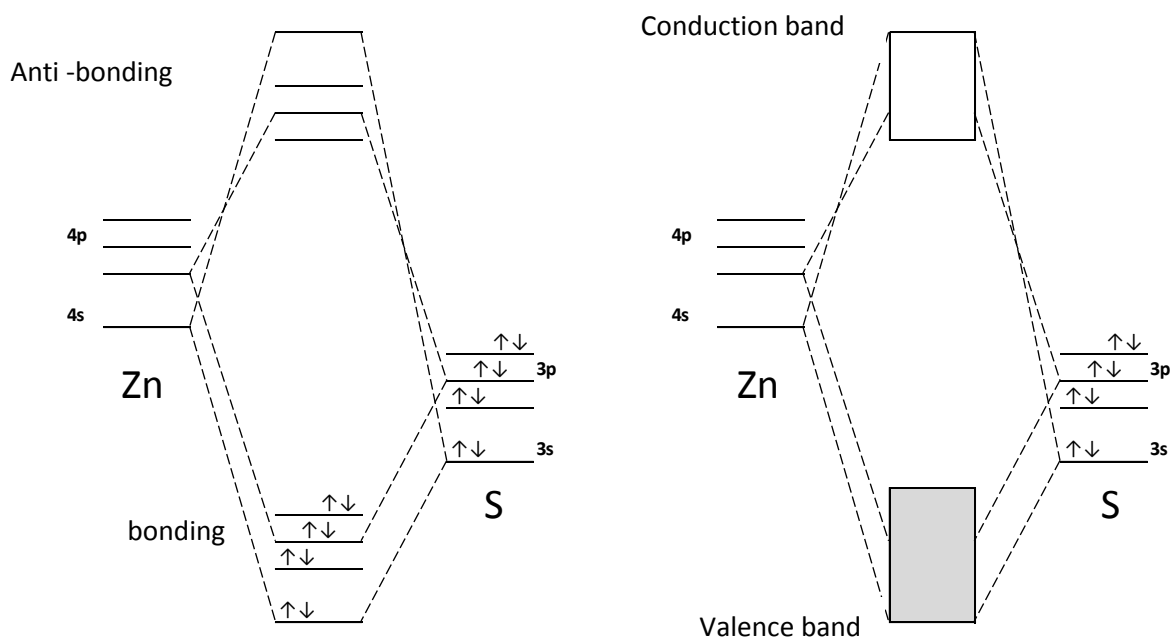


Figure 2.5: Molecular orbitals of a ZnS_4 cluster and the corresponding band model. (Osseo-Asare, 1992)

A macroscopic solid mineral consists of many atoms that generate many molecular orbitals. These orbitals are close together in energy and so numerous that they effectively form continuous bands as shown in the right of Figure 2.5. The valence electrons in bonding molecular orbitals form the valence band. Similarly for the antibonding orbitals, an antibonding band known as the conduction band is formed. These bands are separated by a forbidden region of energy known as the band gap. Band theory is the basis for understanding the electronic structure of semiconductors, and for understanding electron transfer between the semiconductor and a redox couple in solution.

Sphalerite is a convenient simple example often given in the literature (Osseo-Asare, 1992; Vaughan and Tossell, 1983). The chalcopyrite crystal is more complex, being a ternary structure with iron and copper replacing zinc at alternate positions in the tetrahedral lattice. Some authors considered the structure as alternate CuS_4^{7-} and FeS_4^{5-} clusters with molecular orbitals as shown in

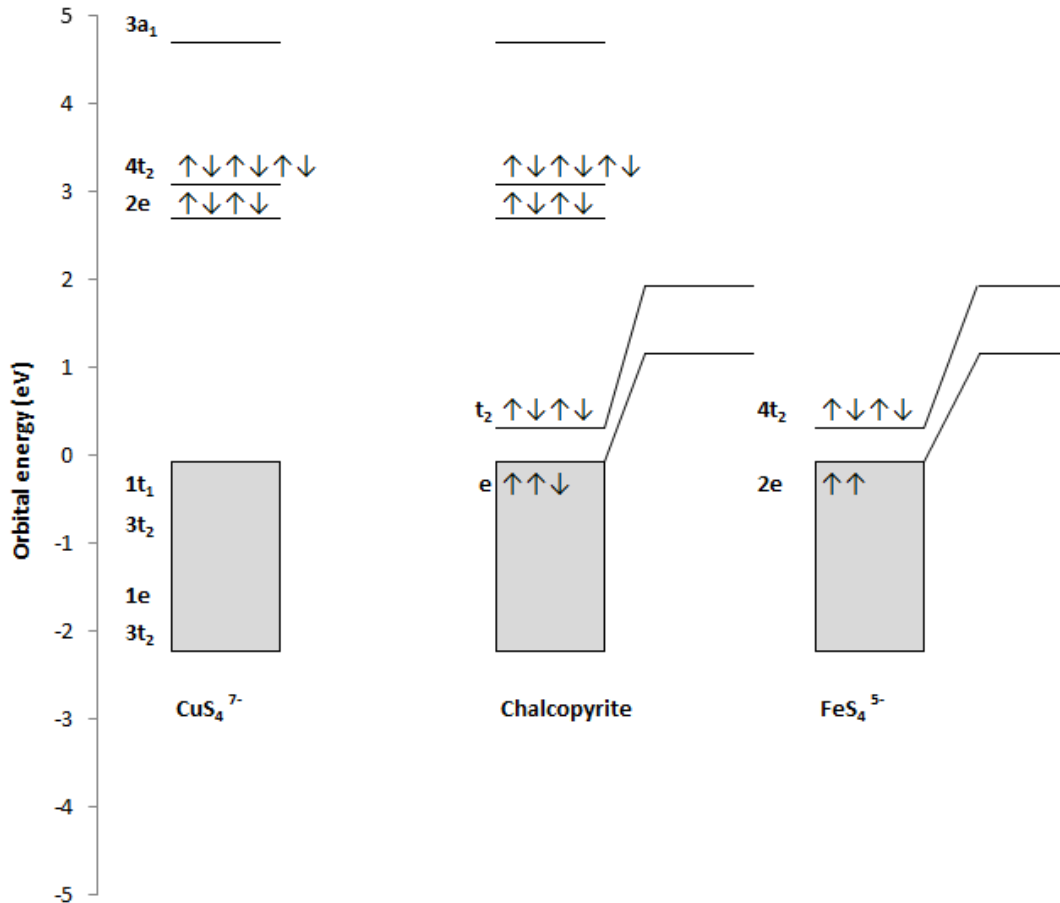


Figure 2.6 (Tossell et al., 1982). The molecular orbitals of these clusters combine to form the overall molecular orbitals for the mineral as shown in the centre of the diagram.

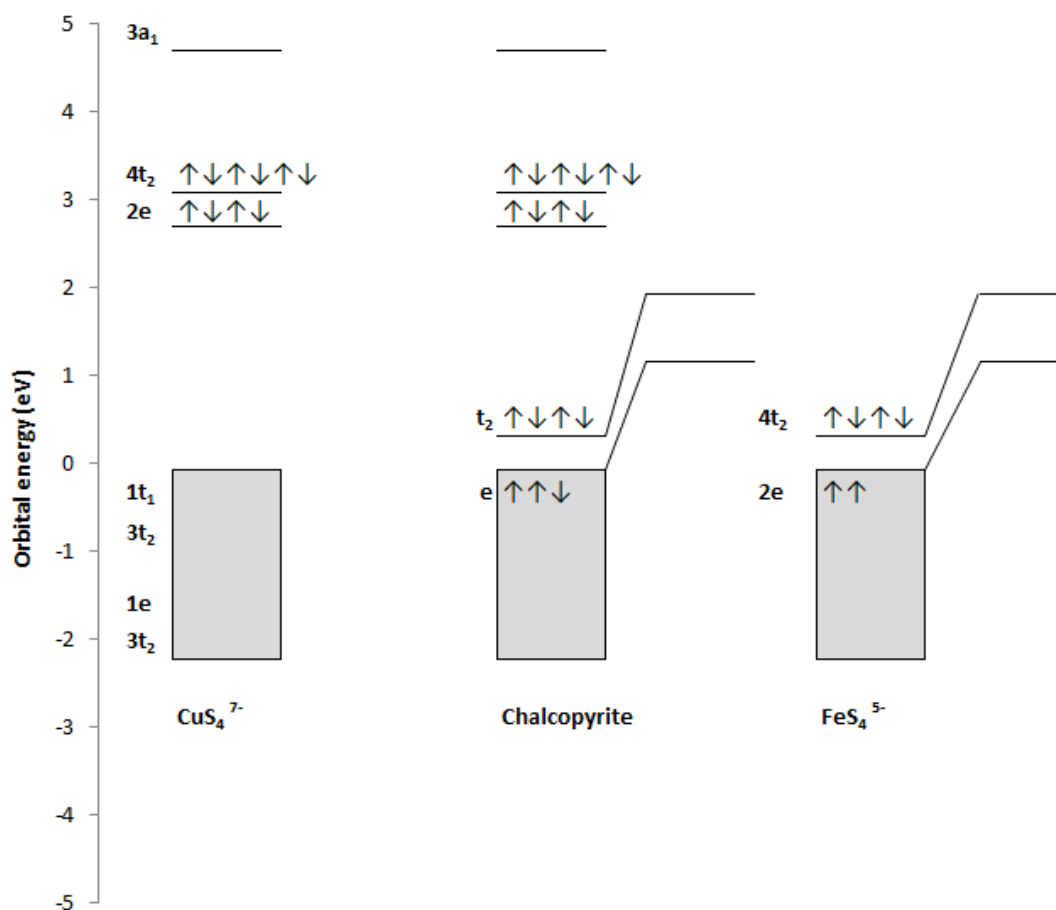


Figure 2.6: Molecular orbital diagrams for CuS_4^{7-} and FeS_4^{5-} that comprise chalcopyrite. The “crystal field” orbitals caused by iron d orbital splitting are also shown (Tossell et al., 1982).

In this diagram the uppermost $3a_1$ orbital represents the conduction band and the $1t_1$ the top of the valence band. This would suggest a band gap of 4.75 eV. The band gap has in fact been shown through optical spectroscopy to be 0.6 eV. This is anomalously small compared to other analogue semiconductors in the chalcopyrite family (Oguchi et al., 1980). This discrepancy is likely due to the influence of iron on the band structure. This has been shown by the effect of iron doping on other chalcopyrite semiconductors, where extra absorption bands are observed with increasing intensity as doping is increased (Teranishi et al., 1974).

The splitting of the iron 3d orbitals, known as the crystal field orbitals, contributes significantly to the electronic structure of the mineral. The $4t_2$ orbitals that were originally iron 3d orbitals form a narrow band within the band gap. The electrons in this band have a lower mobility and hence conductivity than a conventional conduction band. An extra optical absorption edge at 3.7 eV is thought to correspond to the true band to band transition and is the band gap of chalcopyrite if the d band is not considered (Sato and Teranishi, 1976). The electronic structure is complex, and worthy of a dedicated study to further understand the nature of the band gap.

2.3.3 Band structure of semiconductors

An ideal semiconductor is known as “intrinsic”. At absolute zero it has a full valence band and empty conduction band. A real semiconductor may have impurities and imperfections that result in localised energy levels in the band gap, known as “doping”. By being localised, these levels do not allow electrons the physical movement that is seen in bands. In quantum chemistry terminology, the wave function for these levels does not extend through the crystal. In other words, these levels do not form a band.

If the localised level has excess electrons and is close to the conduction band edge, electrons can be readily promoted to the conduction band. This is termed an “n-type” semiconductor. If the level is electron deficient and close to the valence band, electrons can be promoted out of the valence band resulting in a mobile “hole” in the band – a “p-type” semiconductor. For chalcopyrite, conductivity type is determined by a natural metal excess over sulfur. This causes localised energy levels close to the conduction band edge in the band gap resulting in n-type conductivity. P-type chalcopyrite is rare but has been reported in some studies (Pridmore and Shuey, 1976). A schematic diagram of these processes is shown in Figure 2.7.

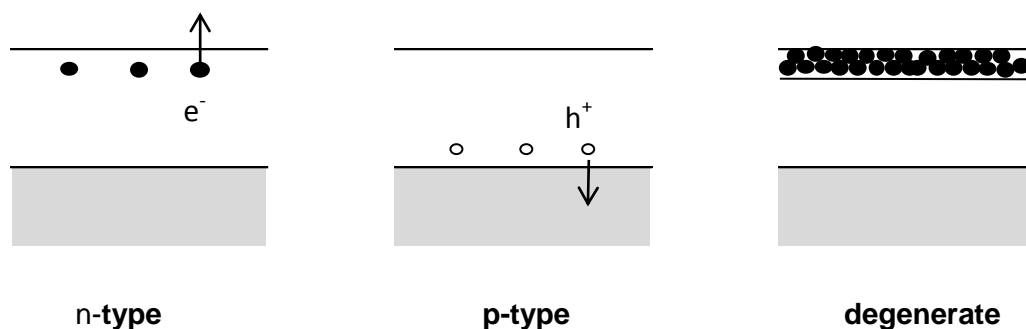


Figure 2.7: n-type, p-type, and degenerate semiconductors.

When doping of a semiconductor is extreme, the dopant atoms are physically close together and the energy levels are no longer localised. These form a new energy band allowing conduction of electrons that result in metal-like behaviour. This is known as a degenerate semiconductor. A high level of impurities could be expected in natural minerals such as chalcopyrite. It has been speculated that for this reason the semiconductor is heavily doped and would not exhibit semiconducting properties during leaching (Nicol et al., 2016).

The effect of doping on degeneracy has been observed in studies on synthetic chalcopyrite samples in the electronics industry. Small amounts of metal doping or sulfur deficiency result in metal-like behaviour, such as a drop in the thermoelectric power as evidenced by the measured Seebeck coefficient (Lefevre et al., 2016; Li et al., 2013; Xie et al., 2016). This would be identifiable in hand specimens as a small or zero thermoelectric power with a hot probe analysis method.

2.3.4 Electron transfer

The description of the band structure of chalcopyrite as outlined in the previous sections is an important foundation for understanding electron transfer during oxidative leaching. The model for electron transfer from a semiconductor requires the energy levels of the semiconductor to correspond to vacant energy levels of the redox couple (Gerischer, 1969). The energy levels of typical redox couples fluctuate due to reorganisation energy of the ion-solvent bond, showing a Gaussian distribution as shown in Figure 2.8 (Memming, 2007). This increases the energy range over which electrons may be accepted from the mineral.

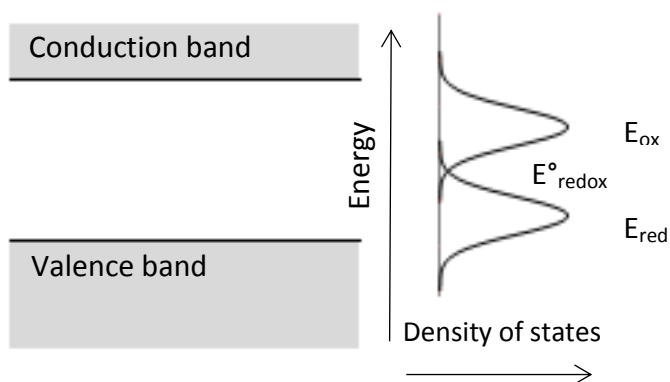


Figure 2.8: Energy levels of a typical semiconductor and redox couple (Memming, 2007).

Dissolution would not be expected from redox couples with a standard potential in the band gap of an ideal semiconductor. If the energy levels of the conduction and valence bands are known then an appropriate oxidant could be selected that would not have an energy corresponding to the gap. The precise energy levels of the band gap in chalcopyrite have not been directly measured due to its antiferromagnetic nature (Shuey, 1975). However in a theoretical study the energy at the centre of the band gap, the Fermi level, was calculated from electronegativity values of the constituent atoms to be 5.15 eV on the absolute scale, or 0.65 V (vs SHE) (Xu and Schoonen, 2000). With a band gap of 0.6 eV spanning the Fermi level, the band edges would be expected to be at 0.95 V (vs SHE) for the valence band and 0.35 V (vs SHE) for the conduction band. A suitable oxidant should therefore have empty energy levels of greater than 0.95 V (vs SHE) or less than 0.35 V (vs SHE). This seems consistent with observations of leaching in strong oxidants, mild oxidants such as triiodide and ferricyanide, and controlled low-potential leaching with ferric/ferrous ions (Guan and Han, 1997; Third et al., 2002; Watling, 2013).

Electrochemical studies have shown that the rate of reduction of a species in solution at the surface of a chalcopyrite electrode is not correlated to the potential of the couple (Parker et al., 1981). Couples with a low potential such as ferricyanide, triiodide and cupric ions are reduced at a faster rate than ferric ions, which has a higher potential. Stronger oxidants such as bromine and nitrate are also reduced faster than ferric. The rates of reduction were said to be related to the semiconducting properties of the chalcopyrite surface (Parker et al., 1981). It has been suggested that the reduction rate is due to the proximity of the redox couple energy to the conduction and valence band edge as can be seen in Figure 2.9 (Crundwell, 1988).

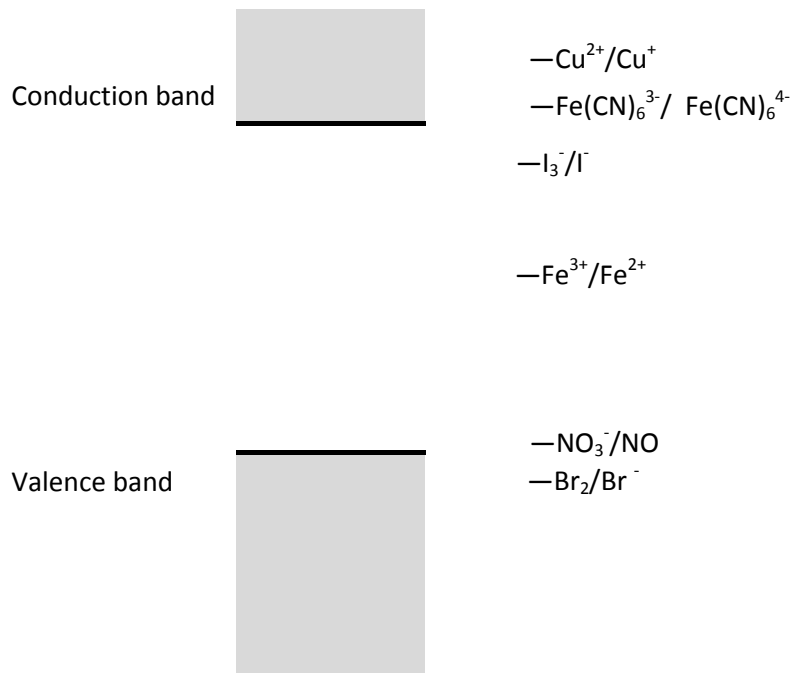


Figure 2.9: Schematic of the energy levels in chalcopyrite and redox couples (Crundwell, 1988)

The standard potentials of the redox couples in Figure 2.9 are for equal activities of oxidised and reduced species in equilibrium. The actual potential can be varied by controlling the concentration of the species in the couple according to the Nernst equation as shown in Equation 2. For example, the ferric/ferrous couple corresponds to the centre of the band gap at 0.77 V (vs SHE). It can be lowered by altering the ferric to ferrous ratio through controlled potential leaching so that it overlaps the conduction band and allows electron transfer. This however lowers the density of unpopulated states in the couple and limits the electron transfer rate. This is shown in the schematic diagram in Figure 2.10.

The Nernst equation for the ferric ferrous couple is as follows:



$$E = E^{\circ} - 2.303RT/F \times \log[a(\text{Fe}^{2+})/(a\text{Fe}^{3+})] \quad \text{Equation 2}$$

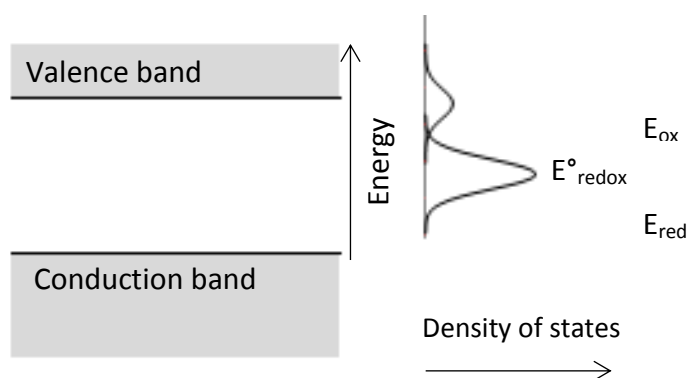


Figure 2.10: Energy levels of a semiconductor and redox couple with a lower concentration of reduced species (Memming, 2007).

2.3.5 Expected electrochemical current-potential behaviour for ideal semiconductors

Chalcopyrite and other semiconductors are often studied with electrochemistry. The current potential curves of ideal semiconductors are well known. A schematic is shown in Figure 2.11 (Schmickler, 2010). For an n-type semiconductor, at positive applied potentials little current would be expected to flow until the potential approaches that of the valence band edge. At this point electrons can hop to the conduction band resulting in mobile holes at the surface that eventually allows dissolution. This generally occurs at about 0.95 V (vs SHE) for chalcopyrite in many studies (Crundwell, 2015; Ghahremaninezhad et al., 2010; Viramontes-Gamboa et al., 2007). At negative applied potentials, current flows freely via the conduction band.

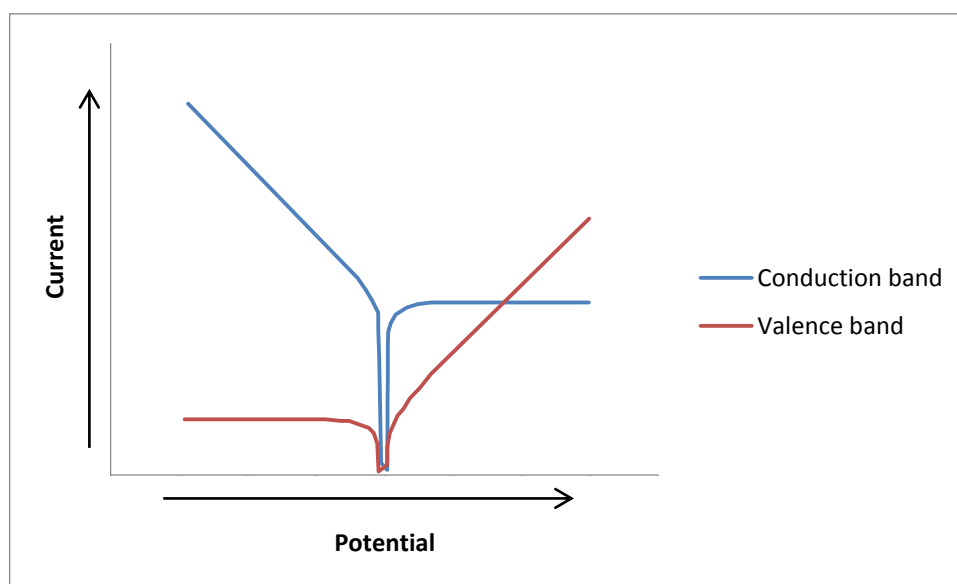


Figure 2.11: Schematic of a current potential curve for a typical n-type semiconductor (Schmickler, 2010).

2.3.6 Implications for leaching and electrochemical behaviour.

Given the electronic structure, it is expected that the dissolution of chalcopyrite would be slow using common oxidants such as Fe^{3+} . Strong oxidants such as dichromate, hypochlorite or bromine that interact with the valence band have been shown to greatly enhance leach rates (Watling, 2013). Oxidants that interact with the conduction band such as ferricyanide, triiodide, cupric or ferric/ferrous with controlled potential also show enhanced leach rates or electrochemical reduction (Chen et al., 1991; Guan and Han, 1997; Parker et al., 1981; Third et al., 2002; Xie, 2006).

The current potential curves of chalcopyrite electrodes presented in literature usually match what would be expected according to semiconducting theory as outlined above. These show a free flowing cathodic current and an inhibited anodic current up to a critical potential where electrons can hop from the valence band to the conduction band (Crundwell, 2015). This is an alternative to the idea that this critical potential indicates the breakdown of a passive layer, as it is known for classic metal passivation.

The semiconducting properties of chalcopyrite have been well established in many studies in a variety of disciplines, the most comprehensive is by Shuey and co-workers (Pridmore and Shuey, 1976; Shuey, 1975). Their work has shown that chalcopyrite is predominantly n-type due to a natural non-stoichiometry. The semiconducting nature of chalcopyrite has led to numerous studies for its application in electronics, starting with its discovery in 1875 (Braun, 1875). It is now a name given to a broad family of semiconductors used in industry (Siebentritt, 2006)

Despite this widespread acceptance of the importance of the electronic structure of chalcopyrite for electron transfer, it is generally not taken into consideration when analysing leaching or electrochemical behaviour. A few researchers have claimed that the semiconducting properties are of no relevance to the leaching behaviour and rejected the idea outright. The claim is that chalcopyrite does not behave as a semiconductor; instead it has metallic or alloy properties with a polysulfide passivation layer (Biegler and Swift, 1979; Nicol and Zhang, 2017; Nicol, 2016; Nicol, 2017a; Nicol, 2017b; Nicol, 2017c; Nicol et al., 2016).

2.4 Arguments against the electronic band structure/semiconductor theory

While many authors have not considered the semiconducting nature of chalcopyrite and the implications it has on leaching, only a few have rejected the evidence completely. The claim is that natural chalcopyrite has significant impurities, these dope the semiconductor resulting in a degenerate or metal-like state (Nicol et al., 2016). The degenerate semiconductor then behaves as a metal, with dissolution impeded by passivation.

This is a speculative claim and has not been tested experimentally. Studies of synthetic chalcopyrite doped with zinc have shown a change to metal-like behaviour as evidenced by the thermoelectric effect, but this has not been seen in natural samples that should also be “doped” (Nicol, 2016; Nicol, 2017c; Nicol et al., 2016; Xie et al., 2016). It would be important to differentiate between impurities present as separate discrete inclusions compared to solid solution atoms within the mineral lattice. In any case, it has been shown that deviations from stoichiometry are more influential than such lattice substitutions of impurities (Pridmore and Shuey, 1976).

2.4.1 Early arguments against passivation

The first argument against the semiconducting properties of chalcopyrite as having relevance to its dissolution was in the early 1970s (Springer, 1970). This study is sometimes cited in later work as supporting the idea that there is no relationship between semiconducting behaviour and leach kinetics (Biegler and Swift, 1979; Nicol et al., 2016).

The primary focus of this study however was not on chalcopyrite but on the electrochemical behaviour of pyrite, which showed some characteristics of a metal instead of a semiconductor. This observation seems to have been extended to chalcopyrite, for which only a limited study was carried out. Two criteria were given as evidence for non-semiconducting behaviour of pyrite. Firstly the Tafel slope was measured at 120 mV per decade of current which is typical of a metal. An ideal semiconductor should be 60 mV per decade. Secondly, there was no limiting current present at high potentials that is characteristic of semiconductors.

In this study the Tafel slope of chalcopyrite was not discussed, which in fact turned out to be about 45 mV compared to about 150 mV for pyrite as can be seen in Figure 2.12. Obviously the first criterion that a Tafel slope is similar to that of a metal does not apply to chalcopyrite. It was also claimed that no limiting current was present for chalcopyrite. The limiting current was possibly not seen due to termination of the potential sweep below the onset of the limiting current, as demonstrated by (Zevgolits and Cooke, 1975). The potential sweep in the Springer study stopped at 1.15 V (vs SHE), which is just below the point where current limiting effects are observed by other researchers (Crundwell et al., 2015; Zevgolits and Cooke, 1975).

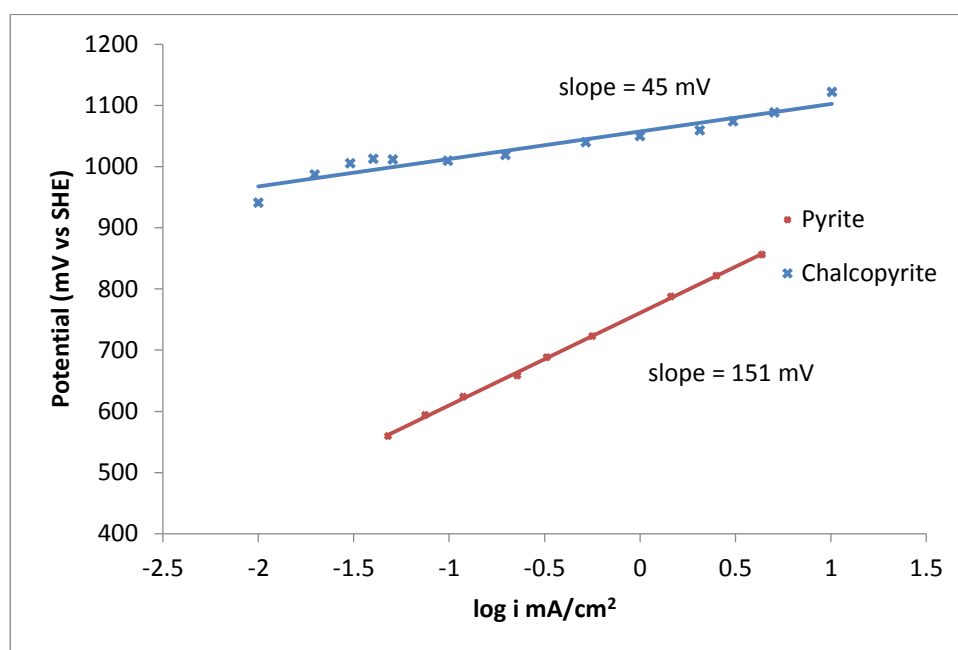


Figure 2.12: Comparison of the Tafel slopes of chalcopyrite and pyrite (Springer, 1970).

Another study critical of the influence of semiconducting properties was by Biegler and Swift (1979). Their criticism was based on a lack of any photo-effects with a chalcopyrite electrode. By using a light that was switched on and off during a potential sweep it was stated that no effect was observed - specifically no “light sensitive limiting current”. The results of this work were not presented in the paper nor were any experimental details given such as the scan rate used. This is a highly unusual way to prove a hypothesis; the conclusion can also be regarded as speculative at best. Other authors, even strong critics of the semiconductor theory, have positively shown an effect from illumination (Crundwell et al., 2015; Nicol, 2016). Also, in a much later study by Klauber (2003), samples from one of the sites in the Biegler and Swift study was shown to be an unusual p-type, which in any case would not show a photo effect at anodic potentials.

Some authors studied the leach rates of chalcopyrite from different localities and determined similar leaching rates for all (Dutrizac, 1982). It was also concluded that along with impurities and dislocation density, the n or p semiconducting type had no effect on leaching rate. The thermoelectric effect (hot probe method) was used to determine semiconductor type on samples before leaching. However, after measurement of semiconductor type the samples were crushed, cyclosized and triple froth floated for leaching tests. The hot probe results were for samples with impurities, the leach results were for purified samples. While this approach is useful for showing that sample location had no effect on leach rates of purified chalcopyrite, the leach rates cannot be connected to hot probe results on impure samples.

A further study on samples from the same locations comparing n and p-type also described variability of conductivity type within a sample (McMillan et al., 1982). These samples were very different in terms of impurities; with the p-type being 98% chalcopyrite and the n-type 82%. The n-type was also high in silver, but with no further description of mineralogy, such as if silver was interstitial in the lattice of chalcopyrite or a discrete mineral in the sample. It is well known that silver catalyses chalcopyrite dissolution and may affect these results (Watling, 2013). A Hall Effect measurement was performed on n and p-type samples according to an ASTM method, however recent literature from ASTM emphasises the importance of a pure, single crystal for such measurements (ASTM, 2016). Recent studies have also shown how n and p-type minerals can exhibit similar behaviour due to electron exchange through surface states (Bryson and Crundwell, 2014).

2.4.2 Recent criticisms

Few papers were written in recent years that were critical of the semiconductor model of chalcopyrite dissolution until Nicol and co-workers published a series of papers in 2016 and 2017 (Nicol and Zhang, 2017; Nicol, 2016; Nicol, 2017a; Nicol, 2017b; Nicol, 2017c; Nicol et al., 2016). This seems to be in response to three papers by Crundwell and co-workers that promoted the idea that the electronic structure played a key role in the leaching behaviour (Bryson et al., 2016; Crundwell, 2015; Crundwell et al., 2015). The fundamental claim of these critics is that natural chalcopyrite is degenerate due to the quantity of impurity elements expected in such samples (Nicol et al., 2016). These impurities cause heavy doping of the semiconductor resulting in degeneracy and metal-like behaviour. Such strong criticism demands a scrutiny of their claims.

The alternative process proposed by these authors is that a polysulfide passivating layer similar to an oxide layer on a metal is formed on the surface. This was said to be similar to a de-alloying process seen in some metal alloys (Lázaro and Nicol, 2003; Nicol and Zhang, 2017; Nicol, 2017a; Nicol, 2017c). The surface can be reactivated by another process called “back alloying” that is claimed to be analogous to a process seen in binary metallic alloys.

2.4.2.1 Photo-effects on the chalcopyrite surface.

It is well known that photocurrents can be produced in a semiconductor when light of energy exceeding the band gap is shined on the surface (Bard and Faulkner, 2001; Brett and Brett, 1993; Memming, 2007). This effect was demonstrated for chalcopyrite in several recent studies (Bryson et al., 2016; Crundwell et al., 2015; Zhou et al., 2015). This idea was criticised by Nicol and co-workers, who produced two studies on the effect of light to claim that the current effects observed by others are thermal in origin and not related to the interaction of light with the electronic structure of chalcopyrite.

In the first study, the anodic and cathodic currents from two p-type chalcopyrite electrodes under visible and laser light of different wavelengths were examined (Nicol, 2016). It was claimed in this work that “for p-type samples, photocurrents should normally be observed using visible sources under anodic but not cathodic conditions”. This is the opposite of what is normally observed, where n-type semiconductors show this behaviour (Crundwell et al., 2015; Memming, 2007). Under visible light, a correlation of current with temperature was shown for the anodic scan which was claimed to be the main factor contributing to the current spikes shown in Figure 2.13. For the cathodic scan, similarities in the response of chalcopyrite and gold metal to light were cited for a lack of a photo effect.

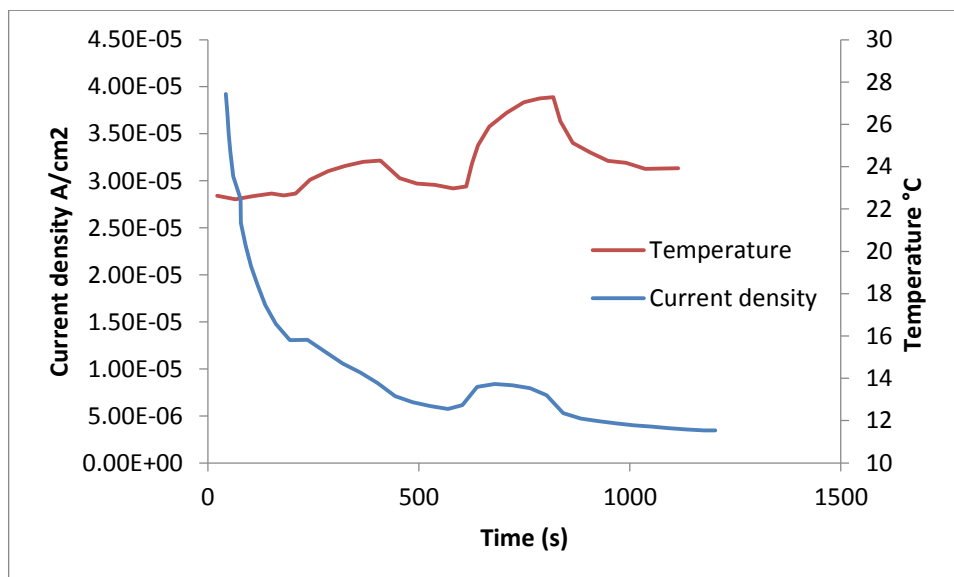


Figure 2.13: Apparent correlation of current density and temperature for a chalcopyrite electrode held at 0.577 V (vs SHE) (Nicol, 2016)

A chalcopyrite band gap of 0.35 eV was quoted in this work, which would show photo effects across the visible range. Lasers of different wavelengths were used in an attempt to induce a photocurrent as shown in Figure 2.14. Higher energy lasers indeed induced a photocurrent at anodic potentials. Strong current responses with green and violet light and a weak response from red light indicated that the band gap was between 2.3 eV and 3.1 eV. It was claimed that this response suggested the oxidised surface was a p-type semiconductor. The reasoning is unclear, as anodic photocurrents indicate n-type behaviour. This conclusion of a p-type surface layer is not consistent with other researchers as claimed. Instead the opposite has been observed where the surface was said to be n-type and the bulk p-type (Ghahremaninezhad et al., 2010).

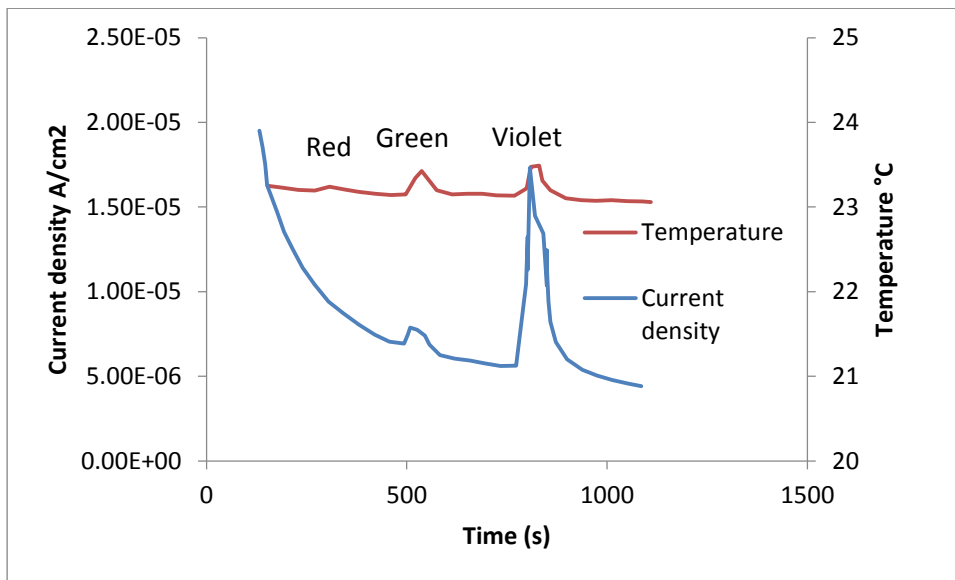


Figure 2.14: The effect of red, violet and green lasers on current density and temperature.

The effect of light of different wavelengths can be attributed to the complex nature of the band gap of chalcopyrite. The photo effects observed in Figure 2.14 with light of energy greater than the band gap appears to be due to transitions to higher levels that are observed during reflectance studies (Oguchi et al., 1980). The band gap of 0.6 eV that would be for visible light is for the valence band and the iron 3d band transition. This band has different properties such as lower mobility which may contribute to the effects observed.

In a second paper, an n-type sample was used and the opposite claim that “photocurrents would not be expected to be observed for a cathodic reaction involving an n-type semiconductor.” (Nicol et al., 2016). In this paper a small correlation between temperature and current was demonstrated for cathodic potentials and it was concluded that temperature was the contributing factor as shown in Figure 2.15. This current effect was not of the same order observed for the p-type sample in the previous paper.

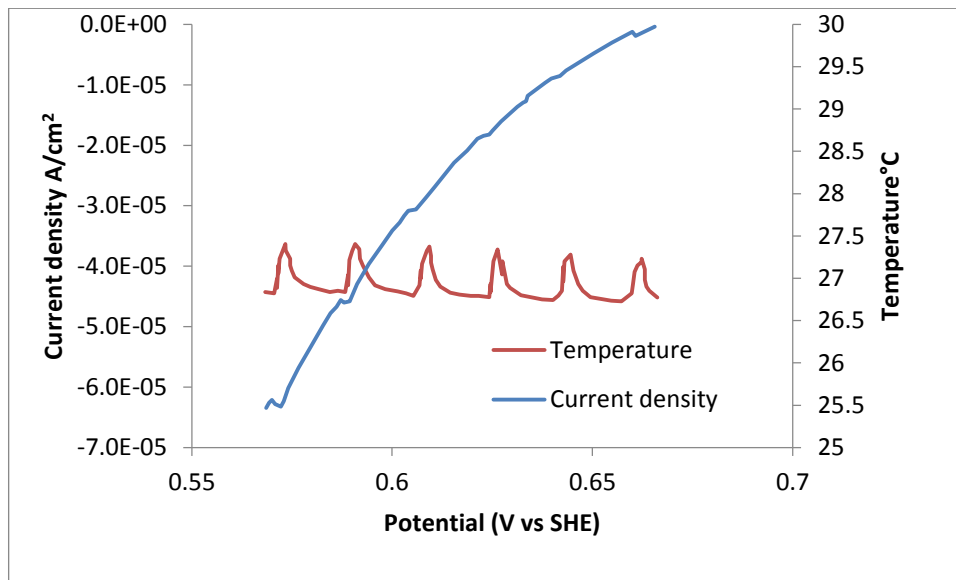


Figure 2.15: Voltamogram for the reduction of iron (III) on chalcopyrite with periodic illumination by a violet laser.

Unfortunately, no anodic results were shown for this n-type sample. If anodic scans under light were carried out, they could be compared to the results for the p-type sample given in the previous paper and a much stronger case presented. It should also be pointed out that the band gap of 0.35 eV quoted by Nicol is probably derived from theoretical calculations and is rarely used by most researchers (Li et al., 2014). It can't be ruled out that an error was made in claiming p-type conductivity in the first paper and that both were in fact n-type. This would explain a distinct photo effect for anodic scans and a minor effect for cathodic scans.

Follow up work by Bryson et al. (2016) using a light chopper has comprehensively shown that the photo effects are due to light and not thermal effects. A light chopper allows short bursts of light to shine on the surface at a rate faster than a thermal response. The current response is shown in Figure 2.16. This technique is well utilised in semiconductor physics and would require strong evidence to refute (Seeger, 2004). This work of Bryson et al. has not been taken into account in any subsequent criticisms.

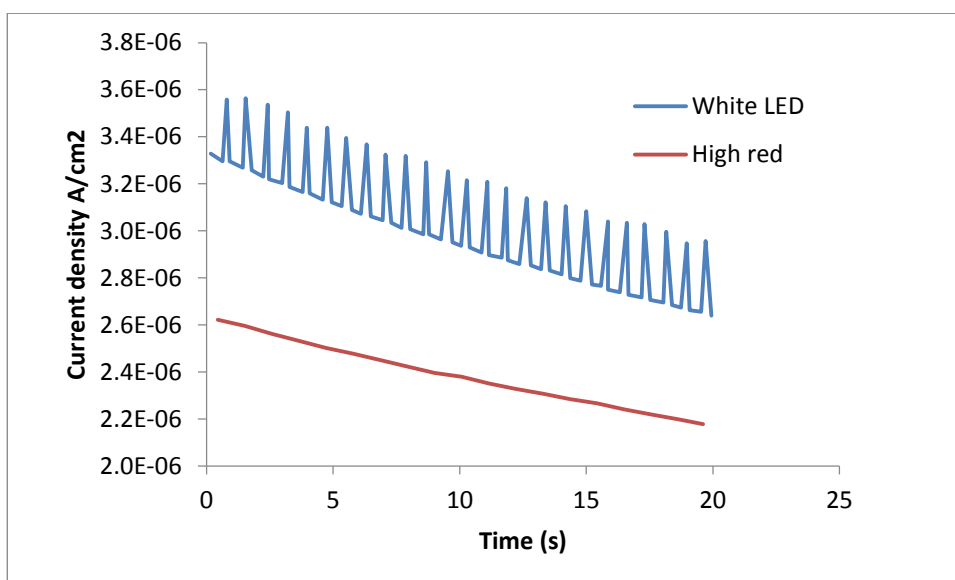


Figure 2.16: Current density of chalcopyrite held at 550 V (vs Ag/AgCl) with pulsed light from a light chopper.

2.4.2.2 The redox potential of Cu(II) complexes compared to hydrated ions.

It has been shown that the reduction of Cu (II) is faster than Fe (III) on a chalcopyrite electrode in chloride solutions (Parker et al., 1981). Crundwell (1988) claimed that this was due to the favourable energy overlap of Cu^{2+} with the conduction band edge compared to Fe^{3+} (Crundwell, 1988). This was presented in a schematic band diagram as shown earlier in Figure 2.10.

It was pointed out that this was in error because the formal potential of the copper chloride complex is “significantly higher” than the 0.15 V (vs SHE) reported for the un-complexed copper couple (Nicol et al., 2016). The potential in chloride solutions is actually between 0.5 and 0.55 V (vs SHE) for various chloride complexes (Lundström et al., 2009; Zhao et al., 2013). The implication is that this would place the potential for the couple in the band gap and electron transfer should be inhibited, with low rates of reduction.

It is correct that the potential for the Cu(II)/Cu(I) couple is higher in chloride solutions, although some studies have shown that un-complexed cuprous may be present which would have a lower potential (Lundström et al., 2009). Another aspect which might account for observed reduction rates is the reorganisation energy of the redox system as shown in Figure 2.8. This is a Gaussian distribution of energy states which can overlap the conduction band edge, even if the standard potential of the couple is in the band gap. The electron transfer rate depends on the density of states in the electron acceptor, which for copper is higher than for iron since it is closer to the conduction band edge and has more overlap.

This is consistent with rate constants for the reduction of Cu (II)/Cu (I) being higher than Fe (III)/ Fe (II). The rate constant for Cu (II)/Cu (I) is 48×10^7 m/s and Fe (III)/ Fe (II) only 0.32×10^7 m/s. By contrast, both species have a rate constant greater than 500×10^7 m/s measured on a platinum metal electrode (Nicol et al., 2016).

2.4.2.3 Limiting current

Semiconductors normally show a limiting current at high potentials as was discussed in the work of Springer (1970). This is due to the limit in the transport of holes in the valence band to the surface. Crundwell et al. (2015) observed this electrochemically on chalcopyrite through a potential step method. With 10 minutes duration at each step, a limiting current was shown at potentials above 1.1 V (vs SHE) to 1.5 V (vs SHE). Other authors disagreed that a limiting current is normal for chalcopyrite by comparing with selected studies that did not show it (Nicol, 2017a). This lack of evidence of a limiting current was claimed to demonstrate a lack of semiconducting behaviour of chalcopyrite.

A close examination of the studies presented for comparison of limiting currents shows some major differences in the measurement procedure (Nicol, 2017a). These use high scan rates at 20 mV/s and 100 mV/s compared to the slow potential step method used by Crundwell et al. High scan rates have been shown in some studies to mask the presence of a current plateau (Ghahremaninezhad et al., 2010; Viramontes-Gamboa et al., 2007). For the studies presented by Nicol, the high scan rates resulted in much less charge being passed at the potential where limiting currents are observed. While high currents were observed in these studies, it was for a brief time during the fast potential sweeps. This would explain the lack of a limiting plateau in these studies.

This effect of scan rate is shown clearly in one of the works cited in the comparative study. In the work of Ghahremaninezhad et al. (2010), different scan rates were used to show the effect on the current - potential curve as shown in Figure 2.17. The scan rate of 50 mV/s was chosen to demonstrate a lack of a limiting current at high potentials as shown by the green curve (Nicol, 2017a). However, a comparison with slower rates does show a drop in current that approaches the limiting current observed by Crundwell. The other curves presented in the comparative study terminated their anodic sweeps at around the potential expected for the onset of a limiting current. This was also illustrated in the early work of Zevgolis and Cooke, (1975) that showed that limiting currents can occur above the highest potential used in a potential sweep.

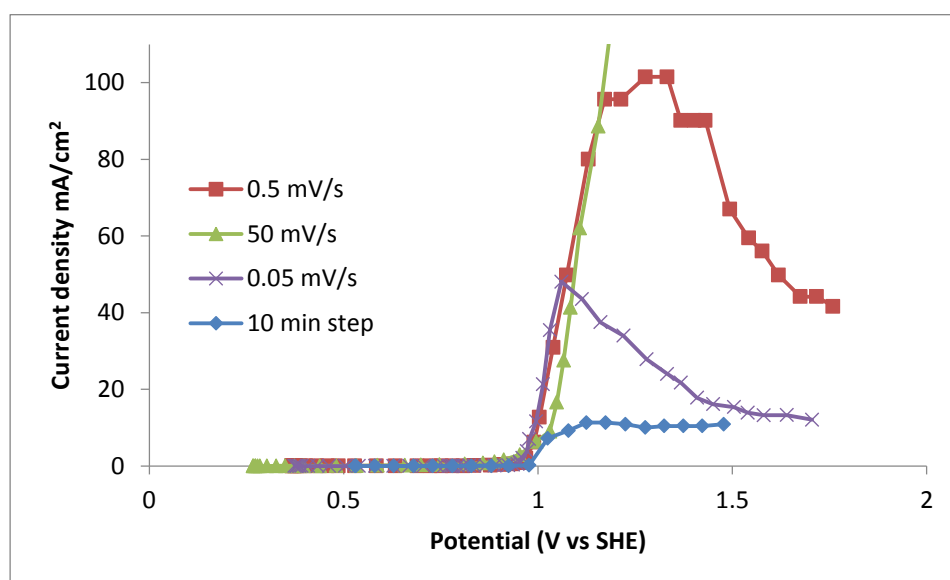


Figure 2.17: The effect of scan rate on observation of a possible limiting current. (Crundwell et al., 2015; Ghahremaninezhad et al., 2010).

2.4.2.4 Capacitance Measurements

The capacitance of the chalcopyrite-solution interface has been measured by some authors to demonstrate the semiconducting nature of the chalcopyrite surface (Crundwell et al., 2015; Ghahremaninezhad et al., 2010; Olvera et al., 2016). Of particular interest is the difference between passive and transpassive states at around 1 V (vs SHE). This approach has been criticised for two reasons (Nicol, 2017c). The first is that the system is not at steady state for the measurement; the second reason is that the frequency chosen for the capacitance measurement is not appropriate and results in unreliable data.

The argument for a steady state requirement is based on the length of time required to measure an electrochemical impedance spectrum (EIS). However, none of the studies that were criticised presented a full EIS study, only a capacitance measurement at a single frequency after a potential step of 10 to 20 minutes duration. It was assumed these studies instead used a linear potential sweep of unknown rate, but they in fact specified that the potential step method was used. Despite criticising this method, the same supposedly inaccurate measurement of capacitance was used as evidence for a passive layer formation and breakdown (Nicol, 2017c). This is obviously self-contradictory.

It was also claimed that an incorrect measurement frequency was used to determine capacitance. The correct frequency for measuring capacitance was said to come from the linear region of a Bode plot of impedance versus frequency, citing a study of passivated metallic nickel as a reference (Darowicki et al., 2006). However, the source for this claim makes no reference to this fact or to Bode plots at all. This paper also explicitly states that the measurement frequency has no effect on determining the semiconducting type. This is the most important property discussed by other authors. The change from n-type to p-type during a scan is said to coincide with passive layer breakdown or inversion of semiconducting type (Crundwell, 2015; Ghahremaninezhad et al., 2013). It should also be pointed out that a Bode plot should show the impedance and phase angle versus frequency, however only plots of impedance were presented in this critical paper (Nicol, 2017c).

The capacitance of a semiconductor/electrolyte interface is well known to vary with frequency and is reported in many textbooks and papers (Gomes and Vanmaekelbergh, 1996; Schmickler, 2010). The choice of measurement frequency will indeed affect the calculated donor density, but this is not critical for demonstrating the semiconducting nature of chalcopyrite. The studies that were criticised show the same capacitance behaviour regardless of frequency, that is n-type behaviour up to about 0.95 V (vs SHE) followed by an inversion to-p type (Nicol, 2017c).

2.4.3 Summary

The literature reviewed showed that criticisms of the semiconductor theory as it applies to chalcopyrite leaching are speculative at best. No measurements have been made that demonstrate the effect of doping of the mineral with impurities – which is the fundamental claim of the critics. Photo effects have been shown to be genuine and not thermal in origin. Claims regarding the observation of limiting currents and capacitance are based on incomplete data and misinterpretations of measurement techniques by other authors.

2.5 The passive layer

The alternative to the semiconductor model is that chalcopyrite is a degenerate semiconductor with metal-like properties. Its leaching is inhibited by a passive layer similar to that of oxides on metals.

2.5.1 Passivation as understood in corrosion science

Passivation, as it is understood in corrosion science, is caused by the formation of an oxide layer on a metal. A general Eh-pH diagram for corrosion of a metal is shown in Figure 2.18. This shows the region of solubility at low pH, immunity at low redox potentials and passivity at high pH. A small window for corrosion is also observed at very high pH for many metals.

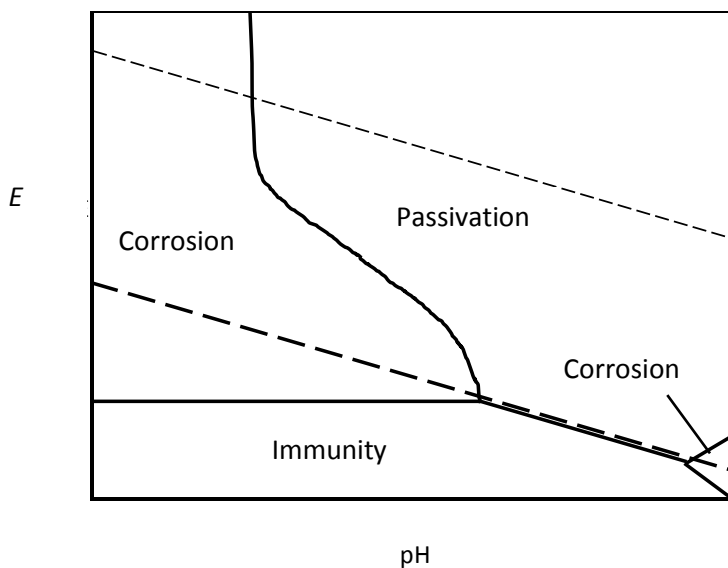


Figure 2.18: General Eh-pH diagram showing passivation and corrosion (Brett and Brett, 1993)

The classic passivation current-potential curve generated in electrochemistry for metals is superficially similar to that for chalcopyrite and shown in Figure 2.19. However, metals have different passivation behaviour to the observed “passivation” of chalcopyrite. Firstly, passivation is less favoured at acidic pH for metals, whereas lower pH provokes passivation on chalcopyrite (Córdoba et al., 2008). The passivation potential as shown in Figure 2.19 decreases with increasing pH for metals, but no such behaviour is reported for chalcopyrite (Viramontes-Gamboa et al., 2007). The critical current density for metal passivation decreases with pH, but no such effect is seen with chalcopyrite.

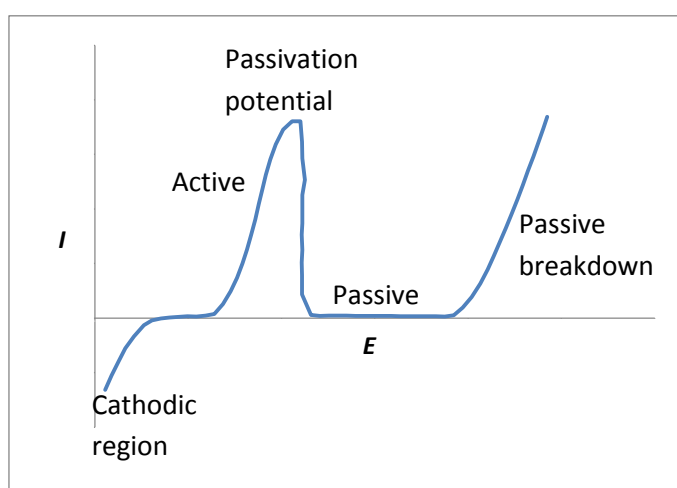


Figure 2.19: Typical current potential curve showing a passivation and passive breakdown.

The term “passivation” was not used by early researchers studying chalcopyrite dissolution, possibly since there was no relation to the well-known effect in corrosion science. Many authors have recognised this since that time and avoided the use of the term (Klauber, 2008). The term will be used in this review when it has been used in a cited paper.

2.5.2 Early theories- elemental sulfur

The first references to an inhibiting surface layer appeared in the 1960s, although it wasn't termed "passivation" at the time. In alkaline ammonia solutions, a loose iron oxide film was thought to limit charge transfer but was overcome through agitation (Beckstead and Miller, 1977; Stanczyk and Rampacek, 1966). In acid solutions, it was suggested a layer of sulfur was responsible for the slowing of leach rate (Dutrizac et al., 1969). The dissolution rate was linear with the square root of time and described as parabolic as shown in Figure 2.20. Unlike alkaline ammonia solutions, the rate was insensitive to disk rotation. This is consistent with what would be expected for transport through a surface film. Acid concentration also had no effect beyond keeping iron in solution. Sulfur was detected with XRD and was proposed to be the reason for parabolic kinetics.

Interestingly, the leach rate for a pure synthetic sample was much faster than for a natural sample. This is the opposite of what would be expected if the natural sample was a doped semiconductor as was discussed in Section 3.3. Doping of the mineral would result in degeneracy and metal-like behaviour. It was suggested porosity or impurities may have influenced the leach rate.

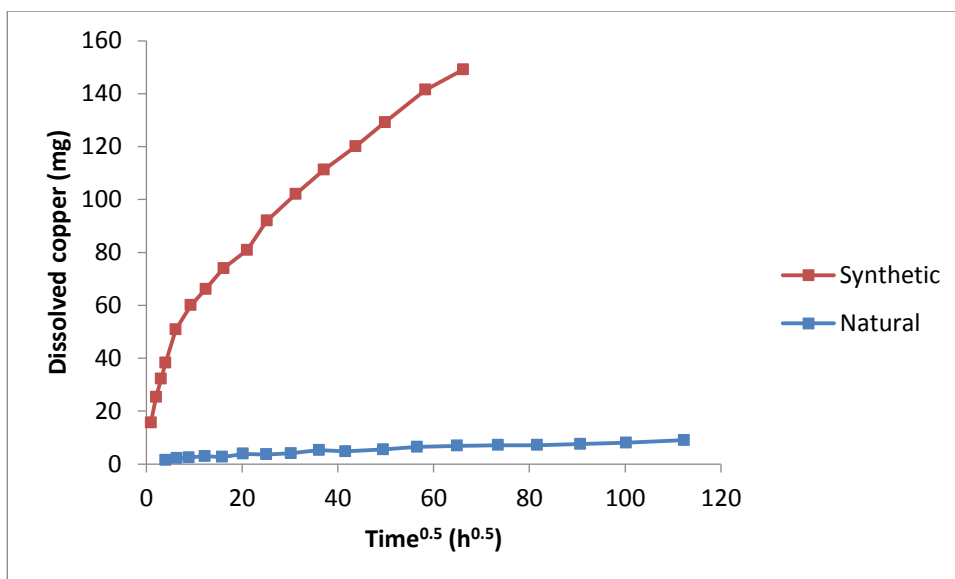


Figure 2.20: Comparison of natural and synthetic dissolution of chalcopyrite (Dutrizac et al., 1969).

2.5.3 Metal deficient models

The proposal for a rate controlling surface layer of sulfur was not universally accepted. Linge (1976) examined the leach rates from previous work and found they were far too low for that expected for pore diffusion through an elemental sulfur layer. Variations with temperature and oxidant concentration were also not consistent with the pore diffusion model. Linge disagreed with the elemental sulfur proposal and instead proposed a limitation by solid state diffusion.

It was observed that iron was solubilised at twice the rate of copper. Using the fact that a unit cell of chalcopyrite is $(\text{CuFeS}_2)_4$ and to maintain charge neutrality in the lattice, it was proposed that the only metal deficient layer possible was $\text{Cu}_3\text{Fe}_2\text{S}_6$ or a proton-stabilised $\text{Cu}_3\text{Fe}_2\text{H}_3\text{S}_8$. Further disruption to the lattice would result in a chalcocite phase which would dissolve rapidly. This is the only attempt to date to fully describe the stoichiometry of a metal deficient phase, other studies published since then use a broad term such as $\text{Cu}_{1-x}\text{Fe}_{1-y}\text{S}_2$.

2.5.4 “Passivation” by metal deficient layers

The first use of the term “passivation” in regards to acidic leaching of chalcopyrite was in 1977 for synthetic chalcopyrite disks in chloride solutions (Ammou-Chokroum et al., 1977). It was proposed that the accumulation of Cu_2S in a porous sulfur network covered the surface as shown in Figure 2.21. This gradually thickened and blocked the surface resulting in a decrease in reaction rate. The idea of “passivation” was immediately criticised for the use of un-sintered synthetic disks, which would show an initial rapid rate as fines are consumed (Dutrizac, 1978). Despite this, the term “passivation” was widely used from this point to describe the leaching kinetics of chalcopyrite.

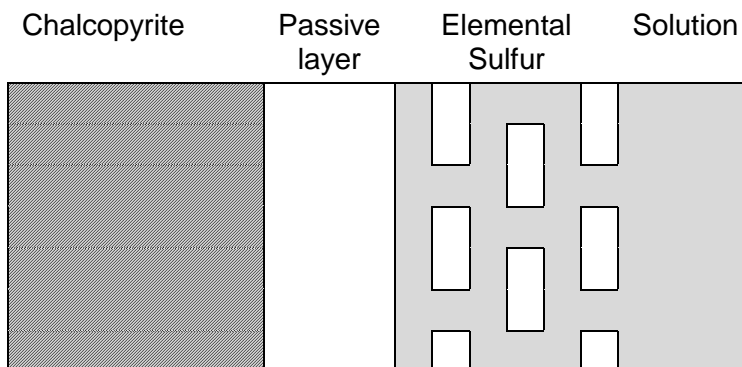


Figure 2.21: Model of passive layer by Ammou – Chokroum (1977)

Biegler and Swift (1979) attempted to generate a passive layer on a chalcopyrite electrode that would be significantly thick enough to observe and characterise. It was ultimately unsuccessful and the surface retained the appearance of chalcopyrite after lengthy oxidation times. X-ray analysis did not reveal any other phases present. Support for a passivating layer was not explicitly stated, but it was claimed that a thin layer formed during a linear sweep by oxidation of the surface through a “pre-wave” process. The pre-wave process was equated with the metal deficient layer suggested in the earlier work by Linge (1976). This pre-wave was later affirmed to be due to the formation of a passivating film (Biegler and Horne, 1985).

2.5.5 The metal deficient polysulfide

The idea of a metal deficient passivating layer was further developed with the introduction of the term “metal deficient polysulfide” (Parker et al., 1981). A key feature of this proposal is that the film is unstable and breaks down upon removal of an applied potential, resulting in a reactivated surface. This was observed through successive chronoamperometry scans, with rest periods at the OCP for various times as shown in Figure 2.22. This feature is of critical importance because it suggests that any attempt to observe the passive layer ex situ will be in vain – it is no longer present once removed from solution. This surface reactivation behaviour was also observed in other studies (Lu et al., 2000; Nicol, 2017a).

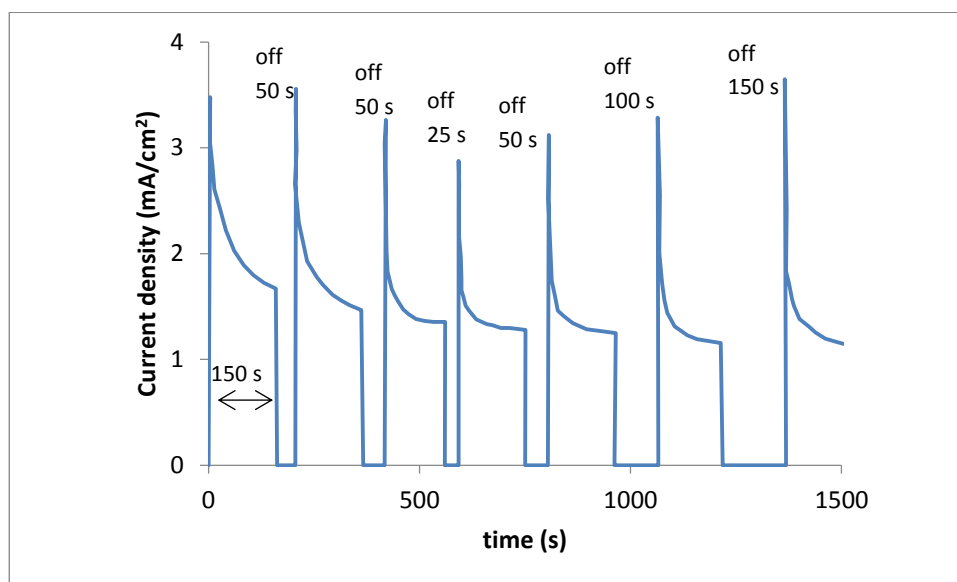


Figure 2.22: Chronoamperometry curves with rests at the OCP for times indicated (Parker et al., 1981).

Sulfur was formed on the surface in this study but was shown through dissolution in CS_2 to not be passivating. The authors acknowledged the semiconducting properties of chalcopyrite and proposed that the passive layer was also a semiconductor. This was based on the different rates of reduction of various oxidants at the same applied potential. A simple resistive layer such as sulfur was said to not differentiate between these oxidants. The presence of a limiting current suggested an n-type semiconducting surface.

Biegler and Horne (1985) revisited the pre-wave feature of earlier electrochemical studies. In this work, the prewave was said to be an indication of the formation of a passive layer. Unlike Parker's work, this layer apparently did not break down upon removal of potential. The break down process was suggested to be temperature dependent and not to occur at ambient temperature. The studies are however not directly comparable since a chronoamperometry measurement was not performed for direct comparison to Parker. Instead, cyclic voltammetry was performed with a rest at the OCP. The absence of a prewave on subsequent cycles was given as the reason for the lack of a reactivation. Later studies contradict this finding, where chronoamperometry does indeed show a reactivation at ambient temperature (Lu et al., 2000; Nicol and Zhang, 2017). The prewave is therefore not likely to be a feature of passive layer formation but is likely an artefact of surface preparation. It should be noted that this artefact formation process was considered by Biegler et al., but ultimately rejected.

Further electrochemical studies inferred a passive layer with still vague descriptions of its nature. A new term was introduced for the metal deficient phase – the Solid Electrolyte Interphase (SEI) (McMillan et al., 1982). This was said to be electronically insulating as is an oxide film on a metal, but did allow the transfer of ionic species from chalcopyrite to solution. Contrary to this work, (Warren et al., 1982) proposed two electrically conducting passive intermediates: $\text{Cu}_{1-x}\text{Fe}_{1-y}\text{S}_2$ and Cu_2S . The claim of passivity was based on polarisation curves and chronoamperometry. The passive species was tentatively suggested to be bornite and covellite, but it is known that these are more reactive than chalcopyrite and should hardly be passivating. It was conceded that chalcopyrite does not demonstrate the classical passivating behaviour of metals.

2.5.6 Surface analyses of the passive layer

Until the early 1980s no direct evidence for a passivating metal deficient sulfide layer on chalcopyrite was available. Buckley and Woods (1984) used XPS to examine the surface oxidised in air, ammonia and acid solutions. The surface species generated in air and ammonia were similar with an overlayer of iron oxide/hydroxide. Below this layer it was proposed that a metal deficient sulfide, in this case CuS_2 , was present due to a shoulder in the sulfur peak of Figure 2.23. This is now commonly referred to as the disulfide component of the peak, the main component is the monosulfide that is the lattice sulfur of CuFeS_2 (Klauber, 2008).

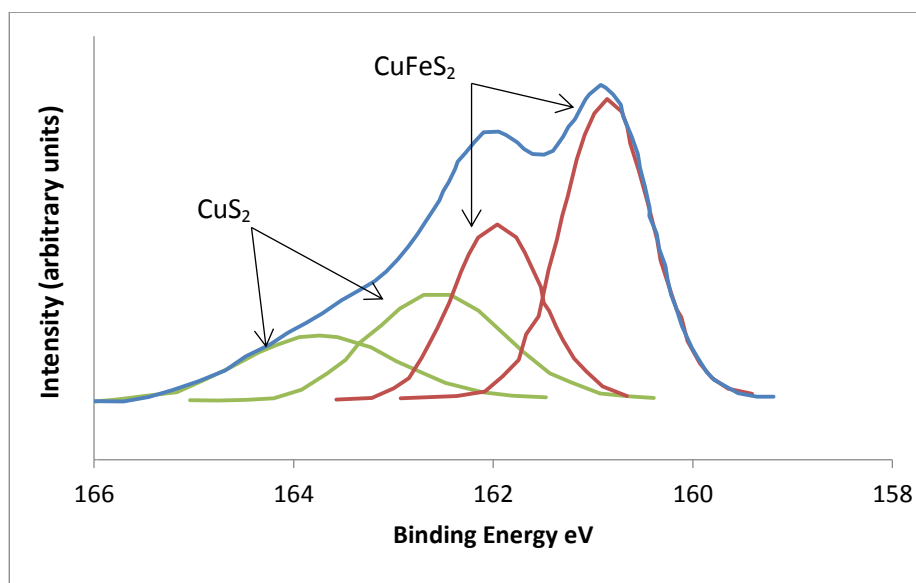


Figure 2.23: Sulfur peak for chalcopyrite exposed to air for three days (Buckley and Woods, 1984)

In acid solutions no iron-oxyhydroxide overlayer was detected, but the surface was said to comprise $\text{CuS}_{1.8}$. Iron and some copper were removed from the lattice leaving sulfur in its original position. No description is given for the unsatisfied valence on the remnant sulfur, but it was suggested that the layer could be called a polysulfide. The sulfur was said to not restructure to form pyritic S_2^{2-} groups.

Another example of XPS analysis of chalcopyrite was by Hackl et al. (1995). XPS and Auger spectroscopy was used to compare the surface of a pressure-leached and an unleached surface of chalcopyrite. The leached surface was that of a sample that had been exposed to a leaching solution of 5 g/L Fe^{3+} , 98 g/L H_2SO_4 at 110°C and 1.38 MPa O_2 pressure for three hours, the dissolution curve is shown Figure 2.24.

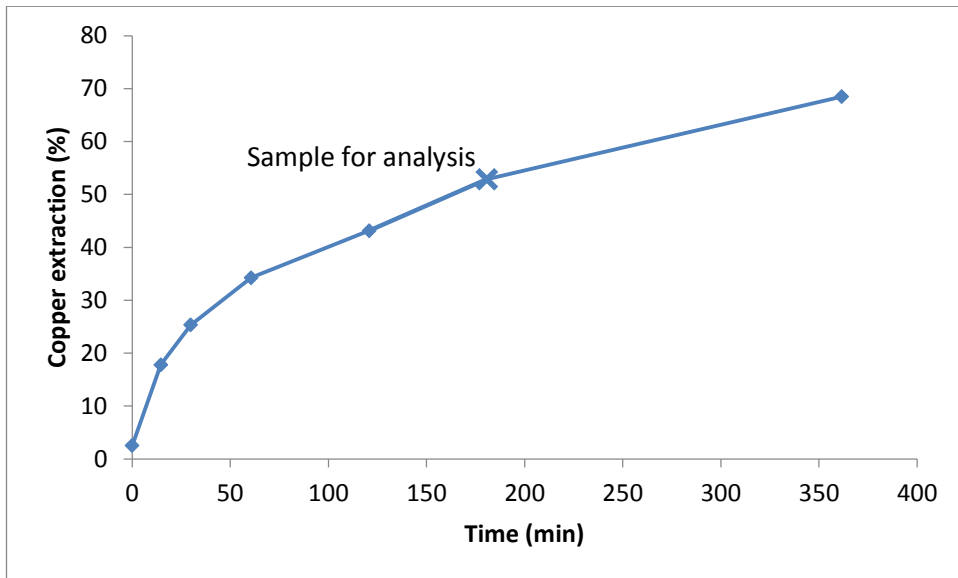


Figure 2.24: Leach curves at 110°C and 1.38 MPa oxygen pressure (Hackl et al., 1995).

It was proposed that distinct disulfide and polysulfide species were present on both the leached and unleached surfaces. These were thought to represent an “iron deficient sulfide” and “copper polysulfide” respectively. Both species formed on exposure to air where the metal deficient sulfide was 18%, polysulfide 10% and the lattice sulfide 68% of the total surface sulfur. During leaching, the lattice sulfur still made up over half the sulfur at 54%, disulfide was 8% and polysulfide 35%. A comparison of leached and unleached XPS is shown in Figure 2.25.

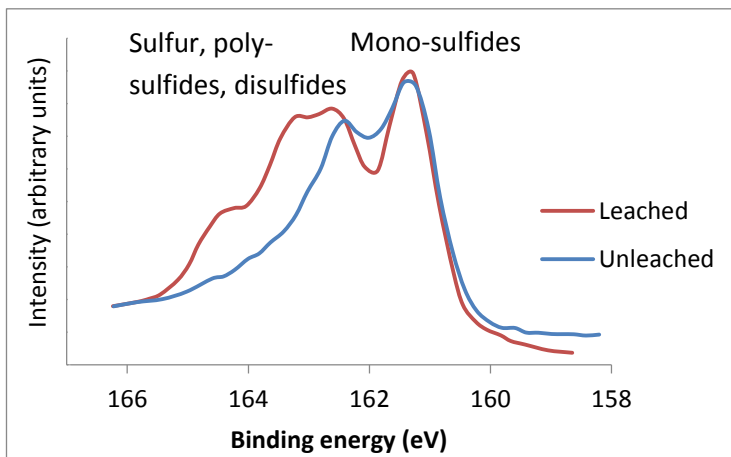


Figure 2.25: Comparison of sulfur peak for leached and unleached chalcopyrite (Hackl et al., 1995)

The iron deficient sulfide was said to form in an initial reaction and was non-passivating. The polysulfide formed in a second step that passivated the chalcopyrite. It was not explained how the polysulfide could passivate when it comprised only 35% of the total sulfur, which itself comprised only 35% of the mineral. It is questionable that polysulfide is in fact passivating, since the data shows that about 50% of the copper was extracted in only three hours at the time of sampling, and was still dissolving.

Other authors came to an opposite conclusion to Hackl in regards to the passivating species (Ghahremaninezhad et al., 2013). These authors claimed instead that polysulfides were non-passivating and metal deficient sulfides were passivating. In this work, a chalcopyrite electrode was held at various potentials in the passive and non-passive region and the surface examined with XPS. Components of disulfide and monosulfide were attributed to a metal deficient layer, and a distinct component to polysulfide. It is strange that the monosulfide was attributed to the metal deficient species. This is normally thought to be due to lattice sulfur (Buckley and Woods, 1984).

It was noted that the polysulfide appeared at potentials where active dissolution was observed, whereas the disulfide and monosulfide decreased in relative abundance in this potential region (Figure 2.26). This was interpreted as the breakdown of the passive layer that is comprised of mono and disulfides.

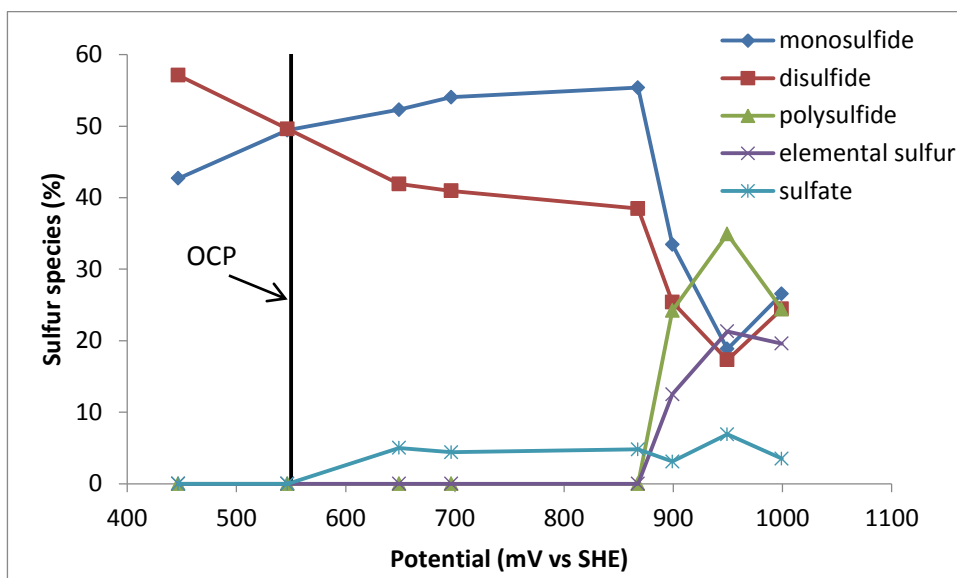


Figure 2.26: Proportion of various sulfur species as a percentage of total sulfur (Ghahremaninezhad et al., 2013)

Interestingly, the monosulfide and disulfide are present in samples held at the OCP and even at reducing potentials below the OCP. These are supposed to represent a passive metal deficient species that are the result of oxidation. The fact that it is present at the OCP and reducing potentials is inconsistent with this idea. The drop in relative contribution of mono and disulfides to the total sulfur peak shown in Figure 2.26 probably not due to a loss of these species on the surface, but the addition of other species such as sulfate, elemental sulfur and polysulfides.

Accompanying this change in sulfur speciation and passive layer breakdown was a change in the trend of capacitance with potential. This indicated a change from n-type to p-type semiconductor at the surface. This was interpreted as the breakdown of an n-type layer to reveal a speculated p-type bulk. Other studies with confirmed n-type chalcopyrite show the same behaviour, which can instead be attributed to the formation of an inversion region of a semiconductor at high potentials (Crundwell et al., 2015). Unfortunately the bulk was not actually characterised as p-type by Ghahremaninezhad et al. and this claim is speculative. It is highly improbable to be p-type given its rarity in nature (Pridmore and Shuey, 1976).

In his 2008 review, (Klauber, 2008) criticised the assignment of sulfur peak components to metal deficient sulfides and polysulfides in XPS traces. It was pointed out that the selective removal of a metal from chalcopyrite will destroy the crystal lattice. To remove a component of the lattice and yet retain the lattice structure is not possible. It was considered that metal deficient sulfide's existence is questionable let alone its passivation ability. Polysulfides are naturally unstable and oxidise readily to elemental sulfur. XPS peak shifts as evidence for polysulfides was also doubtful. The origin of the apparent polysulfide component assignment was traced through several historical papers and is based on misquoting results in the original work.

2.5.7 Other layer proposals

Another recent proposal for chalcopyrite passivation has been to compare it with de-alloying of binary alloys (Lázaro and Nicol, 2003; Nicol and Zhang, 2017; Nicol, 2017c). The polarisation curves of such alloys show characteristic features that are superficially similar to those for chalcopyrite (Ateya et al., 2002; Laurent and Landolt, 1991; Moffat et al., 1991). For these alloys, at potentials just above the OCP the current density is low and does not vary with potential. This low current is due to the dissolution of the less noble component of the alloy. The surface then becomes enriched in the more noble component which suppresses further dissolution. Above a critical potential the current increases rapidly with increasing potential. This process is known as gross or global surface roughening, resulting in a porous network of the more noble component.

The chalcopyrite alloy is said to comprise Cu_2S , FeS and FeS_2 (Lázaro and Nicol, 2003). This would actually be a ternary alloy rather than a binary. If the de-alloying model is to be adopted, it would be assumed that Cu_2S is the more noble component and FeS and/or FeS_2 the less noble. The initial low current region would represent the dissolution of the less noble FeS and/or FeS_2 components. This would lead to a surface enrichment in Cu_2S which suppresses further dissolution. At the critical potential this layer would break down and rapid de-alloying takes place with accelerated dissolution of FeS and FeS_2 . By the global surface roughening model this would result in a porous network of insoluble Cu_2S . Clearly this does not happen, since at the critical potential copper is rapidly dissolved; it does not form a porous network.

A further proposal to account for surface reactivation seen after a rest at the OCP is that of “back alloying” (Nicol and Zhang, 2017). This involves migration of the more noble components – in the case of chalcopyrite FeS and FeS_2 to the surface if the applied potential is removed in the passive region. This typically takes place over hours or days for metal alloys (Ateya et al., 2002). By contrast, the reactivation time observed for chalcopyrite is very fast- 30 seconds (Parker et al., 1981). It would be expected that the back alloying process for chalcopyrite would be even slower than for metals, considering the alloying iron sulfide components are much larger than a metal atom.

It is clear that the de-alloying/back-alloying process is highly speculative and has already been criticised by others (Klauber, 2008). No attempts have been made to address these criticisms in recent work and it is not considered a serious proposal by other researchers.

2.5.8 The Burkin model for metal deficient layers

Burkin studied the metal deficient surface layers formed on several sulfide and oxide minerals, but specifically not chalcopyrite (Burkin, 1969). Despite this, some authors cite this study in support of the metal deficient sulfide passivation theory for chalcopyrite (Córdoba et al., 2008; Lázaro and Nicol, 2003; Nicol, 2017a; Tkáčová and Baláž, 1988). In fact, Burkin stated that chalcopyrite likely had a non-protective porous iron oxide surface layer that was not analogous to the metal deficient layers that are readily observed on other minerals in the study.

A key criterion for Burkin's model is that the surface phase should be a stable mineral species that can form a continuous series of solid solutions with the main mineral. This series was readily observed and the cross section measured with a microprobe and optical microscope in a number of cases. Chalcocite was found to have a covellite layer, with intermediate digenite and non-stoichiometric phases forming a continuous gradient to the bulk mineral. The covellite layer is visible in hand specimens and is long known for being directly responsible for chalcocite's two stage leaching kinetics (Sullivan, 1933, Stanczyk and Rampacek, 1966). Chalcopyrite has no such solid solution series and hence no obvious metal deficient layer, despite some researchers' efforts to generate one (Biegler and Swift, 1979).

2.5.9 Passivation in alkaline pH

Relatively few studies of chalcopyrite dissolution have been carried out at alkaline pH. The key difference with an acidic medium is the insolubility of iron, which results in a layer of iron oxyhydroxides (Beckstead and Miller, 1977; Stanczyk and Rampacek, 1966). These studies showed that high agitation improved leach rates through the abrasion and removal of this layer (Figure 2.27). This is different to what is observed in the acid leaching process, where stirring has no effect or reduces the leach rate (Li et al., 2013b). For temperatures above 50°C and pressures above 690 kPa, dissolution rates were comparable to other copper minerals.

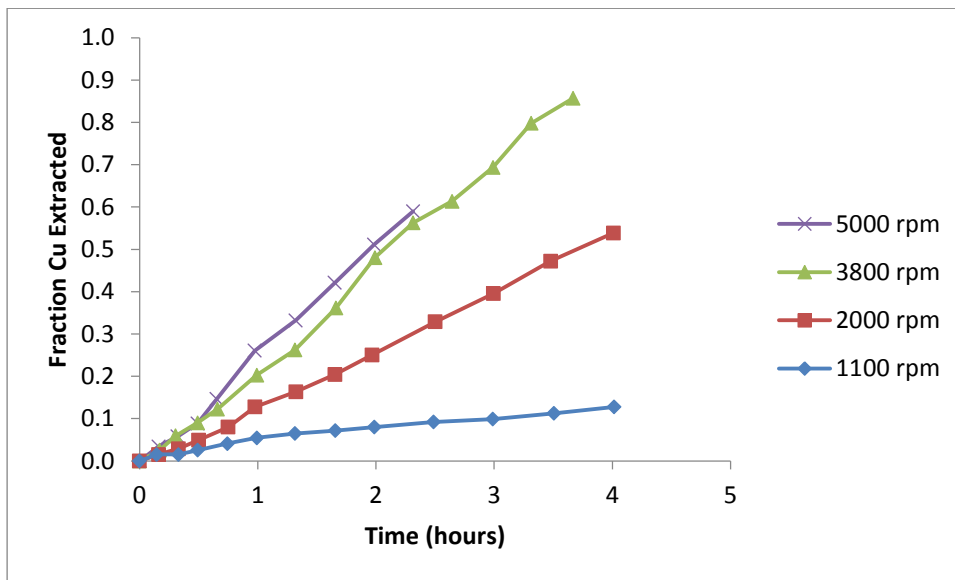


Figure 2.27: Effect of agitation on leach rates in alkaline ammonia solutions (Beckstead and Miller, 1977).

Some authors have mentioned the porosity of the iron oxyhydroxide layer and suggested that it is not expected to have a major effect on chalcopyrite dissolution rates (Burkin, 1969; Warren and Wadsworth, 1984). Warren and Wadsworth (1984) claimed that underlying the iron oxide layer is a copper deficient layer that is responsible for passivation. The idea of a metal deficient layer underlying an iron oxide coating has also been proposed in many studies of flotation at alkaline pH (Wills, 2015). These underlayers don't seem to cause any detrimental effects with collector attachment and flotation, suggesting they are a reactive species.

The need for a passivation model in alkaline systems seems superfluous when electrochemical experiments are examined. In alkaline solutions with a complexing agent, the apparent passivating effect that is observed in the acid range is notably absent. This can be seen in the anodic sweeps in alkaline ammonia solutions in Figure 2.28 (Warren and Wadsworth, 1984; Warren et al., 1982). Here, the current increases with applied potential. By contrast, in sulfuric acid solution little current flows up to a potential of about 1 V (vs SHE). This lack of a passivating region has also been noted by other researchers in alkaline ammonia solutions or at pH 13 where copper is soluble (Nicol and Zhang, 2017; Yin et al., 1995).

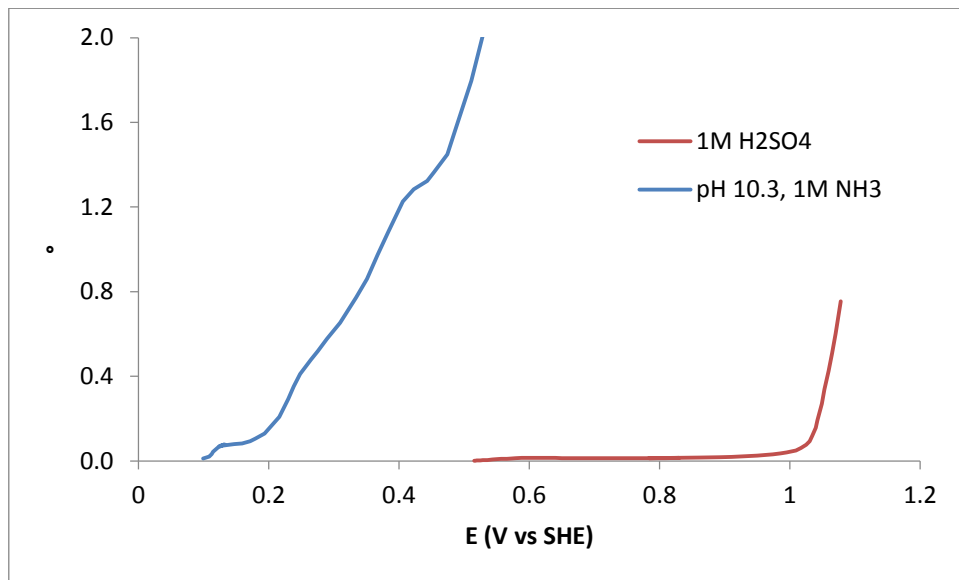


Figure 2.28: Comparison of alkaline (A) and acid (B) current potential curves. Scan rate 30 mV/minute (Warren and Wadsworth, 1984; Warren et al., 1982).

The idea of passivation layers inhibiting chalcopyrite leaching is so well accepted by some researchers that passivation is claimed even when it is clearly not observed in current potential curves. In one study it was claimed that passivation was evident even though very high anodic currents of around 4 or 5 mA cm⁻² were recorded at potentials just above the OCP (Hua et al., 2018). By comparison, “passivated” chalcopyrite typically only yields a few hundredths of a mAcm⁻². Regions labelled as passive on the current potential curve show an increase in current with potential. The authors also admitted that the leach reaction stops due to volatilisation of ammonia, which questions the need for a passivation model.

In conclusion, the slow leach rate in alkaline solutions is likely not due to any form of passivation, but due to the lack of a sufficient oxidant. Studies of oxygen reduction on chalcopyrite in alkaline solutions have shown that it is a poor oxidant, with copper (II) being more effective in both ammonia and glycine at alkaline pH (Moyo et al., 2015; Nicol, 2017b). Triiodide ion has also been shown to be viable as an oxidant (Guan and Han, 1997). Further research into viable oxidants is needed for alkaline systems.

2.5.10 Arguments against passivation

There are relatively few studies that argue directly against the passivation model. Dutrizac criticised the term “passivation” immediately after it was first proposed in 1978, suggesting that the consumption of fines was responsible for early high leach rates (Dutrizac, 1978). Dutrizac favoured an elemental sulfur inhibiting species, as did Klauber who argued strongly against the metal deficient sulfide and polysulfide model (Dutrizac, 1989a; Dutrizac, 1989b; Klauber, 2008). Mikhlin concluded through electrochemical and spectroscopic techniques that the surface layers measured in the passive region do not break down in the trans-passive region and so are not responsible for passivation (Mikhlin et al., 2004). Electrodes with thick surface layers showed no appreciable difference in electrochemical behaviour to a freshly abraded sample.

It has been shown that surface species formed in flow through leaching studies were not passivating (Acero et al., 2007). Surface species identified included elemental sulfur and polysulfides. Long term flow through experiments showed no decrease in copper concentration with time. It was suggested that parabolic kinetics can be caused by fine particles or by a reactive surface caused by grinding.

The most critical authors of the passivation theory have been Crundwell and co-workers (Bryson et al., 2016; Crundwell, 1988; Crundwell, 2015; Crundwell et al., 2015). These authors have shown instead how fundamental inorganic chemistry can be applied to understand the reactivity of chalcopyrite. This concept was described in the previous section, and they have also applied this to other sulfide minerals (Bryson and Crundwell, 2014; Bryson et al., 2016; Crundwell, 1988; Crundwell, 2015; Crundwell et al., 2015; Holmes and Crundwell, 2013).

2.5.11 Summary of the passivation proposals

No conclusive evidence has been put forward to demonstrate a passivating metal deficient sulfide or polysulfide layer on chalcopyrite. Klauber (2008) described the acceptance of this model as: “metal deficient phases transformed from a convenient accounting model to a belief in a physical existence”. Original proposals for the layer were tentative, using language such as “passive-like”, “thought to be an iron-deficient altered sulfide”, “postulated metal deficient pre-wave” (Biegler and Swift, 1979; Hackl et al., 1995; Parker et al., 1981; Warren et al., 1982). It should be emphasised that that this is still a tentative proposal and should not be accepted as fact.

The literature is inconsistent in describing the passive layer. It can be either a metal deficient sulfide, a metal deficient polysulfide, or these can be simply just different names for the same species (Buckley and Woods, 1984). There is no explanation of how the layer can retain the structure of chalcopyrite with the removal of metals from the lattice. The surface appears to reactivate after the removal of applied potential in electrochemistry experiments with a breakdown of the passive layer. It is not explained how the surface species measured ex situ can then be claimed as a passivating species.

Metal deficient layers have been readily observed for other minerals, such as a covellite layer on chalcocite. A similar layer is not observed for chalcopyrite, where the layer has only been inferred from XPS. Here it is inferred from a disulfide component, but that component is also present on un-leached, and therefore an un-passivated surface. Alkaline systems have also been suggested to have a passive layer – either of iron oxides or an underlayer of a metal deficient sulfide. This idea is not reflected in current-potential curves that increase from the OCP.

2.6 Glycine leaching systems

2.6.1 Introduction – alkaline leaching systems

The lack of an apparent passive region in alkaline chalcopyrite leaching systems makes it an attractive field for further study. Alkaline ammonia systems have been used for over 100 years, but have problems with volatility and environmental considerations (Benedict, 1917; Dutrizac, 1981). Recent work at Curtin University in Western Australia has demonstrated that the amino acid glycine may be an effective alternative to ammonia as a complexing agent for a range of base and precious metals. Glycine acts to form a bidentate ligand with copper at alkaline pH, allowing dissolution instead of the formation of insoluble copper oxides. Both the cupric and cuprous complexes are possible although the cupric glycinate dominates in all cases.

2.6.2 Glycine leaching

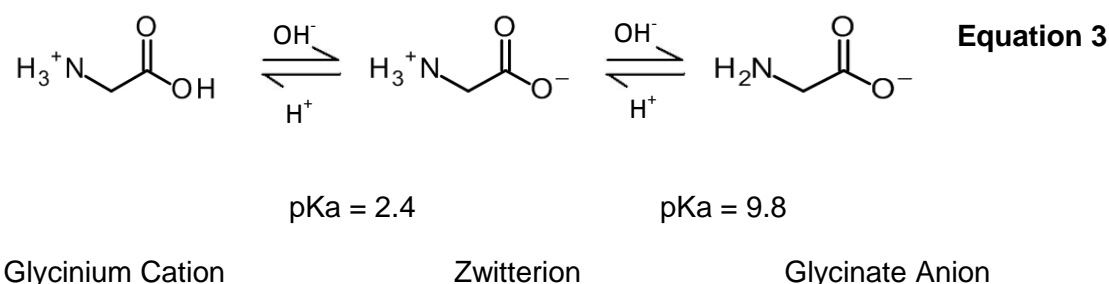
The use of glycine as a complexing agent in the alkaline leaching of copper minerals is currently being investigated at several institutions (Eksteen et al., 2017; Kuhar et al., 2018; Oraby and Eksteen, 2015; Perea and Restrepo, 2018). The most appropriate application to date appears to be for copper gold ores, where glycine can reduce cyanide consumption through the dissolution of copper minerals. Glycine has not yet been used in an industrial leaching operation, and little research has been carried out on fundamental electrochemical properties in a metallurgical context.

The simplest system for an initial review is metallic (native) copper. Although native copper is relatively rare as an ore mineral, its electrochemical properties are still of interest in extractive metallurgy for the recovery of copper from converter slag, electronic waste and from oxide and secondary sulfide deposits. These leaching operations are typically carried out at acidic pH, due to the low solubility of copper at neutral and alkaline pH in the absence of a complexing agent (Altundoğan and Tümen, 1997; Cui and Zhang, 2008; Schlesinger et al., 2011). With a complexing agent present, native copper readily dissolves at alkaline pH, such as with cyanide in gold operations.

Ammonia is a well-known example of a complexing agent for copper leaching at alkaline pH and is frequently studied (Arbiter and McNulty, 1999; Reilly and Scott, 1977; Stanczyk and Rampacek, 1966; Warren and Wadsworth, 1984; Weiss, 1976). It is yet to be proven financially viable for copper leaching, particularly for open-air applications where losses due to volatility render the process unfeasible (Dutrizac, 1981; Greenawalt, 1912; Nicol, 2017b). Volatile ammonia losses are also a problem in other industries where copper dissolution is important, such as in the preparation of integrated circuits. This has prompted fundamental studies into many alternative complexing agents such as glycine and other organic acids (Aksu and Doyle, 2001; Drissi-Daoudi et al., 2003; Halpern et al., 1959; Keenan et al., 1976). These studies did not explore in depth the conditions that enhance copper dissolution for a metallurgical application such as the effects of temperature or the higher concentrations of glycine expected to be used in a copper leaching environment. These are gaps that need to be addressed to understand the fundamentals of the copper-glycine system.

2.6.3 Properties of glycine

Like other amino acids, glycine is an amphoteric molecule. Its neutral form is the zwitterion, which has a positive charge on the amine group and a negative charge on the carboxyl group to give an overall neutral charge. It can gain a proton to form a cation or lose a proton by reaction with hydroxyl to form an anion as shown in Equation 3 (Streitwieser and Heathcock, 1985).



For the purpose of this study, the term “glycine” will refer to the sum of the zwitterion and glycinate anion in solution. The terms “zwitterion” and “glycinate” will refer to these species specifically. Glycinium was not present at the alkaline pH used for this study.

Several authors report that the glycinate anion concentration is strongly correlated to copper dissolution at alkaline pH (Aksu and Doyle, 2001; Halpern et al., 1959; Keenan et al., 1976; Pearlmutter and Stuehr, 1968). The ratio of glycinate to zwitterion increases with pH and is determined from the pKa and pH as shown by Equation 4. The glycinate form dominates when the pH is greater than the pKa.

$$\log\{\text{Gly}^-\} / \{\text{HGly}\} = \text{pH} - \text{pKa} \quad \text{Equation 4}$$

Where: “HGly” designates the glycine zwitterion and “Gly⁻” the glycinate anion.

Experimental data indicate that the pKa of glycine decreases linearly with increasing temperature, it is 9.8 at 25°C and 9.0 at 60°C (Izatt et al., 1992). The variation of the glycinate mole fraction with pH for different temperatures according to Equation 4 is shown in Figure 2.29. Higher temperatures and pH are favourable for the glycinate ion formation.

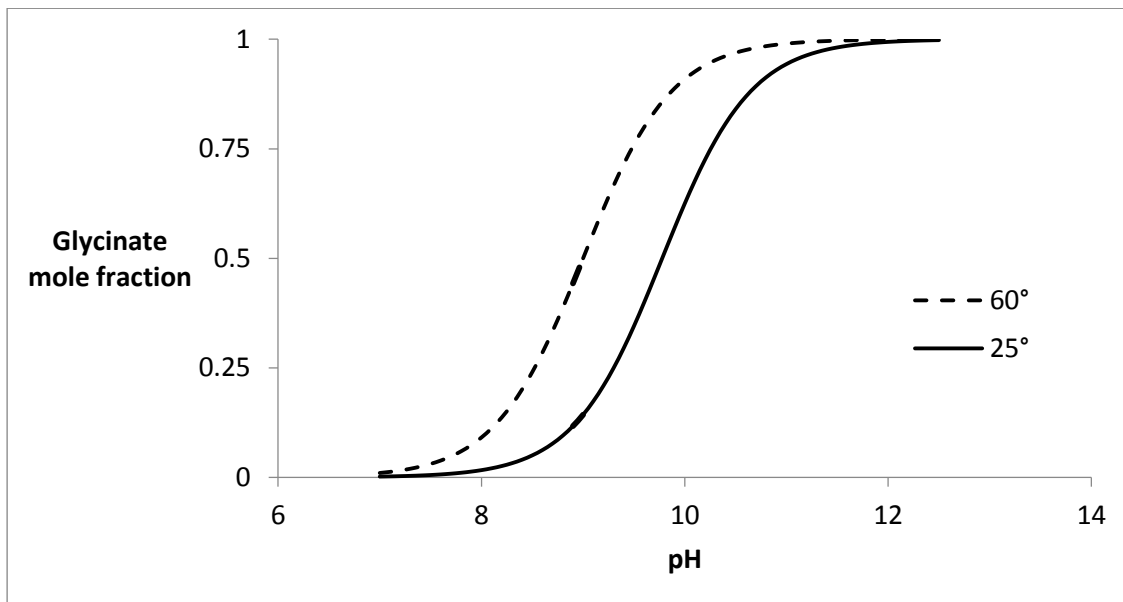
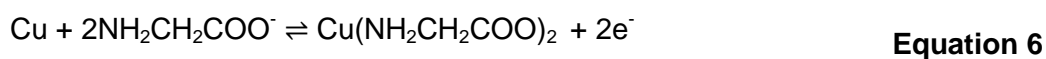


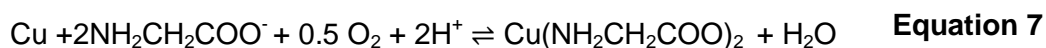
Figure 2.29 Variation of the glycinate ion mole fraction with pH at 25°C and 60°C

2.6.4 Glycine reactions with copper

The thermodynamics of the copper-glycine aqueous system are extensively described in the literature (Aksu and Doyle, 2001; Patri et al., 2006; Tamilmani et al., 2002). The essential aspects as applied to the metallurgical leaching of copper are described in this section. The half-reactions for copper dissolution are shown in Equations 5 and 6.

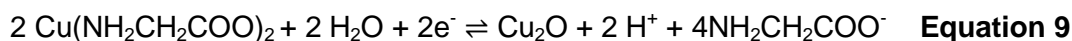
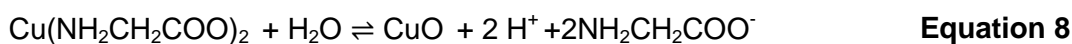


Combining these results in the overall reaction for copper dissolution according to Equation 7.



Unlike the amino and cyanide complexes, the glycinate complex of cupric copper is neutral.

Changes in pH at the copper surface resulting from Equation 5 can be countered by the buffering action of excess zwitterion in solution, as per Equation 3. At low zwitterion concentrations where buffering capability is limited, the equilibrium between copper oxides and copper glycinate can be established as in Equations 8 and 9.



At pH values greater than 11, the zwitterion concentration effectively reduces to zero as shown in Figure 2.29. Above this pH, the ability to buffer the solution is lost and the equilibria of Equation 8 and Equation 9 are driven to the right to favour CuO and Cu₂O. These species occupy and block active surface sites and will slow the dissolution of copper. They are insoluble and may thicken and eventually passivate the copper surface as a duplex layer through a complex series of nucleation and precipitation steps (De Chialvo et al., 1984; Kunze et al., 2004; Speckmann et al., 1985; Strehblow et al., 2001). When glycinate is in excess over copper in solution, copper (II) glycinate can be reduced to copper (I) glycinate as per Equation 10 with a standard reduction potential of -0.167 V (vs SHE) (Aksu and Doyle, 2001; Drissi-Daoudi et al., 2003; Tamilmani et al., 2002). Metallic copper at the surface is oxidised in the process.



This cuprous species can be oxidised back to copper (II) glycinate by oxygen in solution and is then available for further oxidation of the copper surface. This process has the potential to enhance copper dissolution and is well known as autocatalytic corrosion (Habashi, 1965).

Temperature also has a major effect as can be seen in the Pourbaix diagrams for 25°C and 60°C as shown in Figure 2.30. These were created from the thermodynamic database within Outotec HSC Chemistry software (HSC Chemistry Version 8.1.4, 2015). At higher temperatures, the stability region for copper glycinate contracts considerably. While this is unfavourable for leaching, it is countered to a degree by the lowering of the pKa to 9.0 for glycine/glycinate, making high-temperature leaching feasible at lower pH.

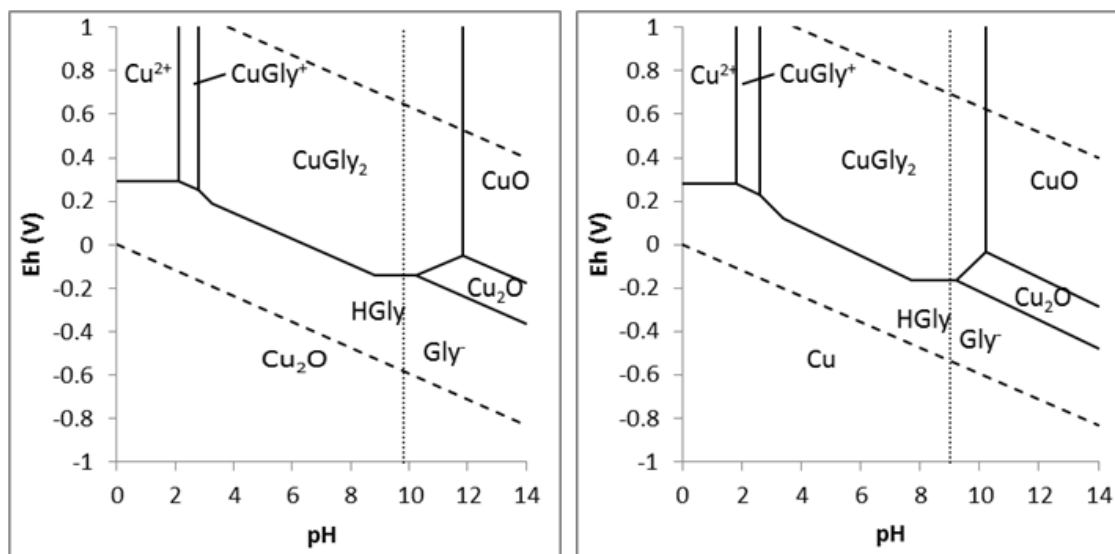


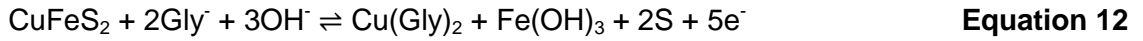
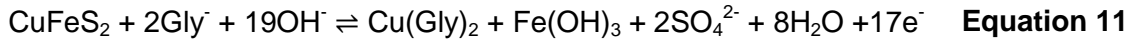
Figure 2.30: Eh-pH diagrams for the copper-glycine system at 25°C (left) and 60°C (right).

2.6.5 Passivation of Copper Metal

Passivation of metals occurs as a direct oxidation of the metal surface in the absence of acid or a complexing agent (Habashi, 1965). In the case of copper metal, the passivating species has been shown to be a duplex layer of CuO and Cu₂O (De Chialvo et al., 1984; Kunze et al., 2004; Speckmann et al., 1985; Strehblow et al., 2001). In the presence of a complexing agent such as glycine, the effect of copper passivation is minimised, but has been shown to occur at pH values greater than 11 with a passivation potential dependent on glycine concentration (Aksu and Doyle, 2001; Skrypnikova et al., 2008; Tripathi et al., 2009). These studies were conducted with a glycine concentration less than 0.1 M, but for metallurgical applications, the passivation effect needs to be investigated in unstirred solutions and at higher concentrations of glycine that are expected for a leaching process (Eksteen et al., 2017; Oraby and Eksteen, 2014). This research will also provide a background for future studies on the passivation of copper minerals, which are sometimes claimed to behave as metal with a passivating oxide layer (Nicol, 2017c).

2.6.6 Glycine reactions with Chalcopyrite

The chemistry of the glycine chalcopyrite system is still relatively unstudied. The anodic dissolution of chalcopyrite in glycine solutions may form elemental sulfur or sulfate by the following half reactions:



Other iron species such as FeOOH , Fe_2O_3 or Fe_3O_4 may also form in alkaline solutions and are collectively referred to as iron oxyhydroxides (Grano et al., 1997). Other sulfur species such as thiosulfate may also form and will be the topic of further research. Chalcopyrite dissolves much slower than supergene and copper oxide minerals in glycine solutions (Eksteen et al., 2017; Tanda et al., 2017). This is also true for a variety of leaching systems in the acidic pH range and in alkaline solutions with ammonia or cyanide as complexing agents (Marsden, 2006; Razzell and Trussell, 1963; Stanczyk and Rampacek, 1966; Watling, 2013). Such slow rates of dissolution have prevented the development of a financially viable hydrometallurgical process for copper leaching from chalcopyrite.

The Eh-pH diagram (Figure 2.31) for chalcopyrite is similar to that for the copper glycine system. At high pH, copper oxides are favoured over the copper-glycinate complex. This region expands at high temperatures, suggesting that lower pH should be used at high temperatures. The position of the conduction and valence bands are superimposed to show the favoured potentials for leaching. The region between these lines would be expected to have slow kinetics for an ideal chalcopyrite semiconductor.

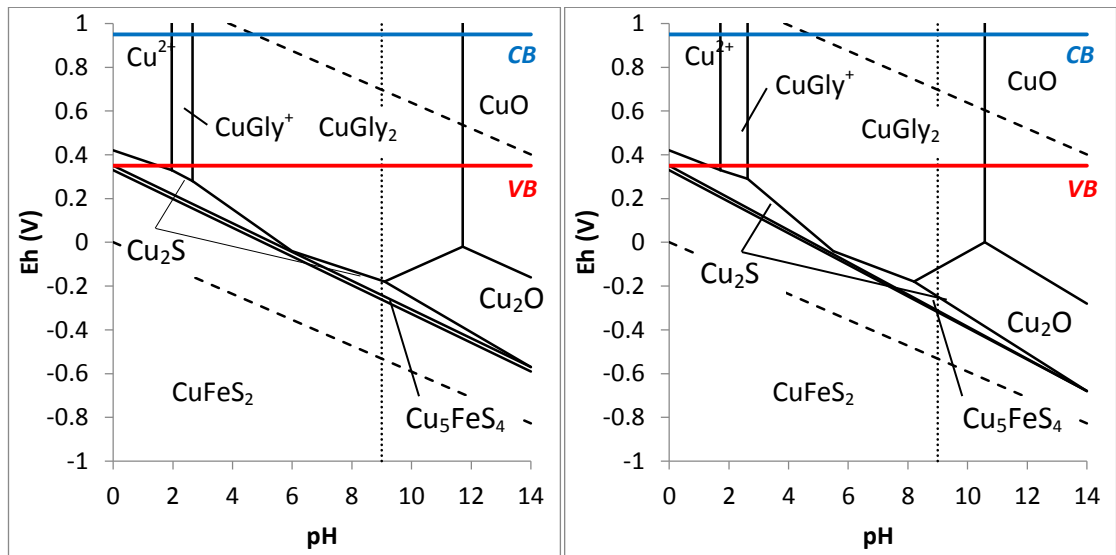
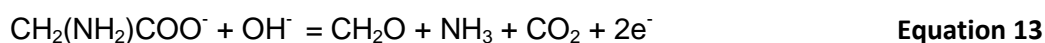


Figure 2.31: Eh-pH diagrams for chalcopyrite at 25°C, left and 60°C, right. The relative positions of the valence and conduction bands are labelled “VB” and “CB” respectively.

2.6.7 Oxidation of glycine

The oxidation of complexing agents as a side reaction has been a topic of interest in the electrochemical study of some metal-ligand systems, particularly for gold-thiosulfate (Breuer and Jeffrey, 2002; Zhang and Nicol, 2003). These side reactions can yield a significant current response resulting in an overestimation of the corrosion current (i_{corr}) in electrochemical studies. From a practical standpoint if the complexing agent is consumed it raises the costs of an operation by reducing the ability to recycle the reagent (Konishi et al., 1991). For the glycine system, oxidation reportedly occurs at relatively high potentials of around 0.8 to 1.1 V (vs Ag/AgCl) at pH values of 12 to 13 (Marangoni et al., 1989; Ogura et al., 1998; Skrypnikova et al., 2011). The oxidation products of glycine are reported to be formaldehyde, ammonia and carbon dioxide as shown in Equation 13:



It is important to acknowledge this reaction if oxidising agents are to be considered at an industrial scale.

2.7 Oxidants for chalcopyrite-glycine system

Parker et al (1981) identified several potential oxidants for chalcopyrite in their electrochemical work. While these have been shown to be effective, many of the stronger oxidants would likely destroy glycine if attempted. This is well-known in the treatment of municipal water with hypochlorite. Two oxidants with lower oxidising potential are ferricyanide and the triiodide ion. These have standard potentials of 0.35 V (vs SHE) and 0.54 V (vs SHE) respectively and have been discussed in previous studies (Crundwell, 1988).

Little work has been carried out with these oxidants with respect to chalcopyrite leaching. Ferricyanide has been shown to leach chalcopyrite readily as a side reaction in its application for silver leaching (Xie and Dreisinger, 2007). The triiodide ion has been used in one study with ammonia as a lixiviant at alkaline pH (Guan and Han, 1997). These authors identified the need for a suitable oxidant for chalcopyrite leaching and selected triiodide for its ease of recycling in a leaching system. A rotating disk was used to measure the extraction of copper in terms of moles/cm² with various concentrations of iodine and pH. It is difficult to judge the performance of this system in isolation. A comparison with acid systems found in the literature shows that leaching with triiodide is relatively fast (Figure 2.32). Allowances must be made for differences in methodology, but this does warrant further investigation.

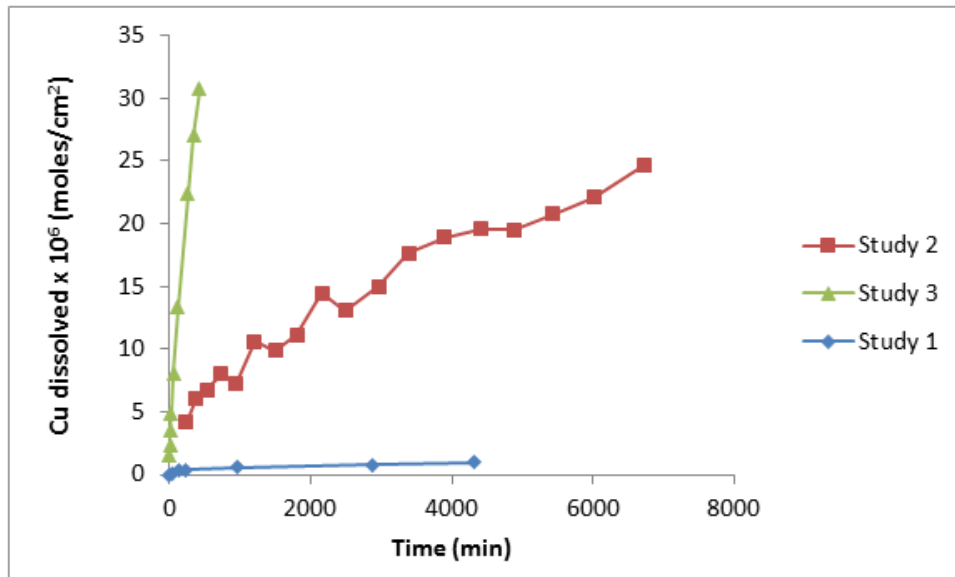


Figure 2.32: Comparison of alkaline iodide-ammonia leaching with ferric sulfate acid leaching. Study 1: 0.1 M Fe³⁺, pH 1, 25°C (Ammou-Chokroum et al., 1977); Study 2: 0.1 M Fe³⁺, 0.1 M H₂SO₄ 75°C (Dutrizac et al., 1969); Study 3: 2M NH₃, pH 9.8, I₂ 0.005 M, 25°C (Guan and Han, 1997).

2.8 Conclusion

Chalcopyrite leach rates are known to be slower than for other copper minerals in a variety of leaching systems. Many fundamental studies have been carried out in an attempt to identify the reasons for this with the aim of identifying a viable leaching process. The majority of these studies have proposed an inhibiting layer that is often termed “passivating”. This term is used tentatively by many researchers due to it having little resemblance to the well-known process in corrosion science.

The inhibiting layer is often described as being an extremely thin metal deficient sulfide or polysulfide. This layer has never been measured directly, unlike other metal deficient layers such as copper deficient species on chalcocite. Instead it has only been inferred from XPS by the presence of a disulfide component in the sulfur peak. The nature of this layer, such as whether it is a sulfide or polysulfide, or if the layer breaks down in an electrochemical system upon removal of potential shows wide disagreement.

It has been shown that the fundamental electronic structure of chalcopyrite can explain the leaching behaviour. The mineral is a natural n-type semiconductor with a band gap that corresponds to the standard potential of common redox couples such as ferric/ferrous. Leaching will be slow with such couples, but has been shown to be faster with couples that have a standard potential outside the band gap. This proposal is disregarded by some authors who assume that natural impurities can “dope” the mineral, causing it to become a degenerate semiconductor and behave more like a metal.

The questions of passivation and the influence of the electronic structure on the leaching of chalcopyrite in alkaline glycine solutions will be addressed in this research. The electrochemical behaviour of metallic copper will be compared to semiconducting chalcopyrite to determine if natural chalcopyrite's behaviour does resemble metallic behaviour. The surface species on chalcopyrite electrodes held at various oxidising potentials will be compared with the current density to determine any passivating effects. Leaching of chalcopyrite with oxidants that have a standard potential both inside and outside the band gap will be conducted to complement electrochemistry with leaching of a chalcopyrite concentrate.

Chapter 3 Electrochemical Behaviour of Copper in Alkaline Glycine Solutions

3.1 Introduction

Alkaline glycine leaching of base and precious metals is a new technology and fundamental aspects are still to be explored. The simplest system for an initial study is metallic copper, which is free from complications that may be caused by iron and sulfur in a natural chalcopyrite mineral sample. Native copper has a small but significant occurrence in supergene oxide and sulfide deposits, and its properties are also of interest for its recovery from electronic waste and converter slag.

Fundamental studies of copper metal dissolution using complexing agents for such as glycine and other amino acids have been carried out for other processes such as for the preparation of integrated circuits. (Aksu and Doyle, 2001; Drissi-Daoudi et al., 2003; Halpern et al., 1959; Keenan et al., 1976). These studies did not explore in depth the conditions that enhance copper dissolution for a metallurgical application such as the effects of temperature or the higher concentrations of glycine expected to be used in a copper leaching environment. This chapter will address these gaps, as well as the relevance of passivation and glycine degradation through oxidation for a leaching operation.

An additional reason to study metallic copper is to establish a baseline of electrochemical behaviour for comparison to semiconducting chalcopyrite. Natural chalcopyrite is said to contain impurities that can render the semiconductor degenerate, meaning that it has metal-like properties and the semiconductor approach is irrelevant (Nicol et al., 2016). By establishing an understanding of copper metal behaviour in alkaline glycine solutions in this chapter, comparisons can be made with the proposed degenerate behaviour of chalcopyrite.

The objectives of this chapter are to:

- Compare the electrochemical behaviour of copper in alkaline glycine solutions with previous studies, and extend the conditions studies to higher temperatures and concentrations.

- Establish the conditions under which passivation in glycine solutions will occur.
- Study the capacitance of the metal-solution interface for later comparison to a semiconductor-solution interface.
- Examine the surface with Raman spectroscopy for evidence of a surface layer.

3.2 Experimental

3.2.1 Potentiodynamic polarisation

All electrochemical tests were carried out using a Bio-logic VMP3 potentiostat. The working electrode was a static copper (99.99%) sample embedded in epoxy resin with an exposed surface area of 1.16 cm². Test solutions were made from analytical grade glycine (99%, Sigma Aldrich) and sodium hydroxide (98%, Sigma Aldrich) using Mili-Q deionised water with a resistivity of 18.2 MΩ.cm.

The working electrode was progressively polished to 1200 grit SiC paper, washed and immediately placed in the test solution. For these experiments the solution was agitated with a magnetic stirrer, the speed was adjusted by manual control to 600 rpm and the temperature adjusted to target within ± 1°C accuracy.

The experiments were carried out in a three-electrode electrochemical cell with a working volume of 150 mL. The reference electrode was single junction Ag/AgCl (3.5 M) held in a Luggin capillary placed close to the working electrode to minimize any error due to iR drop. The same distance was maintained between the reference and working electrodes for all tests. The counter electrode was platinum-coated titanium mesh or Hastelloy C.

Potentiodynamic polarisation tests were conducted ten minutes after immersion of the working electrode in the test solution to allow stabilisation of the open circuit potential (OCP). A potential range of ± 0.250 V vs. the OCP at a sweep rate of 0.1667 mV/s was employed (ASTM, 2014). The corrosion current, i_{corr} was estimated from the linear polarisation resistance at ± 25 mV from the OCP, using the Stern – Geary relationship shown in Equation 14:

$$i_{\text{corr}} = \frac{\beta_a \cdot \beta_c}{2.303(\beta_a + \beta_c) R_p}$$

Equation 14

where β_a and β_c are the anodic and cathodic Tafel slopes and R_p is the polarisation resistance. Tafel slopes of 0.12 V were used in this study based on a charge transfer coefficient of 0.5 for typical metal solution interfaces (Crundwell, 2013; Free, 2013). This approach has been shown to be useful for screening experiments to reveal trends in corrosion and extractive metallurgy (Silverman, 2011).

Confidence intervals were determined according to Equation 15 (Napier-Munn, 2014).

$$CI = t \pm \frac{s}{\sqrt{n}} \quad \text{Equation 15}$$

Where CI is the confidence interval, s is the sample standard deviation, t is the t-value for a 95% confidence interval and n is the sample size.

The variation in passivation behaviour with pH was measured with the same cell arrangement as the potentiodynamic polarisation tests. The scan was started at the OCP, with a scan rate of 1 mVs⁻¹ and terminated at 1.05 V (vs SHE) in quiescent solutions. The effect of disk rotation on passivation was measured at pH 12 with the setup described in the next section.

3.2.2 Evans diagrams and diffusion study

A rotating copper disk electrode with an area of 0.3 cm² was used with a larger cell of 500 mL in order to accommodate the rotation mechanism for these experiments. For the anodic scans, the solution was sparged with 99.99% nitrogen for 1 hour prior to testing to remove dissolved oxygen. The scan was then carried out under a nitrogen atmosphere. For the cathodic scan, the solution was sparged with air for 30 minutes to achieve a constant dissolved oxygen level of 8.6 ± 0.2 ppm for all tests. 0.1 M sodium sulfate (>99%, Sigma Aldrich) was used as a supporting electrolyte to boost the solution conductivity for the cathodic scans and to counter the effects of ion migration (Luo et al., 1997; Prasanna Venkatesh and Ramanathan, 2010). Copper glycinate reduction was analysed by dissolving copper sulfate in glycine solutions. Separate anodic and cathodic scans were carried out starting from the OCP at a scan rate of 1 mVs⁻¹. The anodic scan terminated at 0.100 V with respect to the OCP, the cathodic scan terminated at -0.500 V with respect to the OCP.

3.2.3 Staircase Potential Step and Capacitance

A staircase potential sweep measurement was carried out with 40 steps from the OCP to 1.0 V (vs SHE). Each step was held for 20 minutes with the current recorded, followed by capacitance measurements at 1 to 100 kHz with a sinus amplitude of 17 mV. Capacitance measurements recorded with a frequency of 1 kHz are reported here.

3.2.4 Raman spectroscopy

A Labram 1B dispersive Raman spectrometer with a 632.817 nm source and 2mW power was used to determine the presence of surface species. IR spectra were collected with a Nicolet iN10 MX infrared microscope, but since the surface showed no IR active species the spectra are not presented here.

3.2.5 Cyclic voltammetry

A glassy carbon electrode with a surface area of 0.3 cm² was used to measure the oxidation of glycine and copper glycinate complex in quiescent solutions. Copper sulfate (99% Sigma Aldrich) was added at 0.08 M to assess the oxidation of the copper glycinate complex. Cyclic voltammetry was used at 10 to 100 mV/s. The potential window was between -0.3 V relative to the OCP and 2.7 V (vs SHE), starting with the anodic scan and finishing at the open circuit potential.

3.3 Results and Discussion

3.3.1 Conditions for optimal copper dissolution

A series of potentiodynamic polarisation experiments were carried out at pH 9.0, 10.0, 10.5 and 11.5, at temperatures of 22°C and 60°C and glycine concentrations of 0.1 M and 0.3 M. Some examples of these measurements showing the effects of pH, temperature and glycine concentration can be seen in the voltamograms in Figure 3.1.

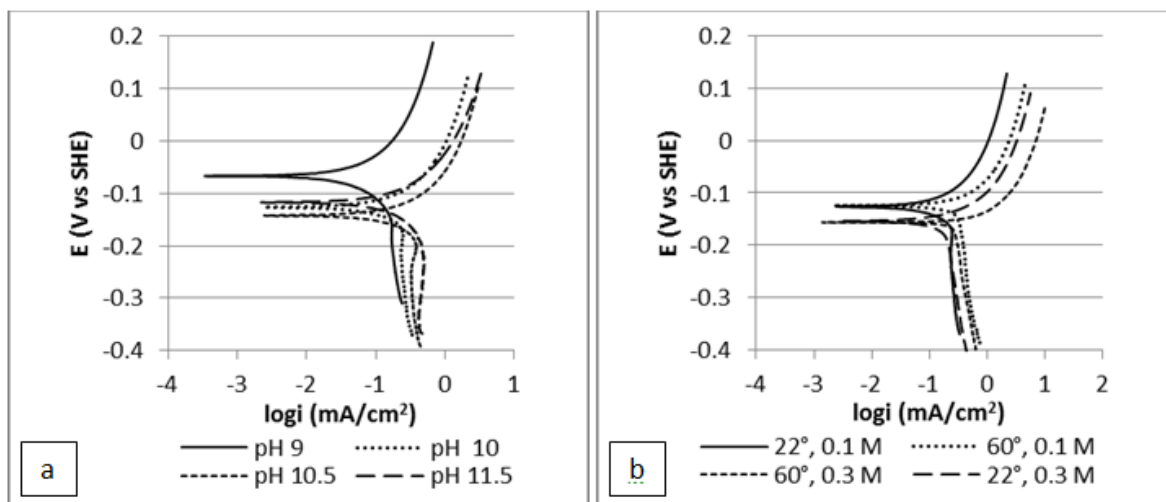


Figure 3.1: Potentiodynamic polarisation curves: (a) effect of pH at 22°C and 0.1 M glycine. (b) Effect of temperature and concentration of glycine at pH 10.

A summary of electrochemical parameters calculated from these curves is presented in Figure 3.2. The corrosion current, i_{corr} , has a distinct maximum at pH 10.0 at 60°C and 10.5 at 22°C. Above this pH, i_{corr} values generally level off or drop in value. This is consistent with the increase in glycinate mole fraction with pH and temperature, and the thermodynamic prediction of oxide formation at higher pH. This trend is in agreement with ambient temperature studies (Aksu and Doyle, 2001) and shows that it extends to higher temperatures and glycine concentrations. The pronounced i_{corr} peak for 0.3 M glycine at 60°C suggests an interaction effect between these factors.

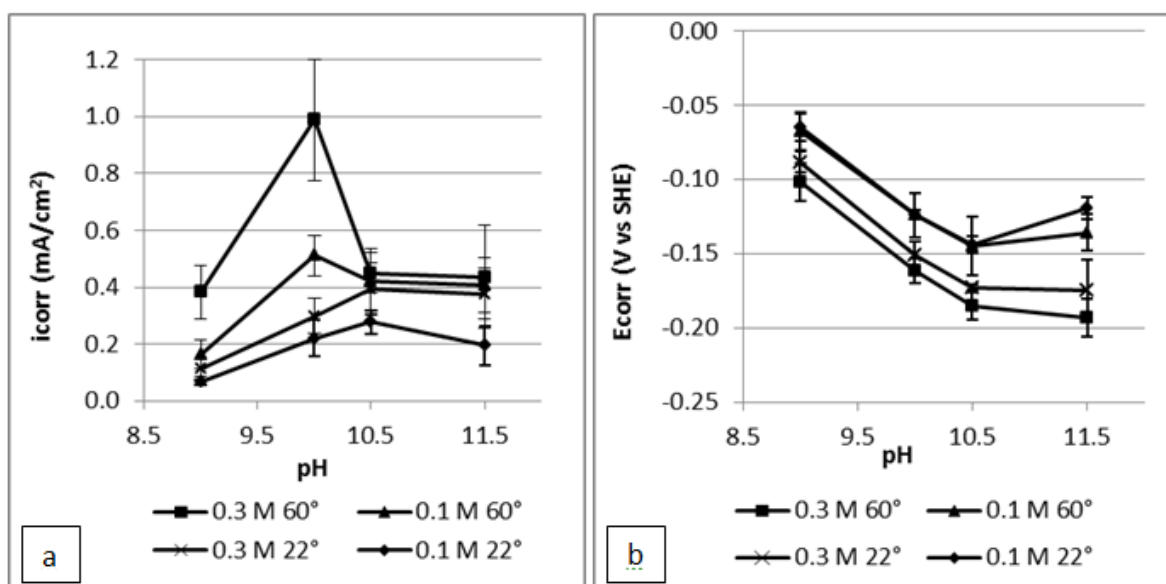


Figure 3.2: (a) Variation of i_{corr} with pH. (b) Variation of E_{corr} with pH.

The E_{corr} decreases with pH from 9.0 to 10.5 and as glycine increases from 0.1 to 0.3 M. It levels off or rises slightly between 10.5 and 11.5, likely due to the formation of surface oxide species. Temperature has little overall effect on the E_{corr} , possibly due to it affecting both anodic and cathodic reactions as discussed in the next section.

3.3.2 Evans Diagrams

The observations in the preceding section were investigated further by using a rotating disk electrode and observing the anodic and cathodic reactions in isolation. Parameters studied were rotation speed, glycine concentration and temperature. Rotation speed had no effect on the anodic curves as shown in Figure 3.3. The cathodic scans were influenced by mass transport of O_2 at low rotation speeds, with the curve at 250 rpm returning significantly lower current densities than those at higher rotation speed.

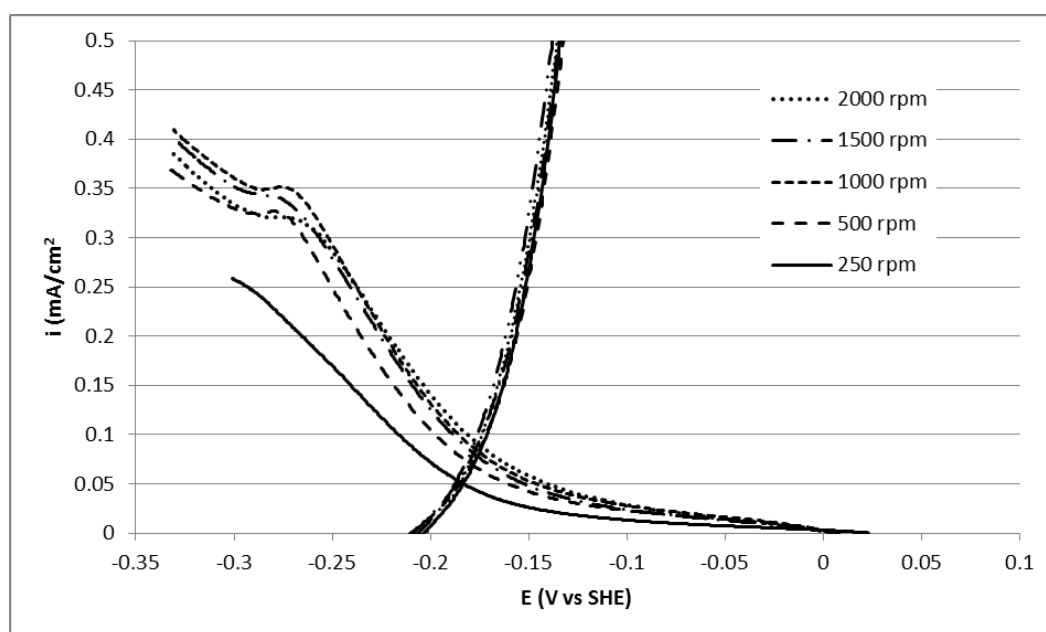


Figure 3.3: Effect of rotation speed (rpm) on anodic and cathodic scans in solutions of 0.3 M glycine at 25°C at pH 10.

The effect of concentration and temperature on the anodic and cathodic curves can be seen in Figure 3.4. Increasing the glycine concentration shifts the anodic curve to more negative values, resulting in a lower E_{corr} and a higher i_{corr} . Increasing the temperature shifts the cathodic curve positive and the anodic curve negative. At 60°C, the curves cross in a steep section of the cathodic curve, meaning a small variation in glycine concentration results in a large change in the i_{corr} .

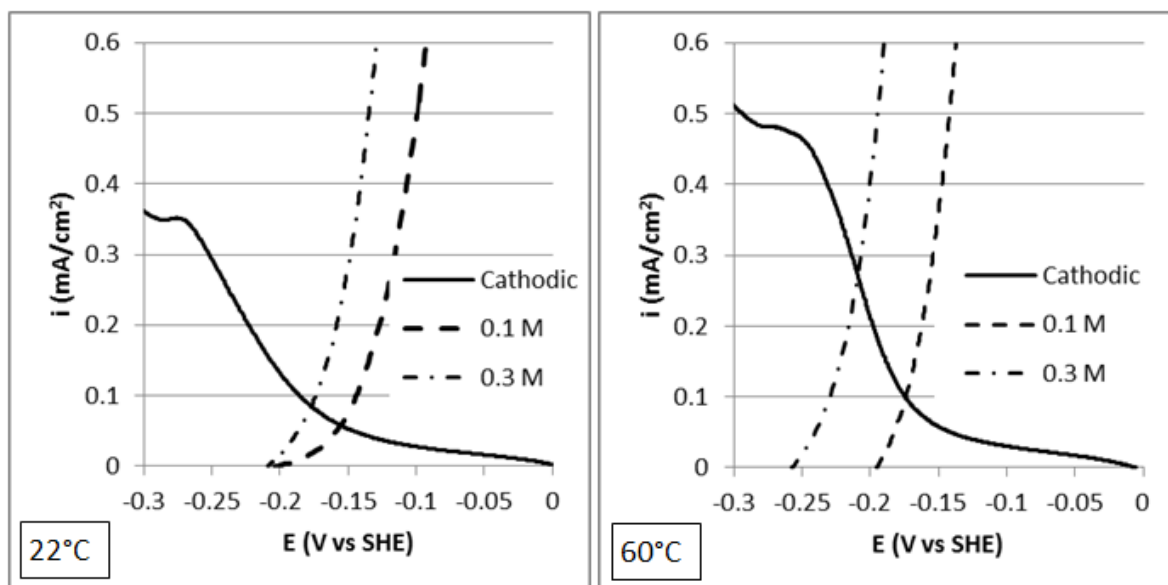


Figure 3.4: Effect of glycine concentration on the anodic curves at 22°C, left and 60°C, right, with a superimposed cathodic curve in a glycine-free solution. Rotation rate 1000 rpm and pH 10.

The trends in these diagrams are consistent with Figure 3.2, but i_{corr} values at the intersection of the anodic and cathodic curves are significantly lower. This may be simply due to the arbitrary use of 120 mV for the Tafel slopes in calculations of i_{corr} , or because glycine was not present for the generation of the cathodic curves when it may in reality contribute to the cathodic current. To clarify this, cathodic curves were generated for the reduction of both glycine and for copper glycinate which may be present during potentiodynamic polarisation due to the dissolution of copper near the OCP.

Copper (II) glycinate was formed in solution by adding CuSO_4 to excess glycine (Drissi-Daoudi et al., 2003). The cupric glycinate reduction can be seen in the cathodic curves shown in Figure 3.5. Glycine alone showed no significant difference in the i_{corr} over oxygen, but the addition of cupric ions showed increasing cathodic currents, particularly at 60°C. The i_{corr} values from Figure 3.5 range from 0.2 to 0.3 mAcm^{-2} at 22°C and 0.8 to 1.4 mAcm^{-2} at 60°C and are in the range of the values calculated from potentiodynamic polarisation. These results suggest that the two half reactions are not completely independent of each other as has been shown in other systems (Robertson et al., 2005). These results also show that the copper (II) glycinate complex may be effective as an oxidant in an autocatalytic process (Habashi, 1965).

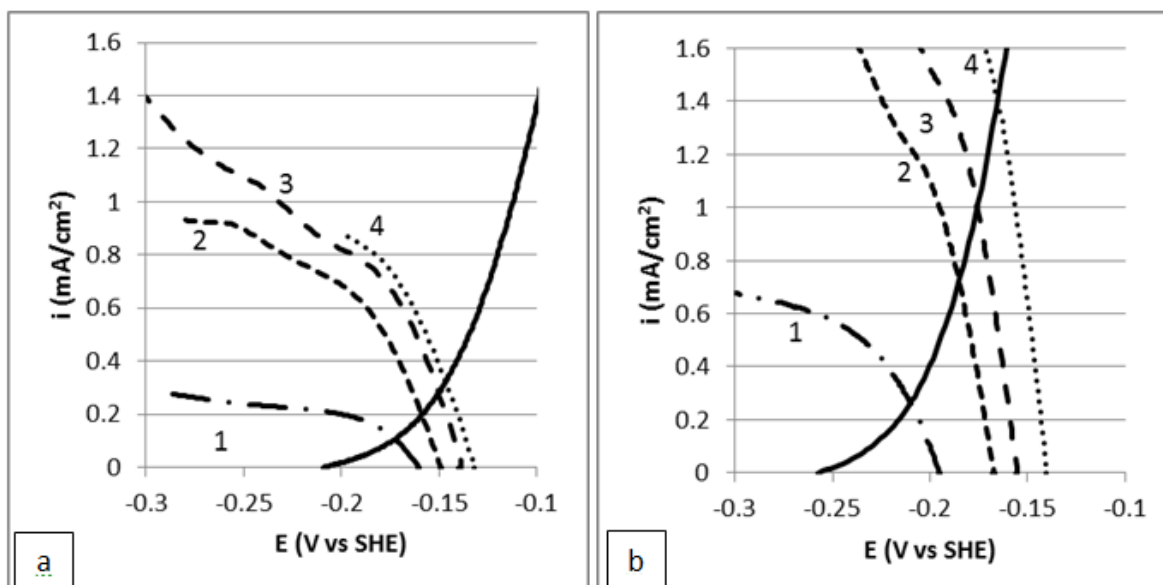


Figure 3.5: Cathodic reduction of aerated pH 10 glycine/copper sulfate mixture at (a) 22°C, (b) 60°C. Solutions of 0.3 M glycine with: 1) 0 M CuSO₄; 2) 0.001 M CuSO₄; 3) 0.002 M CuSO₄; 4) 0.004 M CuSO₄. The anodic scan was obtained from a de-aerated solution.

3.3.3 Passivation

Passivation of the copper surface was only observed at pH 11.0 and 12.0. The passivation potential was dependant on pH, being about 0.5 V (vs SHE) for pH 12 and 0.8 V (vs SHE) for pH 11 as shown in Figure 3.6. This trend is consistent with work by other researchers on the copper-glycine system under similar conditions (Aksu and Doyle, 2001; Skrypnikova et al., 2008; Tripathi et al., 2009). The variation with pH is expected from the thermodynamics summarised in the Eh-pH diagram in Figure 2.30, and if localised depletion of glycine at the surface is considered.

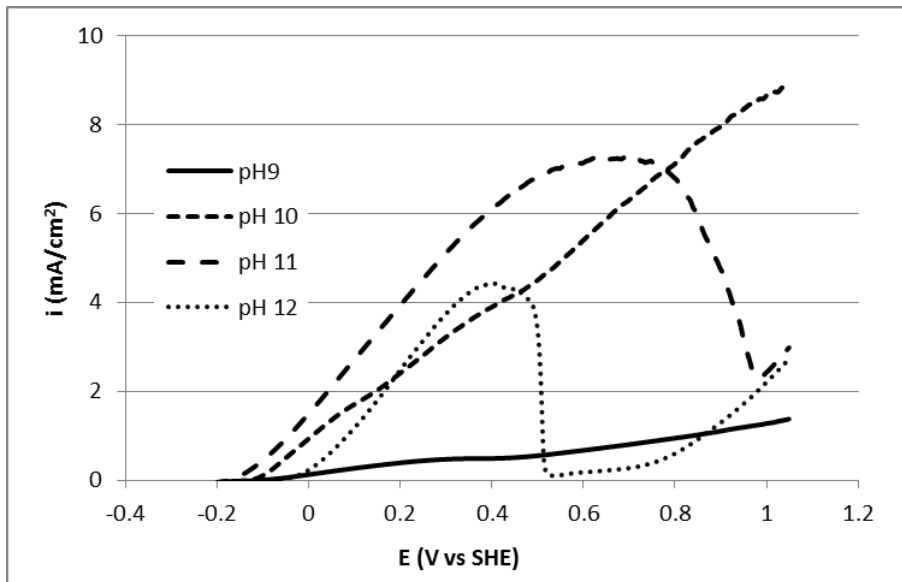


Figure 3.6: Static electrode showing passivation of copper at pH 11 and 12 in 0.1 M glycine.

Using the rotating disc electrode (RDE) gave a slightly lower passivation potential of 0.4 V (vs SHE) under quiescent conditions as shown by the solid line in Figure 3.7. Rotating the electrode had a significant effect, even at a very slow rate of 60 rpm. Passivation was shifted to higher potentials with increasing rotation rate. This is likely due to the increased flux of glycine to the metal surface and prevention of oxide formation by Equations 8 and 9.

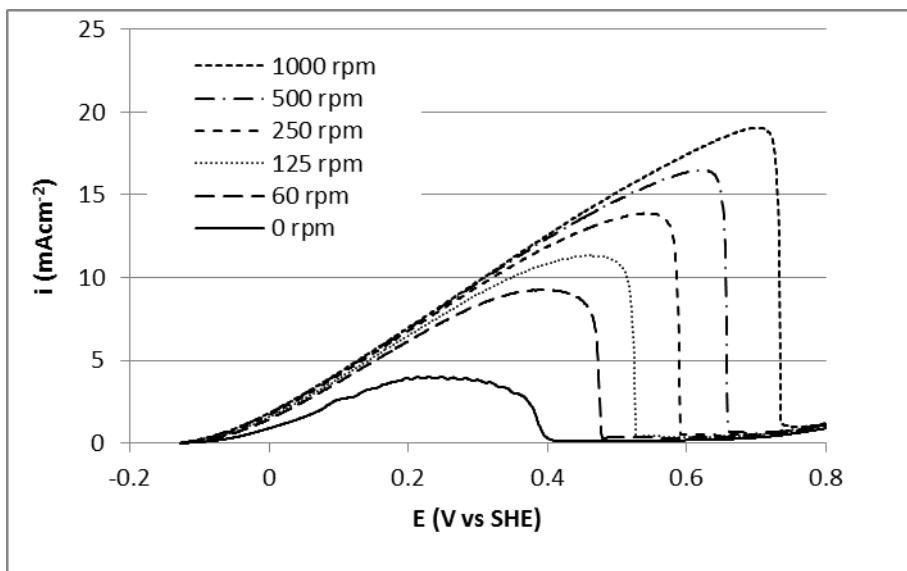


Figure 3.7: Passivation of RDE at pH 12 and 0.1 M glycine showing the effect of rotation speed.

The passive region was investigated further with successive chronoamperometry tests at 0.5 V (vs SHE). Rest periods at the OCP of 30 s and 60 s were included as shown in Figure 3.8. The surface shows a reactivation during the rest periods. When the potential is re-applied, high currents were briefly observed before rapidly decaying to a low steady state. The rotation mechanism was turned on at 400 s during a period of passivation at 1000 rpm, after which no measurable change in current was observed. This suggests a stable coherent passive layer on the copper surface. After the sample was allowed to rest a final time at the OCP with the disk still rotating at 1000 rpm, the last current decay curve maintained a high current of about 15 mAcm^{-2} with no passivation evident. Rotation at 1000 rpm allowed sufficient transport of glycine to the surface and continued dissolution.

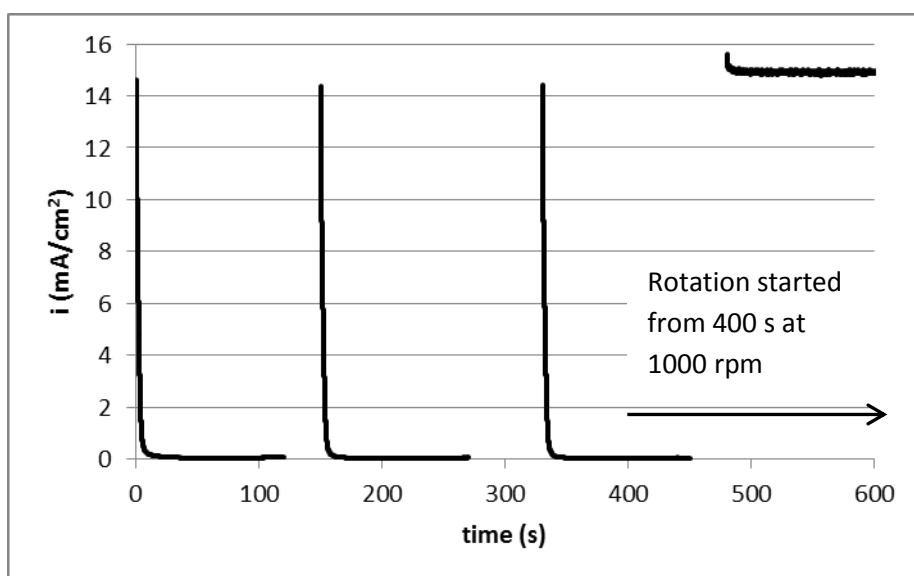


Figure 3.8: Current decay curves in solutions of 0.1 M glycine at pH 12 held at 0.5 V (vs SHE).

3.3.4 Staircase Potential Step and capacitance measurements

Interfacial capacitance measurements are known for describing an oxidised copper surface, represented by two capacitors in series (Grdeń, 2014). These capacitances are generated across the Helmholtz double layer at the electrode-solution interface, and if present, across an oxide layer. The capacitance decreases as this layer thickens and the separation between the opposing charges grows as predicted by the parallel plate model (Bard and Faulkner, 2001). For copper, the oxide layer is a duplex of CuO and Cu₂O. It is a semiconductor, usually p-type, but can be n-type in the early stages of oxidation (Ganzha et al., 2011). Useful values for semiconducting properties of a passive layer from Mott Schottky measurements require long oxidation times to form a thick stable passive layer (Grdeń, 2014). In this study, a qualitative approach was used to compare passive and non-passive surfaces over the relatively short times used.

Non-passivating conditions were observed with 0.3 M glycine at pH 10.5 and a rotation speed of 1000 rpm. Both current and capacitance increase linearly with potential as shown in Figure 3.9. This linear increase of current and capacitance at each potential step suggest Ohmic behaviour, with no significant interference from passivating layer formation.

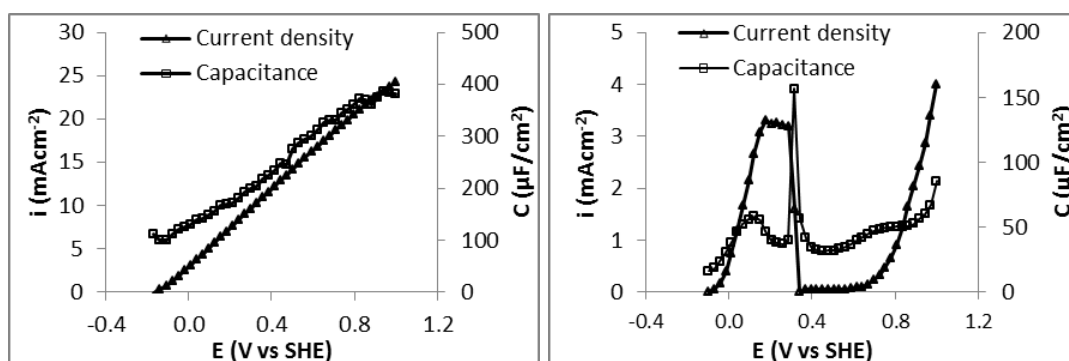


Figure 3.9: Current vs time and corresponding capacitance V potential. (a) Non passivating conditions with 0.3 M glycine at pH 10.5 and 1000 rpm. (b) Passivating conditions with 0.1 M glycine at pH 12 and 0 rpm.

Under passivating conditions at pH 12 with no disk rotation, there is an overall growth of current with potential up to 0.15 V (vs SHE) followed by a plateau. Just before the plateau region the capacitance changes slope and decreases, suggesting a thickening oxide layer consistent with the parallel plate capacitor model (Bard and Faulkner, 2001; Grdeń, 2014). This layer is likely to be Cu₂O that is often a precursor to passivation (Burstein and Newman, 1981; Kunze et al., 2004).

The capacitance continues to decrease in the plateau region but shows a large spike just before the passive region. This has been seen in other studies, and is likely due to oxidation of Cu_2O to soluble copper (II), resulting in an increase in porosity before the formation of CuO (He et al., 2006). The capacitance curve is relatively flat in the initial section of the passive region, but with an increase towards the transpassive region. It then flattens again at the onset of the transpassive region before finally rising again. This suggests complex behaviour involving the semiconducting nature of the oxide layer and further changes in porosity (Grdeń, 2014; He et al., 2006; Speckmann et al., 1985).

3.3.5 Surface analysis

Surface analysis with Raman spectroscopy was consistent with the observations in the previous sections that suggest the passive layer breaks down upon resting at OCP. Three samples were tested: one freshly polished copper sample exposed to the atmosphere, one held at a passivating potential of 0.6 V (vs SHE) for one hour and finally, one held at the OCP for 4 hours. These showed no significant differences in their spectra as can be seen in Figure 3.10. Weak Raman active peaks resembling cuprite (Cu_2O) were detected on all samples. These spectra are similar to those reported in other studies for copper corrosion under various conditions (Hurley and McCreery, 2003; Montes et al., 2014; Rios, 2011).

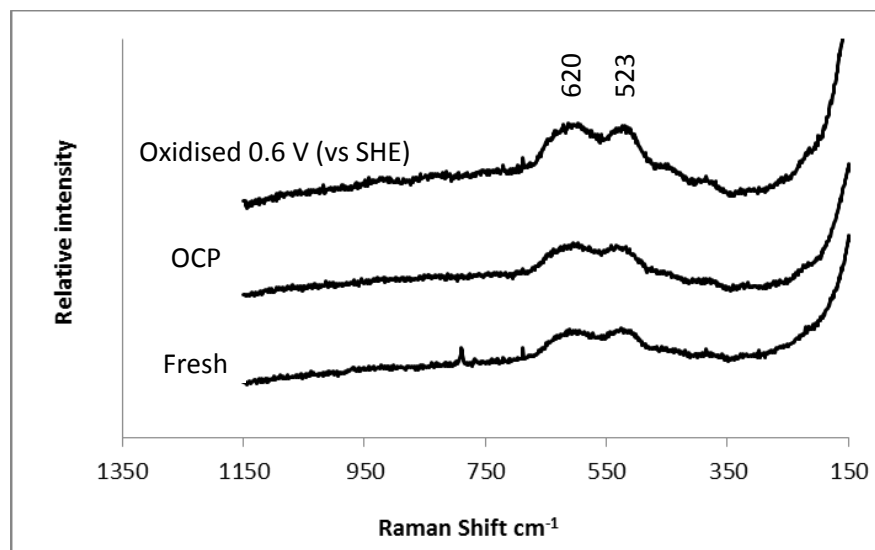


Figure 3.10: Raman spectra of copper that has been oxidised at 0.6 V (vs SHE) held at the OCP, and a fresh sample exposed to air showing a poorly crystalline cuprite layer.

3.3.6 Oxidation of glycine

Cyclic voltammetry was used to investigate the oxidation of glycine at an inert electrode. At scan rates of 10 to 100 mV/s, peaks for oxidation occurred above 1.2 V (vs SHE). This is similar to those reported in the literature of 1.0 V (vs SHE) to 1.3 V (vs SHE) (Marangoni et al., 1989; Ogura et al., 1998; Skrypnikova et al., 2011). The peak potentials shift to higher potentials with scan rate and no peaks were observed on the reverse sweep, indicating an irreversible reaction. A similar result has been reported by several authors studying the adsorption and oxidation of glycine where the adsorption step was reversible, but the oxidation was not (Huerta et al., 1998; Sandoval et al., 2013). The effect was greatest at pH 12 and is shown at 22° and 60° in Figure 3.11.

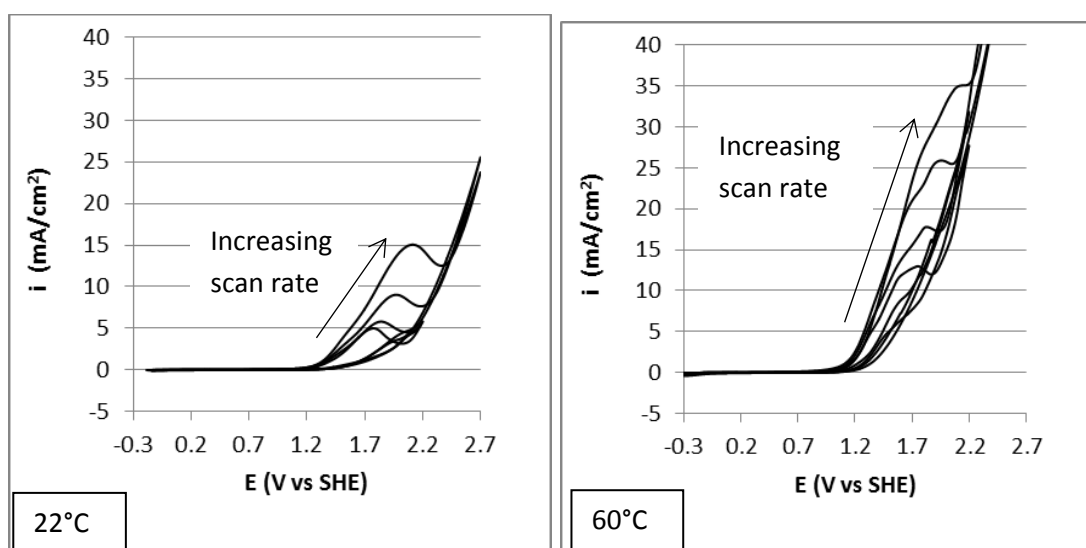


Figure 3.11: Cyclic voltammograms of 0.3 M glycine at pH 12 and 25°C and 60°C with scan rates of 10, 20, 50 and 100 mV/s

3.4 Conclusions

The effectiveness of glycine as a complexing agent in the alkaline leaching of copper is primarily dependent on the pH of the solution, with an optimum pH of 10.5 at 22°C or 10.0 at 60°C. At pH 9.0, dissolution is limited by a low mole fraction of the glycinate ion. Above pH 10.0 or 10.5 the rate is slowed by surface oxide species. Dissolution is particularly enhanced by an interaction between higher glycine concentrations and temperature. Cupric glycinate acts as an oxidant when the glycinate anion is in excess of soluble copper.

For all experiments the passivation potential was greater than 0.4 V (vs SHE) and is dependent on pH, glycine concentration and electrode rotation rate. The passive layer breaks down if the sample is rested at the OCP for 30 seconds, and reforms when the potential is re-applied. Rotating the electrode hinders the reformation of the passive layer.

Metallic copper showed typical behaviour expected of a metal in solution with a complexing agent at alkaline pH. Current potential curves showed classic behaviour discussed in corrosion textbooks with active, passive and passive-breakdown regions (McCafferty, 2010). Observed corrosion currents were consistent with what is expected from thermodynamics, where higher solution pH maximises glycinate mole fraction, but also favours the formation of insoluble copper oxides. The electrode is passivated by these copper oxides as evidenced by low current densities of less than 0.1 mAcm^{-2} at higher pH and low stir rates.

The passive layer generated on the copper surface breaks down after removal of the applied potential. Raman spectroscopy shows weak peaks that resemble a remnant cuprite (Cu_2O) layer, but with no significant difference to a sample exposed to air only. The passivation potential is higher with increased stirring, reflecting the mass transport of glycine in solution.

The main points for comparison of metallic copper to semiconducting chalcopyrite are:

- Current potential curves with well-defined active, passive and trans-passive regions as shown earlier in Figure 3.9.
- Effect of stirring, which shows passivation is directly influenced by the stir rate and the mass transport of glycine through the solution.
- The trend of capacitance with potential shows what would be expected for a parallel plate capacitor. This shows a decreasing capacitance with as the passive layer increases in thickness and the plate separation increases.

Chapter 4 Electrochemical Behaviour and Surface Analysis of Chalcopyrite in Alkaline Glycine Solutions

4.1 Introduction

A review of the literature has shown many inconsistencies regarding the proposal of chalcopyrite passivation. The presence of a passivating surface species such as the metal deficient sulfide can only be considered speculative, no evidence has confirmed it as passivating. Some authors have even questioned the existence of a metal deficient sulfide, which has only been inferred from a disulfide component of the sulfur peak in XPS (Klauber, 2008).

An alternative proposition to passivation is that the fundamental electronic structure of chalcopyrite is responsible for slow dissolution (Crundwell, 2015). According to this theory oxidation will be slow with redox couples that correspond in energy to the band gap of chalcopyrite. A suitable redox couple would have a standard potential outside the energy levels of the band gap, which might explain the higher rates of leaching with strong oxidants at high redox potentials or when the potential is controlled at relatively low values (Watling, 2013).

There is an added complication to understanding the mechanism of chalcopyrite dissolution at alkaline pH. If current potential curves of chalcopyrite in ammonia or glycine are examined, it is evident that there is no passive current (Moyo et al., 2015; Nicol, 2017b; Warren and Wadsworth, 1984). Few surface studies have been carried out under alkaline conditions, but recent work has shown the presence of disulfides which may be linked to a metal deficient sulfide species (Hua et al., 2018).

The objectives of this chapter are to:

- Examine the effect of the electrochemical behaviour of chalcopyrite under different temperature, pH and glycine concentrations.
- Generate surface layers at various potentials to determine if there is a relationship with the observed current density. Surface analyses to be carried out by XPS and Raman spectroscopy.

- Observe the relationship of interfacial capacitance with the applied potential to show conductivity type (n or p).
- Fit observations to the behaviour that could be expected from the fundamental electronic structure of chalcopyrite.

4.2 Experimental

4.2.1 Sample details

A high purity chalcopyrite sample was obtained from Geodiscoveries Australia. Optical microscopy at various times throughout the study confirmed purity at 95% with small inclusions of quartz and feldspars identified by SEM-EDS. The sample was analysed for stoichiometry by electron microprobe and showed a slight excess of metal over sulfur over 140 spot locations. This is consistent with natural chalcopyrite showing n-type conductivity (Shuey, 1975). Metal impurities were highly variable from 0 to 0.02% depending on the spot location, consistent with small mineral inclusions. The main impurities were lead and zinc with an average of 0.01% and silver at 0.003%. The thermoelectric current was measured by heating the positive electrode with a soldering iron and measuring the current with a digital multimeter. The resulting current was highly variable but positive, indicating an n-type semiconductor.

4.2.2 Electrochemical Experiments

All electrochemical tests were carried out using a Bio-logic VMP3 potentiostat. The working electrode was a chalcopyrite core embedded in epoxy resin with an exposed surface area of 0.78 cm². Test solutions were made from analytical grade glycine (99%, Sigma Aldrich) and sodium hydroxide (98%, Sigma Aldrich) using Mili-Q deionised water with a resistivity of 18.2 MΩ.cm.

The working electrode was progressively polished to a 3 μm diamond finish, rinsed with DI water and immediately placed in the test solution. The electrode was rotated at a set rate and the temperature adjusted to target within ± 1°C accuracy. Tests were carried out at 1000 rpm and 25°C unless otherwise specified.

The experiments were carried out in a three-electrode electrochemical cell with a working volume of 500 mL. The reference electrode was single junction Ag/AgCl (3.5 M) held in a Luggin capillary placed close to the working electrode to minimize any error due to iR drop. The same distance was maintained between the reference and working electrodes for all tests. The counter electrode was Hastelloy C with a surface area of 5.5 cm^2 . The working electrode was allowed 60 minutes to stabilise before beginning the experiment.

A staircase potential sweep measurement was carried out with 20 steps from the open circuit potential to 1.0 V (vs Ag/AgCl). Each step was held for 20 minutes and the current was recorded, followed by capacitance measurements at 1 to 100 kHz with a sinus amplitude of 17 mV. Capacitance effects at 1 kHz are presented here, consistent with other studies (Gahremaninezhad et al., 2010; Olvera et al., 2016; Warren et al., 1982) Chronoamperometry measurements were performed at a plateau in the current- potential curve at 0.65 V (vs Ag/AgCl) for periods of 300 s with intermittent rest intervals at the open circuit potential.

4.2.3 Surface Analysis

The chalcopyrite electrode was removed from the solution after a test at a specified potential, rinsed, dried under vacuum before immediate analysis by XPS analysis or Raman spectroscopy. The solution used was 0.3 M glycine at pH 10.5. For XPS a Kratos Axis Ultra DLD X-ray photoelectron spectroscope with a monochromatic Al source at 1486.7 eV was used to characterise the surface species. A survey spectrum was collected at binding energies between 0 and 1200 eV and high-resolution regional spectra were collected for copper, iron, sulfur, oxygen and carbon. Charge compensation was used where sample charging occurred, typically where thick surface layers were present which resulted in a reduction in spectrum resolution. For Raman spectroscopy, a Labram 1B dispersive Raman spectrometer with a 632.817 nm source and 2mW power was used to determine the sulfur speciation.

4.3 Results

4.3.1 General features of current-voltage behaviour

Several researchers have noted that high scan rates for anodic sweeps can hide the effects of a passive layer due to insufficient time for it to form (Ghahremaninezhad et al., 2010; Viramontes-Gamboa et al., 2007). In order to allow time for the formation of a possible passive layer at a given potential, a staircase potential step method was used with each step held for 20 minutes while recording the current. Unless otherwise specified, only the final current after 20 minutes is presented here.

4.3.2 Effect of pH

The effect of pH on the current-potential transient is shown in Figure 4.1. The 0.3 M sulfuric acid run was with no glycine. These curves show the increased current response above pH 9, due to the higher mole fraction of glycinate anion described in other studies (Aksu and Doyle, 2001; O'Connor et al., 2018). Two plateau regions are present for all alkaline pH values. The apparent passive region for the acid conditions is obvious, from the open circuit potential to about 0.77 V (vs Ag/AgCl) where currents are about 0.02 mAcm^{-2} . A rapid increase in current occurs above this potential and continued to increase off the scale of the graph. At alkaline pH in glycine the increase in current is more moderate, likely limited by the complexing ability of glycine. The current eventually drops or forms a plateau at higher potentials as glycine is depleted.

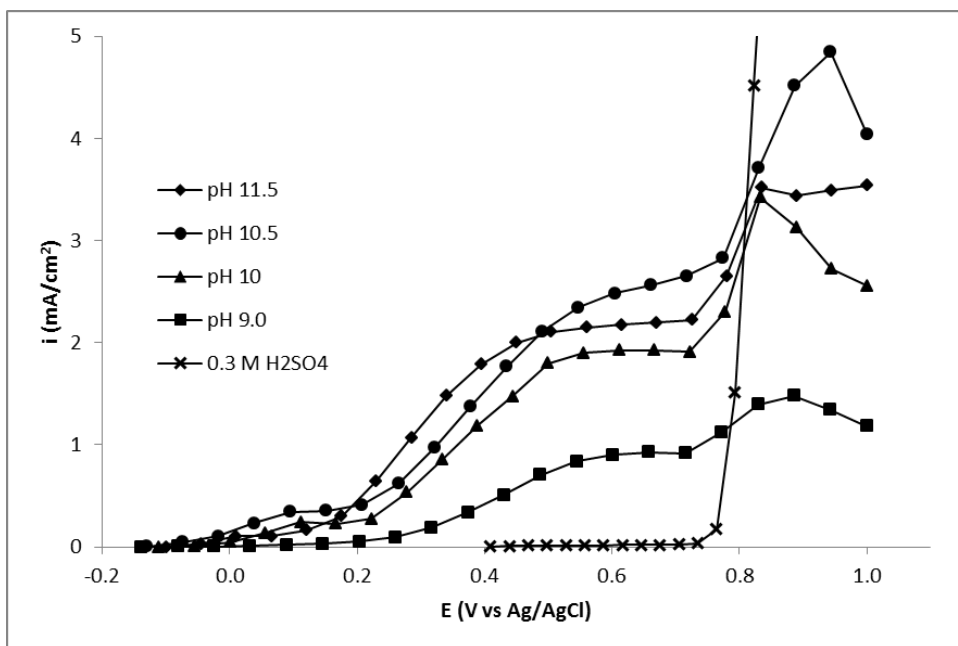


Figure 4.1: Current-potential transients at different pH values in 0.3 M glycine compared to 0.3 M H₂SO₄ solution.

4.3.3 Effect of glycine concentration

The effect of glycine concentration can be seen in Figure 4.2. The general shape of the current-potential curves is similar at all concentration values, but with a less pronounced plateau as the glycine concentration increases. For all concentrations, no significant effect on the current density was observed up to 0.5 V (vs Ag/AgCl). In the plateau region from 0.5 to 0.8 V (vs Ag/AgCl) considerably higher current densities were recorded as the concentration of glycine increased. This is consistent with limitation by transport through a porous layer as opposed to solution diffusion, which would be observed with changes in rotation speed as discussed in section 4.4. This plateau is unlike the passivation for chalcopyrite in acid solutions, where the current is close to zero. The current density is eventually limited by glycine diffusion through the bulk solution at potentials greater than 0.85 V (vs Ag/AgCl) for the 0.1 M and 0.3 M solutions as also shown by the effect of rotation speed.

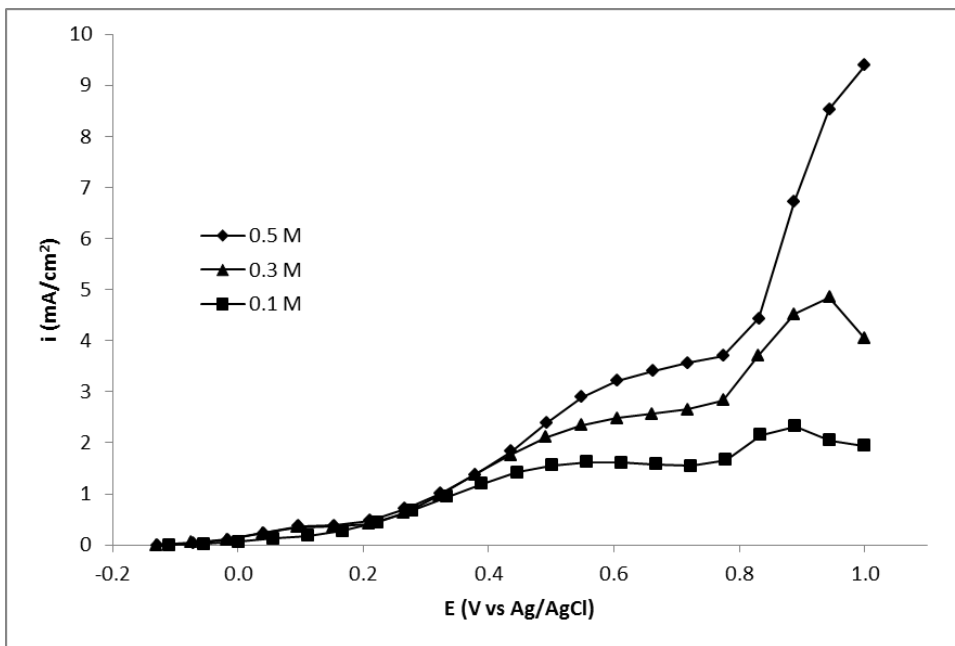


Figure 4.2: Effect of glycine concentration on current potential transient at pH 10.5. Glycine concentration is 0.3 M and temperature is 25°C.

4.3.4 Effect of rotation speed

The effect of rotation speed is shown in Figure 4.3. There is no significant difference in the current potential transients at 500 rpm and above, except at high potentials above 0.9 V (vs Ag/AgCl). This indicates that diffusion through the bulk solution is not the limiting factor for most of the potential range at 500 rpm and above. Other researchers have seen no significant effect of rotation rate in the alkaline studies with ammonia solutions, although not all of these have investigated the effects at 0 rpm solutions (Guan and Han, 1997; Reilly and Scott, 1977; Warren and Wadsworth, 1984). Above 0.9 V (vs Ag/AgCl), there is a dependence of current density for rotation rates of 500 rpm and above. This suggests solution diffusion plays a role at these potentials, but a final steady limiting current density was not observed.

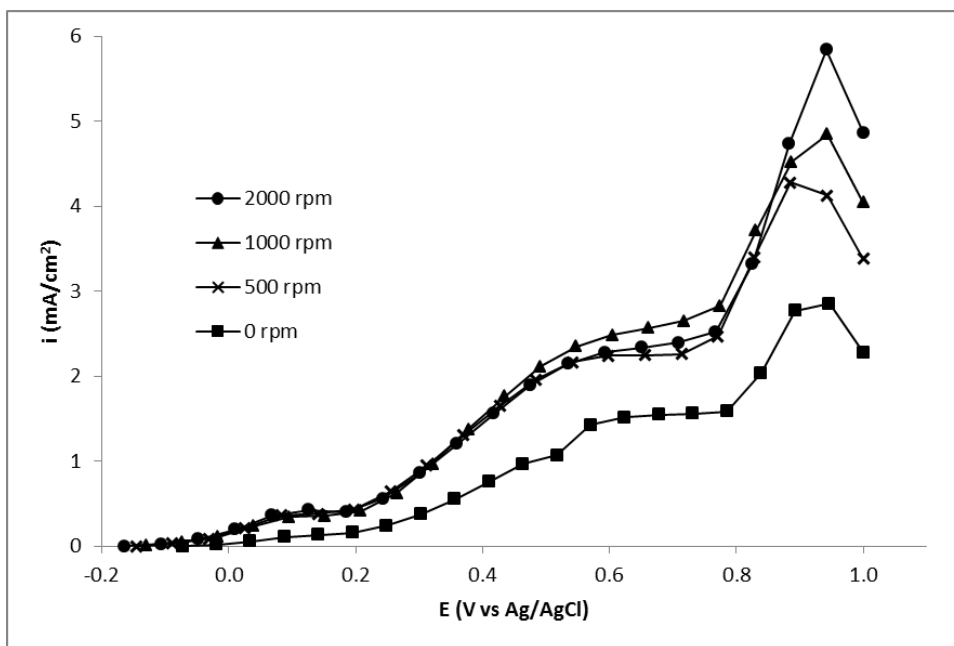


Figure 4.3: Effect of rotation speed on the current potential transients at pH 10.5 and 0.3 M glycine concentration at 25°C.

4.3.5 Effect of Temperature

Increasing the temperature from 25° to 60°C had a positive effect on the current density up to about 0.77 V (vs Ag/AgCl), after which it was slightly lower (Figure 4.4). The curve still shows an increase at 0.77 V (vs Ag/AgCl), but not as great as at room temperature. There is no drop in current at high potentials at 60°C, which in the previous section was attributed to the transfer of glycine to the surface.

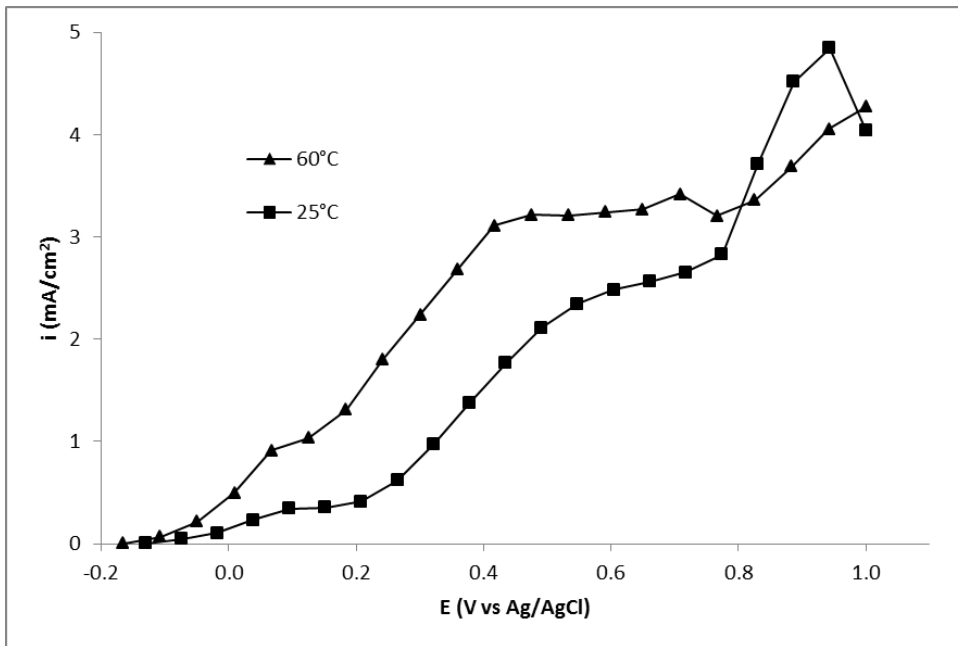


Figure 4.4: Effect of temperature at 25°C and 60°C. Glycine concentration 0.3 M and pH 10.5.

4.3.6 Effect of a pre-oxidised surface layer

During the test program, surface species were readily observed at all potentials after removing the chalcopyrite electrode from the solution. Generally, these were a slightly tarnished surface at potentials less than 0.4 V (vs Ag/AgCl), above this potential was a brown, loosely held layer that is likely to be iron oxyhydroxides that are observed in other alkaline studies (Grano et al., 1997). The effect of this layer was investigated by progressively stepping the potential to 0.65 V (vs Ag/AgCl) before starting a new scan. This generated a thick oxide layer, with the main effect being a lower current in the plateau regions and above 0.9 V (vs Ag/AgCl) as can be seen in Figure 4.5. The thicker oxide layer had little effect on current in the active regions around 0.3 and 0.8 V (vs Ag/AgCl).

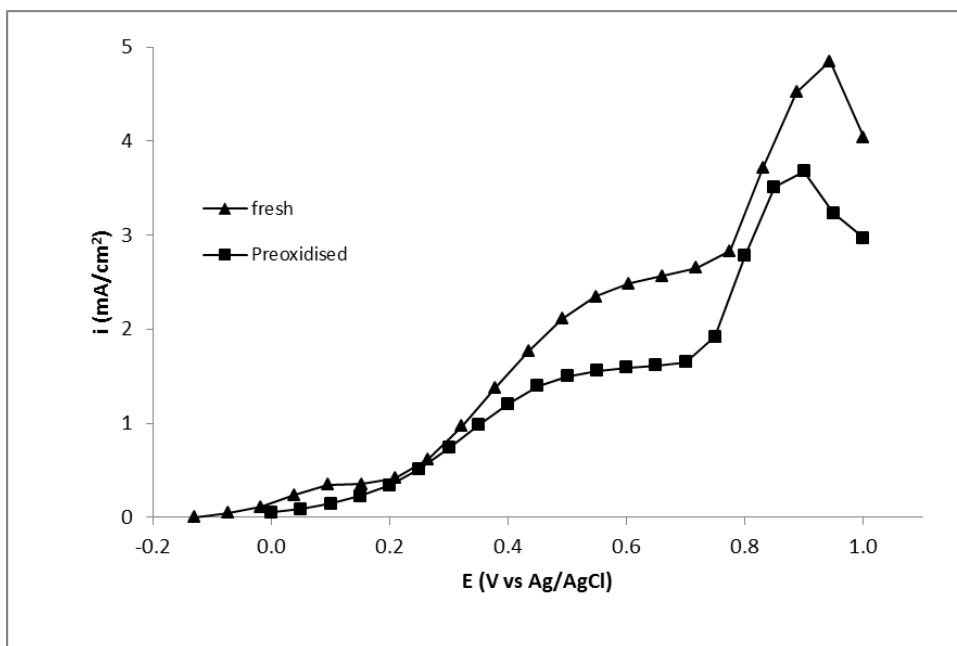


Figure 4.5: Effect of a surface layer generated at 0.65 V (vs Ag/AgCl). Glycine concentration is 0.3 M and pH 10.5

4.3.7 Effect of potential step duration

The time held at each potential step was varied to determine if there was an effect from allowing surface layers more time to thicken and impede transport of reactants to and from the surface. No significant effect was observed up to about 0.5 V (vs Ag/AgCl) as can be seen in Figure 4.6. The sample held for 60 minutes at each step returned a lower current in the plateau region above 0.5 V (vs Ag/AgCl).

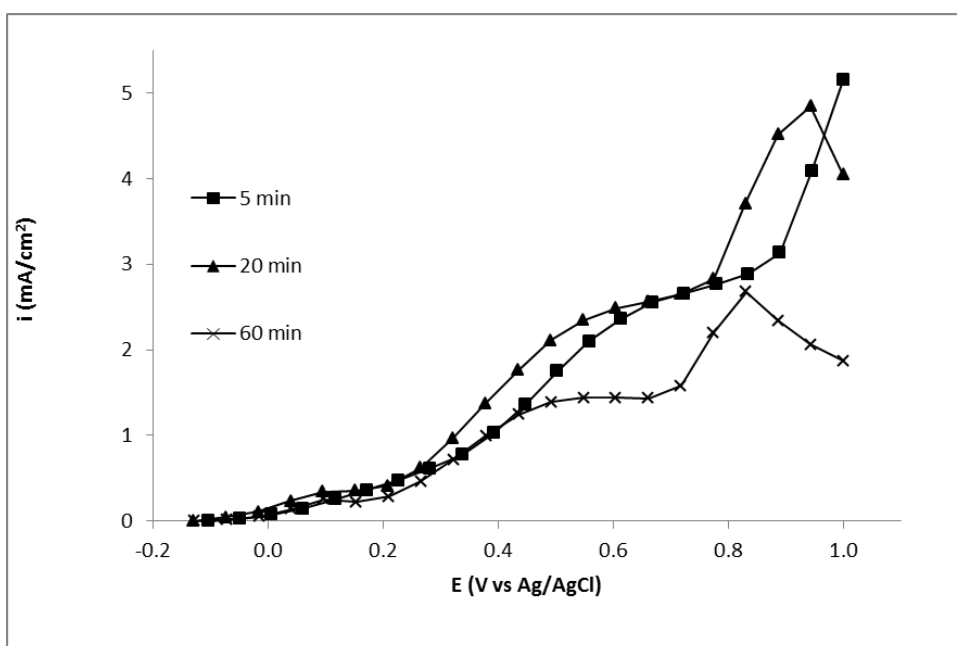


Figure 4.6: Effect of different potential step duration at pH 10.5 and 0.3 M glycine.

4.3.8 Capacitance

Capacitance measurements have been used by several authors for electrochemical impedance and Mott Schottky analyses of chalcopyrite in an effort to understand layer formation in situ (Crundwell et al., 2015; Ghahremaninezhad et al., 2013; Nicol, 2017c). The basis of these measurements is that a mineral-solution interface is considered to act as a parallel plate capacitor where the capacitance, C , is given by Equation 3 (Bard and Faulkner, 2001):

$$C = k\epsilon_0 A/d \quad \text{Equation 16}$$

Where k is the relative permittivity of the dielectric material between the plates, ϵ_0 is the permittivity of free space, A is the area of the charged plate and d is the separation of the plates. Changes in capacitance are therefore a function of these variables. It has been suggested that as a polysulfide passive layer thickens on a chalcopyrite surface, the separation of charge between the bulk mineral and solution grows wider and so the capacitance decreases (Nicol, 2017c). This behaviour of chalcopyrite in acid media was said to be similar to a thickening oxide layer on a metal. At high potentials the layer is thought to be oxidised and breaks down, so the gap narrows, and capacitance increases along with an increase in current. Results in acid solution on the chalcopyrite used in this study are shown in Figure 4.7 and appear to be consistent with this theory and compare well with the trends in the study by (Nicol, 2017c).

However, this model based on charge separation does not fit the observed behaviour of chalcopyrite in an alkaline glycine solution. As can be seen in Figure 4.7, the capacitance decreases with applied potential up to 0.77 V (vs Ag/AgCl). This decrease clearly does not reflect a thickening passive layer because the current increases during this time. At 0.77 V (vs Ag/AgCl) the slope of the capacitance curve changes sign at the same time as an increase in current, as was observed in acid solution. While not consistent with a passive layer formation and breakdown, this behaviour is as expected for the inversion region of an n-type semiconductor seen in Mott Schottky studies (Crundwell, 2015). The curves show little resemblance to copper with a genuine oxide passive layer in glycine solutions, which show a complex behaviour due to porosity and semiconducting properties of the duplex $\text{Cu}_2\text{O}/\text{CuO}$ layer (O'Connor et al., 2018)

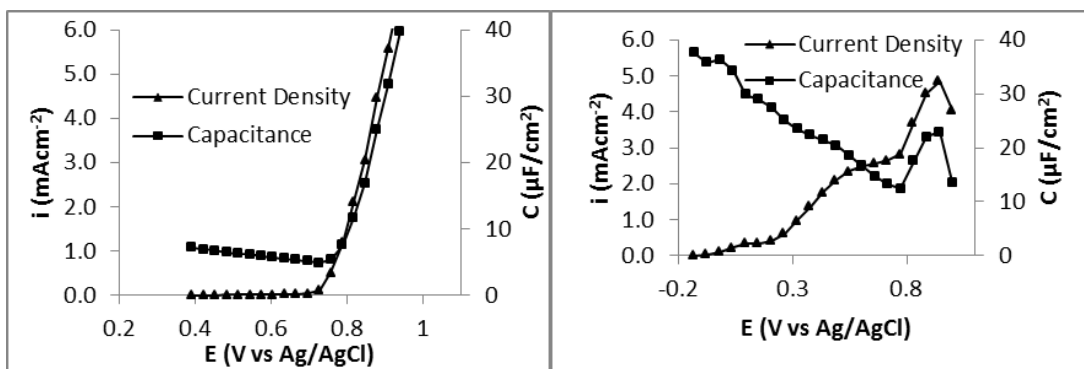


Figure 4.7: Comparison of current and capacitance at 1 kHz in 30g/l H₂SO₄, left, and 0.3 M glycine at pH 10.5, right.

4.3.9 Chronoamperometry

Several authors have proposed that a passivated chalcopyrite surface will reactivate upon removal of potential, based on interpretation of chronoamperometry (Lu et al., 2000; Nicol, 2017a; Parker et al., 1981). This has been attributed to the thermal breakdown of the polysulfide or solid state diffusion of iron and copper in the mineral. A similar reactivation effect was observed for this system when an electrode was held at 0.65 V (vs Ag/AgCl) for five-minute periods with varying rest times at the open circuit potential. The degree of reactivation increased with increased rest times as can be seen in Figure 4.8, consistent with previous research in acid solutions (Parker et al., 1981). Copper metal showed a similar behaviour in alkaline glycine solutions, but with a strong dependence on stirring rate (O'Connor et al., 2018)

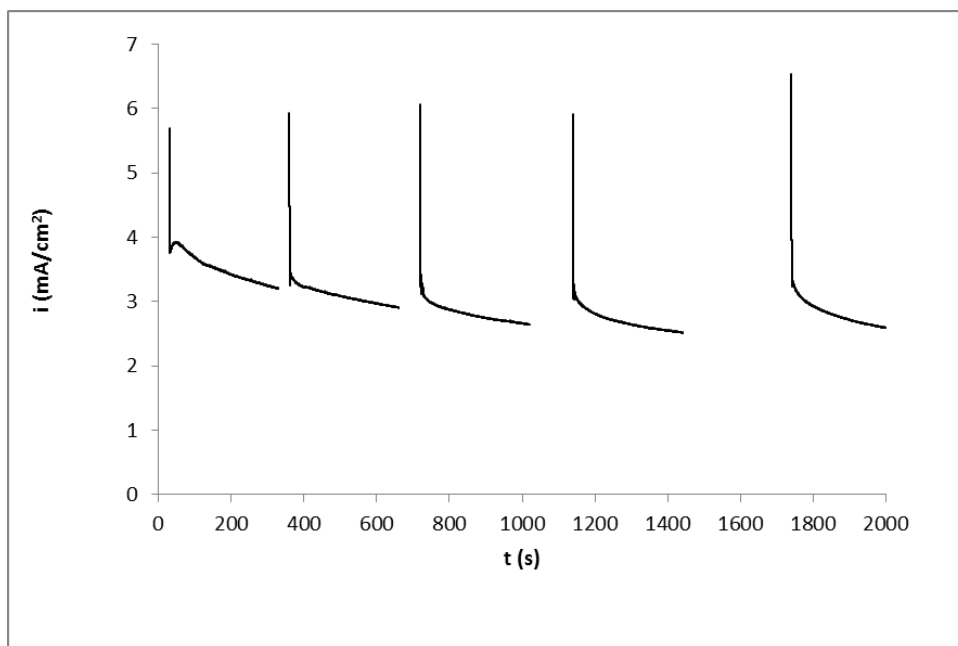


Figure 4.8: Chronoamperometry at 0.65 V (vs Ag/AgCl) in solutions of 0.3 M glycine at pH 10.5.

A close-up view of the first two current transients in Figure 4.9 shows a complex decay curve. For the initial transient a high current drops to a minimum within 1 – 2 seconds, the current then rises to reach a maximum before slowly decreasing again. For the second and each subsequent transient there is a small oscillation that gradually decays, resembling an under-damped second order system. Similar patterns have been observed in other alkaline studies of chalcopyrite but are not well described or understood (Azizkarimi et al., 2014; Yin et al., 2000).

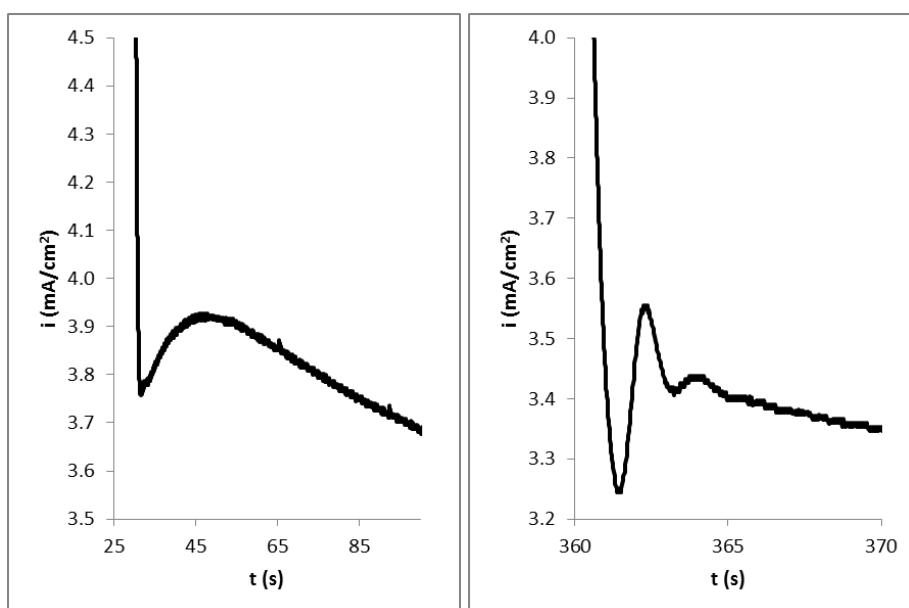


Figure 4.9: Chronoamperometry at 0.65 V (vs Ag/AgCl). Close-up view of the initial and second current transients of Figure 4.8.

A current time transient for a stepped anodic sweep over the whole potential range is shown in Figure 4.10. The most obvious feature is the change in mechanism after 0.77 V (vs Ag/AgCl), where the current accelerates for several steps. Before this point the current shows a spike and rapid decay as expected in a relaxation process (Crundwell et al., 2015). The oscillation feature observed in Figure 4.9 is beyond the resolution of this graph, but was present between 0.26 V (vs Ag/AgCl) and 0.82 V (vs Ag/AgCl). The current decay seen at each step might be argued as evidence of passivation if longer times are employed, but the results from longer step times of 1 hour as shown in Figure 4.6 still yield a current greater than that observed for the passive region in acid solutions.

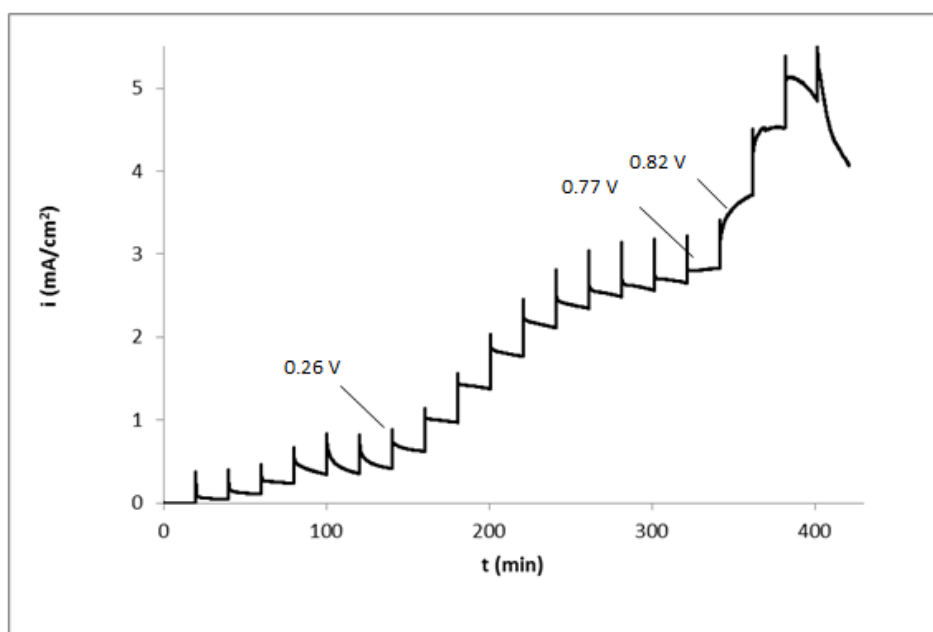


Figure 4.10: Current vs time for a potential step experiment at pH 10.5 with 0.3 M glycine at 25°C

The process of reactivation after a rest at the OCP seen in this study and others suggests that if surface species are responsible for the current decay, they will not be present for analysis at a later time. Analyses of the surface are not likely to be of passivating species, but of other non-passivating reaction products. Alternatively they could be daughter products of a passive or inhibiting species that has altered upon removal from the system.

4.3.10 XPS and Raman Spectroscopy Analysis

Six samples for surface analysis were stepped to potentials ranging from the open circuit potential to 1.0 V (vs Ag/AgCl) and measured by XPS and Raman spectroscopy in solutions of 0.3 M glycine at pH 10.5. A freshly polished sample was exposed to the atmosphere for 12 hours and also measured. At potentials above 0.4 V (vs Ag/AgCl) the samples had a friable overlayer. The surface underneath was also measured in areas where it had detached during rinsing and handling for XPS. Complete deconvolution was only attempted for the sulfur peak. For iron, peaks distinguishing oxide iron and lattice sulfide iron were determined.

4.3.10.1 Samples oxidised in air, at the OCP and at 0.15 V (vs Ag/AgCl)

The spectrum for an air oxidised sample showed typical features of a chalcopyrite surface as can be seen by the uppermost trace in Figure 4.11. Copper is present only as Cu (I). Surface iron is in oxide or hydroxide form and has a low BE shoulder at 708 eV indicating lattice iron bonded to sulfur (Buckley and Woods, 1984; Hackl et al., 1995; Luttrell and Yoon, 1984; McCarron et al., 1990). The sulfur spectrum shows typical peaks for a monosulfide and disulfide species. There is no appreciable indication of polysulfides or an energy loss peak.

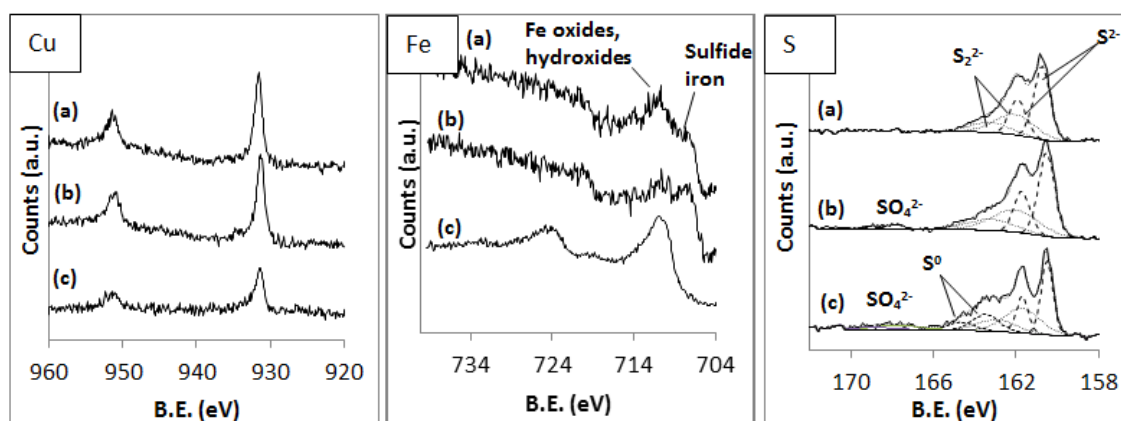


Figure 4.11: Copper, iron and sulfur XPS peaks of chalcopyrite. From top to bottom: (a) air oxidised, (b) oxidised at OCP, (c) stepped to 0.15 V (vs Ag/AgCl). Solution was 0.3 M glycine at pH 10.5.

The Raman spectrum for the air oxidised sample shown in Figure 4.12 shows a relatively broad peak typical of chalcopyrite with the main A_1 mode at 292 cm^{-1} . A B_2/E mode forms a shoulder at 320 cm^{-1} with another at 353 cm^{-1} (Parker et al., 2008). The broad peak width indicates some degree of poor crystallinity compared to those observed at potentials of 0.15 V (vs Ag/AgCl) and above. This is probably an artefact of sample preparation.

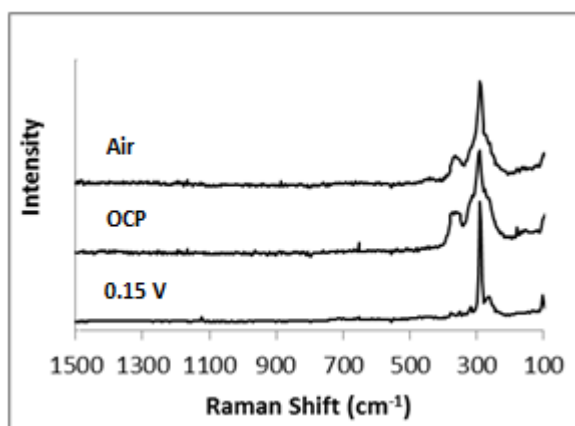


Figure 4.12: Raman spectrum of oxidised chalcopyrite. From top to bottom: (a) Air oxidised, (b) Oxidised at OCP, (c) oxidised at 0.15 V (vs Ag/AgCl). Solution was 0.3 M glycine at pH 10.5.

No significant change was observed in the XPS or Raman spectra for the sample held at the open circuit potential for 12 hours compared to the air-oxidised sample. The iron spectrum shows the same shoulder at 708 eV indicating lattice iron bonded to sulfur, and sulfur shows the same ratio of monosulfide to disulfide as the air oxidised sample. This ratio is similar in other studies that have attributed these species to a metal-deficient sulfide (Gahremaninezhad et al., 2013; Hackl et al., 1995). A minor sulfate peak was also detected.

The sample stepped to 0.15 V (vs Ag/AgCl) showed a tarnished surface typical of a weathered chalcopyrite. The overlayer showed no shoulder at 708 eV in the iron spectrum, indicating the presence of a different surface layer. The surface percentage copper has dropped from 1.0% to 0.3% but still gives a strong signal. The sulfur peak is more complex, with the contribution from monosulfur dropping considerably. A new peak at 163.5 eV is possibly an indication of elemental sulfur. The presence of elemental sulfur in an ultra-high vacuum is possible due to the protective nature of iron oxides (McCarron et al., 1990; Smart et al., 1999). The small peak at 167.9 eV is assigned to sulfate. The Raman spectrum showed a distinct narrowing of the main chalcopyrite peak compared to previous samples as seen in Figure 4.12. This would be expected for a highly crystalline specimen, which suggests that disordered or amorphous chalcopyrite is formed during preparation and dissolved in the initial potential steps. The B2/E modes are visible at 320 cm^{-1} and 353 cm^{-1} .

4.3.10.2 Sample stepped to 0.4 V (vs Ag/AgCl)

In this region the current increased with each potential step and a loose overlayer formed that partially detached from the surface. This allowed both the overlayer and the underlying surface to be measured as shown in Figure 4.13. Copper is still only present as Cu (I). For the overlayer, no shoulder was detected at 708 eV for lattice iron on the surface. The sulfur peak was noisy in this region due to sample charging, but a substantial sulfate peak and decreased monosulfide peaks are evident. Duplicate analyses showed this was a repeatable peak with about 5% variation in calculated sulfur species from the deconvolution process. The underlayer was similar to the fresh surface, with a shoulder for sulfide iron at 708 eV and a sulfur peak consisting of mono and disulfide.

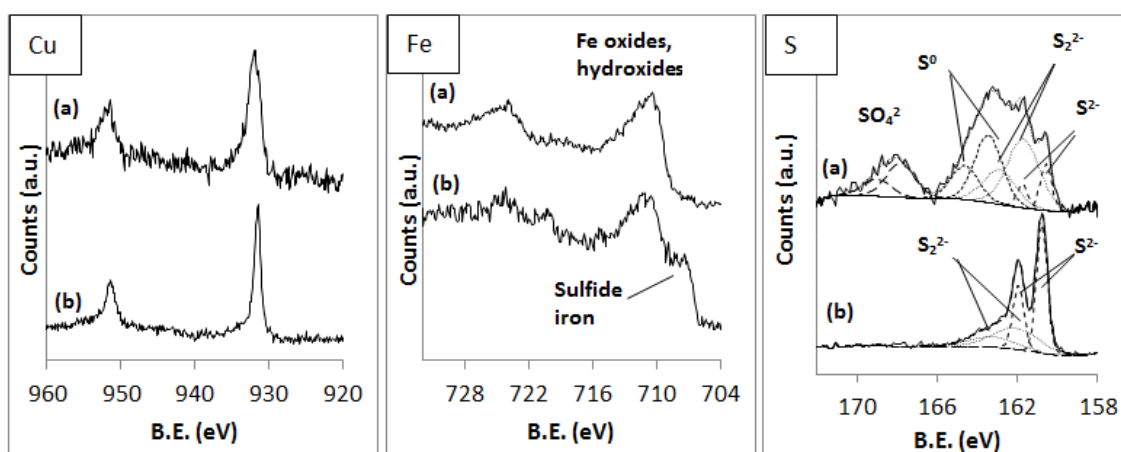


Figure 4.13: Copper, iron and sulfur XPS peaks for chalcopyrite stepped to 0.4 V (vs Ag/AgCl) in 0.3 M glycine at pH 10.5. From top to bottom: (a) overlayer, (b) underlayer

Raman spectra for the overlayer showed mixed spectra of poorly crystalline iron oxyhydroxides, elemental sulfur and chalcopyrite. A broad oxyhydroxide peak is at 1313 cm^{-1} and overlapping peaks are between 650 and 720 cm^{-1} . Elemental sulfur was detected in cracks in this oxide overlayer with distinct peaks due to S-S-S bending at 152 cm^{-1} and 219 cm^{-1} , and S-S stretching at 473 cm^{-1} (Figure 4.14). The surface where the overlayer had detached showed a highly crystalline chalcopyrite peak as with the previous sample and is not repeated here.

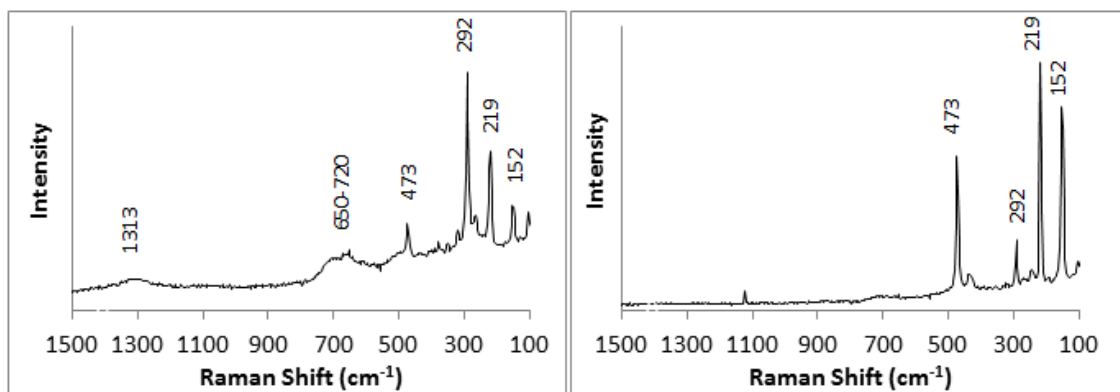


Figure 4.14: Left: Raman spectrum of overlayer showing mixed spectra of chalcopyrite, sulfur and oxyhydroxides. Right: elemental sulfur with minor chalcopyrite in oxide layer cracks. Sample stepped to 0.4 V (vs Ag/AgCl) in 0.3 M glycine at pH 10.5.

4.3.10.3 Sample stepped to 0.65 V (vs Ag/AgCl)

In this plateau region both an underlayer and overlayer were again measured (Figure 4.15). In the overlayer, again no shoulder denoting lattice iron was detected. Copper is almost completely obscured from the surface in this region with peaks barely above noise. As for the previous sample, sulfur has a noisy peak due to sample charging which is difficult to model. It can be stated that the monosulfide contribution has disappeared, leaving a disulfide, elemental sulfur and a sulfate. Another species appears to be present at 165.6 eV that is yet to be positively identified, but is possibly sulfite. The underlayer has features of a chalcopyrite surface in the XPS spectrum as described in previous sections.

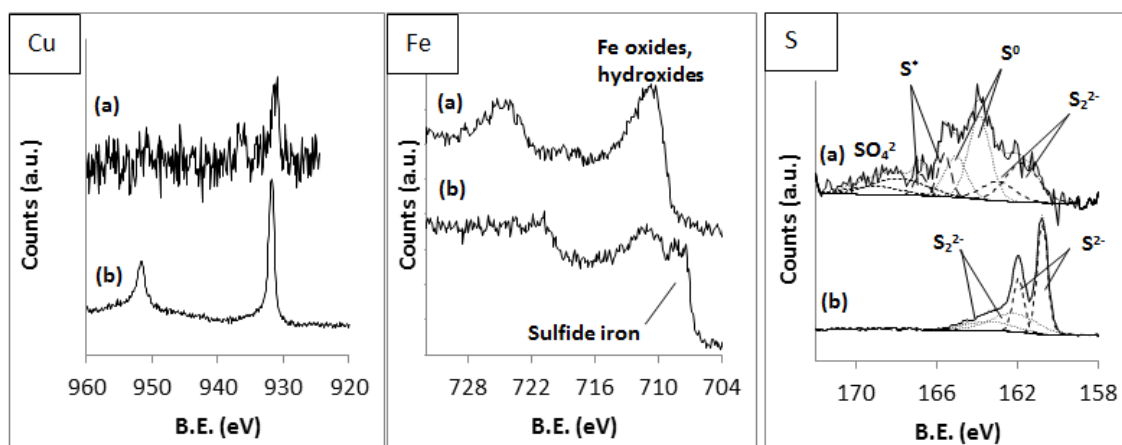


Figure 4.15: Copper, iron and sulfur XPS peaks of chalcopyrite stepped to 0.65 V (vs Ag/AgCl). “S*” denotes an unidentified species- possibly sulfite in 0.3 M glycine at pH 10.5. From top to bottom: (a) overlayer, (b) underlayer.

Raman spectroscopy showed the overlayer to be a mix of poorly crystalline iron oxyhydroxides and elemental sulfur as shown in Figure 4.16. Thick elemental sulfur was detected in cracks in the oxide overlayer as evidenced by a mixed spectrum of sulfur and chalcopyrite. Chalcopyrite in the underlayer was in a highly crystalline form similar to that shown in Figure 4.12.

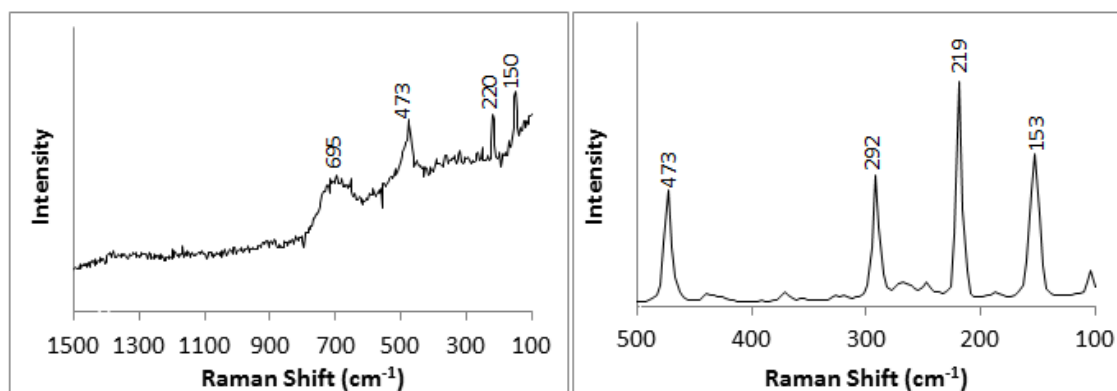


Figure 4.16: Left: Raman spectrum of mixed sulfur and oxyhydroxide in the surface overlayer. Right Elemental sulfur in cracks in the overlayer in 0.3 M glycine at pH 10.5.

4.3.10.4 Sample stepped to 0.85 V (vs Ag/AgCl)

In this active region faint copper peaks were visible in XPS for the overlayer but no positive assignments can be made (Figure 4.17). Sulfur is present as disulfide, elemental sulfur and sulfate. Raman spectra mostly show a mix of sulfur and chalcopyrite spectra in the cracks of the overlayer (Figure 4.18).

The underlayer in this region shows a significantly different sulfur XPS peak compared to other regions, with a contribution from elemental sulfur. Previously it was only detected as a component in the overlayer. Iron again showed the shoulder at 708 eV attributed to iron bonded to sulfur in the lattice.

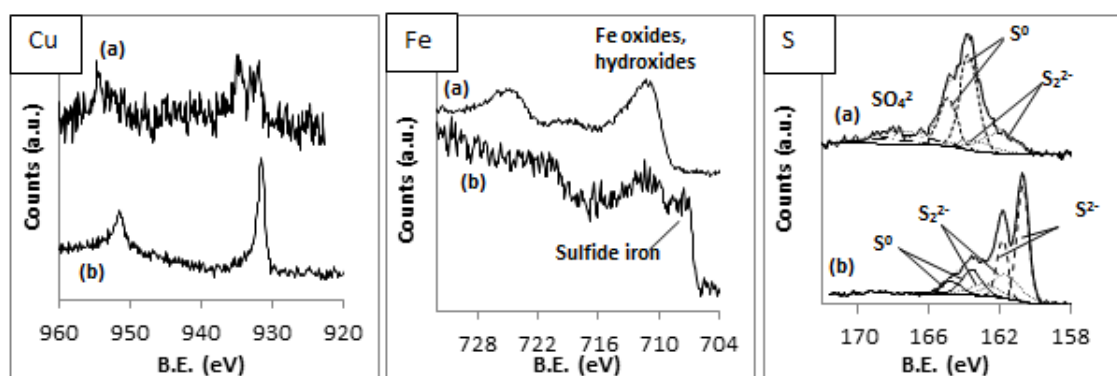


Figure 4.17: Copper, iron and sulfur XPS peaks of chalcopyrite stepped to 0.85 V (vs Ag/AgCl) in 0.3 M glycine at pH 10.5. From top to bottom: (a) overlayer, (b) underlayer.

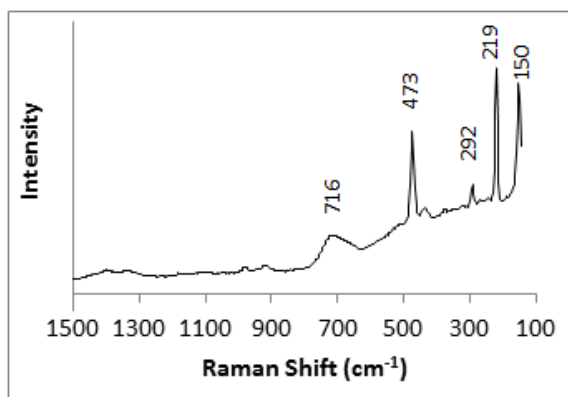


Figure 4.18: Raman spectrum of mixed sulfur, oxyhydroxide and chalcopyrite in overlayer at 0.85 V (vs Ag/AgCl) in 0.3 M glycine at pH 10.5

4.3.10.5 Sample stepped to 1 V (vs Ag/AgCl)

The overlayer in this region is similar to that observed at 0.85 V (vs Ag/AgCl) as shown in Figure 4.19. Sulfur is present as disulfide, elemental sulfur and minor sulfate with no monosulfide detected. The underlayer showed a higher than usual disulfide level, but no elemental sulfur in this case. Raman spectroscopy again showed elemental sulfur in the overlayer cracks and crystalline chalcopyrite elsewhere in the underlayer (Figure 4.20).

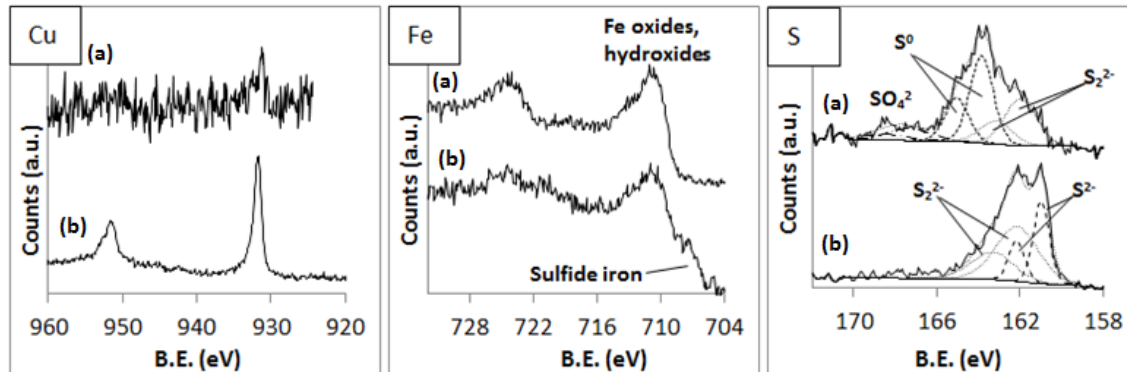


Figure 4.19: Copper, iron and sulfur XPS peaks of chalcopyrite stepped to 1.0 V (vs Ag/AgCl) in 0.3 M glycine at pH 10.5. From top to bottom: (a) overlayer, (b) underlayer.

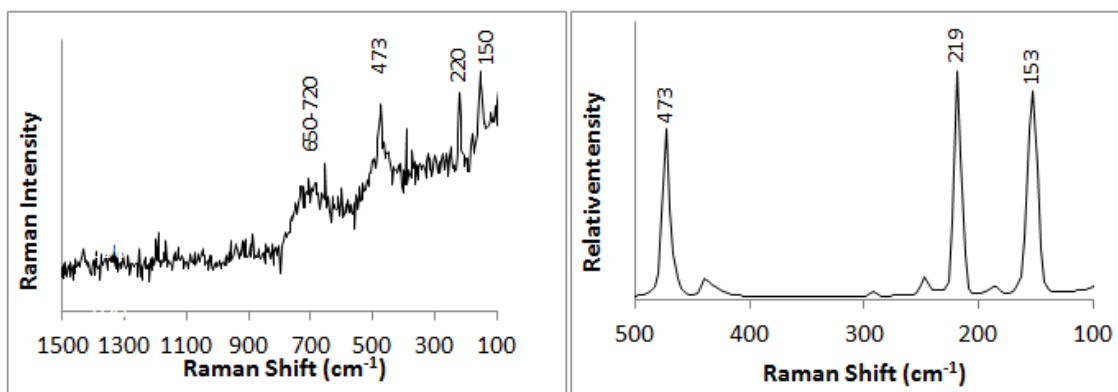


Figure 4.20: Left: Raman spectrum of mixed oxide/sulfur in overlayer; right: elemental sulfur in overlayer crack in 0.3 M glycine at pH 10.5.

4.3.10.6 Summary of XPS Results

The elemental distribution calculated from survey spectra is presented as elemental ratios with respect to copper in Table 4.1. The dominant species in most cases are adventitious carbon, oxygen and nitrogen from the atmosphere. The overlayer shows high iron values due to the presence of iron oxyhydroxides. The surface is rich in sulfur (or copper deficient) except for the underlayer at 1 V (vs Ag/AgCl). The underlayer at 0.88 V has a higher sulfur to copper ratio than the other underlayers, possibly reflecting its status as a reaction product in this region of high oxidation rates.

Table 4.1 Surface elemental distribution from survey scans

Holding potential	Cu	Fe	S	C	O	N
Air	1.0	0.6	5.2	78	13	1.6
OCP	1.0	0.6	5.6	67	13	3.5
0.15 V	1.0	12.0	6.0	199	101	14
0.4 V over layer	1.0	3.5	2.6	95	35	6.4
0.4 V under layer	1.0	1.0	2.9	8.1	5.0	0.4
0.65 V over layer	1.0	14.6	6.9	152	97	15
0.65 V under layer	1.0	1.0	2.6	4.5	1.9	0.3
0.88 V over layer	1.0	11.7	9.3	190	100	21
0.88 V under layer	1.0	1.2	5.7	153	16	5
1 V over layer	1.0	24.3	9.0	176	114	10
1 V under layer	1.0	0.7	1.8	5.8	3.5	0.4

Sulfur speciation is shown in Table 4.2. The monosulfide species is attributed to the bulk chalcopyrite lattice (Klauber et al., 2001). Its contribution to the total sulfur peak diminishes as the overlayer thickens and is not present in this layer at 0.65 V (vs Ag/AgCl) and above. The disulfide peak by contrast is a major sulfur species for both layers in all samples analysed. The disulfide has sometimes been attributed to a passivating metal-deficient sulfide at acidic pH, but in this case there is no correlation with any features resembling passivation in the current potential curves.

Table 4.2: Sulfur species on the friable overlayer and the exposed surface beneath.

Sample	monosulfide		disulfide		elemental S		sulfate		sulfite	
	(eV)	(%)	(eV)	(%)	(eV)	(%)	(eV)	(%)	(eV)	(%)
Air	160.7	60	162.0	40						
OCP	160.5	56	162.0	41			167.9	3		
0.15 V	160.5	36	161.7	37	163.5	18	167.8	9		
0.4 V over layer	160.6	9	161.7	40	163.4	33	167.8	17		
0.4 V under layer	160.8	59	162.1	41						
0.65 V over layer			161.8	29	163.9	40	167.9	19	165.7	12
0.65 V under layer	160.8	58	162.2	42						
0.88 V over layer			162.1	24	163.7	59	167.2	17		
0.88 V under layer	160.7	52	161.7	28	163.5	21				
1 V over layer			162.0	37	163.9	50	167.7	13		
1 V underlayer	160.9	36	162.1	64						

4.4 Discussion

No evidence of the passivation effect that is claimed to be observed in acid solutions was apparent during anodic dissolution of chalcopyrite in alkaline glycine solutions. Unlike acidic solutions, the current-potential curves showed no apparent passive region above the OCP, which is consistent with other studies in alkaline solutions with glycine or ammonia (Moyo et al., 2015; Nicol, 2017b; Warren and Wadsworth, 1984). Trends with capacitance versus potential show no resemblance to a metal with a thickening passive oxide layer as has been suggested for chalcopyrite in acid solutions (Nicol, 2017c). Elemental sulfur and a disulfide species that might be attributed to a metal-deficient sulfide were present in significant amounts in plateau regions and regions of increasing current. These species are clearly not passivating at alkaline pH. This lack of a passive region in alkaline solutions has also been noted by other researchers (Nicol and Zhang, 2017; Yin et al., 1995)

An alternative to the passivation proposal is to apply semiconductor theory. Chalcopyrite in glycine solutions does not behave as an ideal semiconductor, but has characteristics intermediate between a semiconductor and metal. Metal-like behaviour can be seen in semiconductors in several ways. One is by impurities substituting into the lattice, which is utilized in the well-known doping process in the semiconductor industry. Doping has been suggested by some authors as a reason for metal-like behaviour in chalcopyrite, the reasoning being that natural chalcopyrite has high impurity levels (Nicol et al., 2016). Such a heavily doped or degenerate semiconductor is often characterised by the absence of a thermoelectric effect and has been observed for synthetic chalcopyrite doped with zinc (Xie et al., 2016). However, a thermoelectric effect was observed for the sample used in this study and in many others, so there is some doubt that doping of the chalcopyrite lattice is a cause of metal-like behaviour. Studies have shown that impurities in chalcopyrite have little influence on the charge carrier density (Pridmore and Shuey, 1976).

Another way in which metal-like behaviour can be observed in a semiconductor is when surface states are present in high density. These states occur through the termination of the lattice or by adsorbed species that create energy levels within the bandgap (Morrison, 1980). These allow electron exchange at energy levels within the gap, but the surface limitation means a thermoelectric effect is still observed in the semiconductor bulk. This concept of a surface state mechanism has been used to explain the electrochemical behaviour of chalcopyrite and other minerals for many years (Bryson and Crundwell, 2014; Mishra and Osseo-Asare, 1992; Olvera et al., 2016; Springer, 1970; Tributsch and Bennett, 1981).

In addition to the presence of surface states in the band gap, metal-like behaviour can be observed when the semiconductor has an accumulation or inversion layer at the surface surface (Gomes and Cardon, 1982; Morrison, 1980). An accumulation layer is proposed here to occur on chalcopyrite in alkaline solutions from the OCP at -0.1 V (vs Ag/AgCl) up to the conduction band edge at about 0.15 V (vs Ag/AgCl). These electrons are readily removed from the conduction band when the potential is applied, in a similar manner as for a metal (Gomes and Cardon, 1982). Also, if the potential is increased beyond the valence band edge, an inversion layer is created and current will flow via a hole mechanism. For chalcopyrite this would occur at about 0.95 V (vs Ag/AgCl).

Taking these factors into account, band diagrams can be used to visualise the mechanisms via accumulation/inversion layers and via surface states (Figure 4.21). Between the open circuit potential and 0.15 V (vs Ag/AgCl), electrons are removed from the accumulation layer in a one-step process. At potentials in the band gap between 0.15 and 0.75 V (vs Ag/AgCl), electrons tunnel from surface states to the conduction band. In the inversion region electrons tunnel from the valence band edge at the surface to the conduction band with mobile holes generated at the surface. This tunnelling can occur directly or via bulk defects in the mineral.

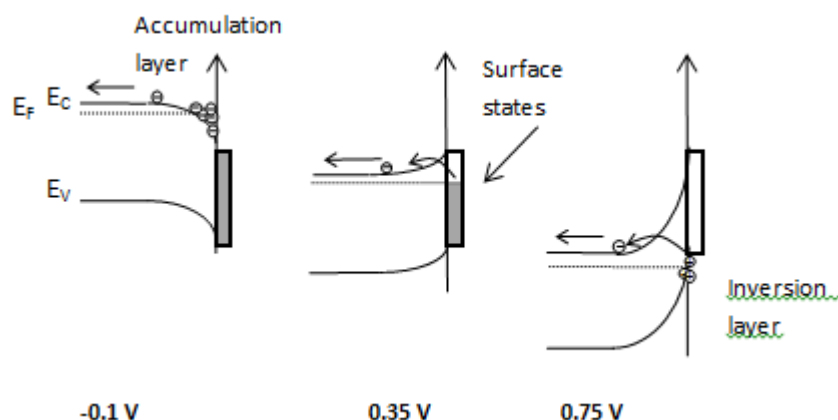


Figure 4.21: Band diagram for chalcopyrite in alkaline glycine solutions at different applied potentials (vs Ag/AgCl).

These three mechanisms are distinguished by different behaviours shown in the current potential curves in Figure 4.1 to Figure 4.6. From the open circuit potential to 0.15 V (vs Ag/AgCl), current increases with each potential step followed by a current decay with time typical of a relaxation process. A small plateau is observed at 0.15 V (vs Ag/AgCl), which coincides with the potential of the conduction band edge. From this point, electron exchange is via surface states and the current decay curves resemble an under damped second order system shown in Figure 4.8. This feature remains up to about 0.82 V (vs Ag/AgCl), after the applied potential crosses the valence band edge.

The two-step surface state mechanism described by other researchers is proposed for the band gap region (Crundwell, 2015; Gerischer, 1969; Vanmaekelbergh, 1997). First, electrons are removed from the surface to form holes at a rate proportional to the density of occupied surface states and the applied potential across the space charge layer. The second step is the reaction of the hole at the surface to form oxidation products such as copper glycinate, iron oxides and sulfur or sulfate. The first step is rate controlling up to about 0.45 V (vs Ag/AgCl) and is characterised by an increasing current with each potential step. Surface layers have no effect on the rate in this region, as evidenced by Figure 4.5 and Figure 4.6. As glycine is depleted at the surface by transport through the porous surface layer, the second step is rate limiting resulting in the plateau region.

The plateau region ends at 0.76 V (vs Ag/AgCl) which is the anticipated potential for the valence band edge. At this point electron exchange is no longer via surface states and so the reaction is not limited by this mechanism. A change in the slope of the capacitance-potential curve indicates an inversion region and a p-type conduction mechanism as seen in other studies (Crundwell et al., 2015). Current increases with potential in this region until it is finally limited by solution diffusion at about 0.9 V (vs Ag/AgCl). The current potential curves obtained in this study closely resemble the calculated curves for a surface state mechanism published by Vanmaekelbergh (1997).

The question remains as to why the behaviour is different to that for acid systems. The surface of chalcopyrite is different under each system, so it is possible that different surface states are involved. The current densities observed are a function of the density and occupancy of surface states. At around 0.75 V (vs Ag/AgCl) both systems undergo an increase in current and a change in slope of the capacitance curves. In this region the surface states would not be expected to play a role.

4.5 Conclusion

Anodic dissolution in alkaline glycine solutions did not show a passive region that is often seen in acidic solutions. This is despite surface species being formed that are often attributed to passivation, such as elemental sulfur and the metal-deficient sulfide. The anodic dissolution behaviour of chalcopyrite can be attributed to it being a non-ideal n-type semiconductor, with a high density of surface states. This research is consistent with recent studies that show the semiconducting properties should be considered in the anodic dissolution of chalcopyrite (Bryson et al., 2016; Crundwell et al., 2015; Olvera et al., 2016; Zhao et al., 2017; Zhou et al., 2015).

Future research on leaching chemistry should focus on applying a more effective oxidant than dissolved oxygen from air. A primary concern is that it should not break down glycine. Some progress has already been made in this area, where Cu^{2+} was shown to be a more effective oxidant than oxygen in glycine solutions (Nicol, 2017b). Optimisation of the process may yield more satisfactory results.

Chapter 5 Comparison of Electrochemical Dissolution of Metallic Copper and Semiconducting Chalcopyrite

5.1 Background

Chalcopyrite is often said to have the properties of a degenerate semiconductor, which means it will be metal-like in its electrochemical behaviour. Its slow leach rate is said to be due to the formation of a metal deficient sulfide or polysulfide that inhibits leaching as would an oxide on a metal in the well-established passivation process in corrosion science.

In the electrochemical experiments presented in this study, no evidence of passivation of chalcopyrite has been observed. The very low currents normally attributed to passivation in acidic media were not evident in alkaline glycine solutions. This is consistent with other studies that have also shown no passivation region in alkaline solutions of ammonia (Moyo et al., 2015; Nicol, 2017b; Warren and Wadsworth, 1984). There are many other differences between a truly passivated metal and a non-passivated semiconductor that is exhibiting its natural behaviour that will be highlighted in this chapter.

5.2 Current potential curves

Metallic copper shows a textbook passivation curve in alkaline glycine solutions, with well-defined active, passive and trans-passive regions as shown earlier in Figure 3.9. It has a passivation potential that varies with stir rate, glycine concentration and pH. The passive region is well defined with current density close to zero.

Conversely, chalcopyrite displays no classic passivation behaviour under the range of conditions studied in Chapter 5. The current generally increases with each potential step and shows no sharp drop that indicates passivation as seen in copper metal. Two plateau regions are observed. One corresponds with the onset of the band gap of chalcopyrite, and the main plateau is shown to be partially caused by surface iron oxyhydroxides in the potential region where surface states are rate determining. A comparison of the metal and semiconductor current-potential curves is shown in Figure 5.1.

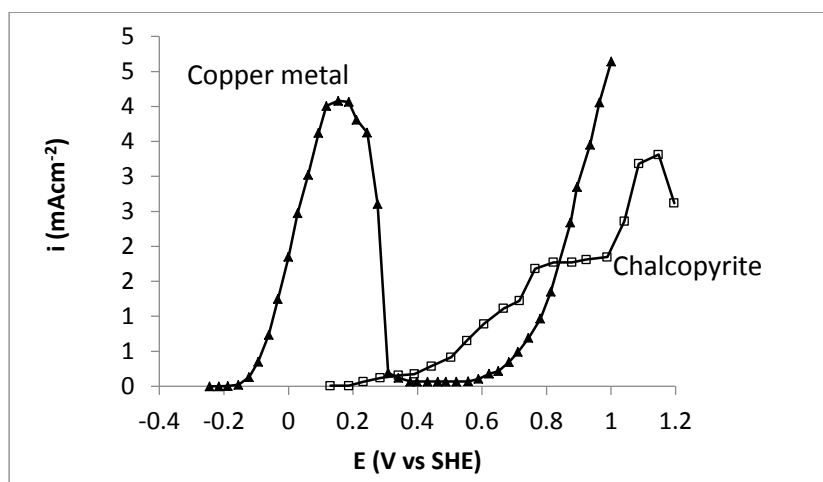


Figure 5.1: Comparison of copper metal undergoing passivation and semiconducting chalcopyrite. Conditions pH 10.5, 0.1 M glycine

5.3 Disk rotation

The metal and semiconductor disks show different behaviours with disk rotation (Figure 5.2). For a rotating copper metal electrode, the current increases with each potential step and remains constant for the step duration. If the electrode is still, the current decays with each step. This suggests transport of reactants through solutions determines the electrochemical response. There is a clear passive region for the non-rotating electrode, and none for the rotating electrode.

For the semiconducting chalcopyrite electrode, the current decays at each step both when rotating and when the electrode is held still. This is consistent with the idea that the current decay curve is determined by the solid state properties internal to the crystal. There is only a relatively small difference in current density between the rotating and non-rotating curves, and certainly nothing resembling passivation.

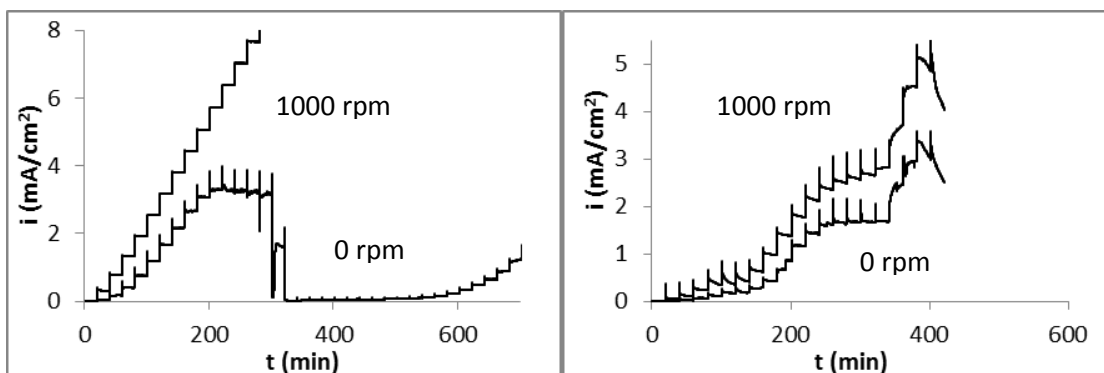


Figure 5.2: Comparison of current versus time graphs for copper metal (left) and chalcopyrite (right) with disk rotation of 0 rpm and 1000 rpm. Glycine concentration 0.1 M, pH 10.5.

This difference in solution as opposed to solid properties was also observed in the chronoamperometry experiments in Chapters 4 and 5. Reactivation of a passivated copper metal electrode occurs when the applied potential is removed and it is allowed to rest at the OCP. If stirring is then applied, high currents are achieved and maintained. If the electrode is held still, high currents briefly flow before passivation is re-established. The semiconductor also shows some increased activation after a rest at the OCP, but stirring does not enhance the current as it does for a metal, again suggesting the current decay is due to the properties internal to the mineral.

5.4 Capacitance

The capacitance of copper metal generally follows what is expected for the parallel plate capacitor model. The capacitance decreases with the increasing thickness of the passive layer as shown in section 3.2.4. For copper, the oxide layer is a duplex of CuO and Cu₂O. For chalcopyrite, the opposite is observed over most of the potential range. Capacitance decreases with potential as the current increases as shown in section 4.2.8. The capacitance is therefore not a reflection of a thickening surface layer but a combination of the capacitances of the interface, surface states, and the space-charge region of the semiconductor.

5.5 Surface analyses

Surface analyses of the metal and semiconductor after polarisation also show differences. The metal shows little sign of a passive layer after removal from the cell. This would be expected after observing the reactivation seen in the chronoamperometry experiments. Chalcopyrite shows a very different surface, with oxidised species present such as sulfur, sulfate and iron oxyhydroxides. Disulfides are also present which are often associated with a metal deficient layer. These are obviously non-passivating, as evidenced by the high currents observed at these potentials and the enhanced activation after a rest at the OCP.

5.6 Summary

In summary, there is little similarity in the electrochemical behaviour of semiconducting chalcopyrite and metallic copper in alkaline glycine solutions. This is observed in current – potential curves, the effect of disk rotation, chronoamperometry, capacitance and surface analyses.

While it may seem sensible to speculate that natural chalcopyrite should contain enough impurities that would render it degenerate and hence metal-like in behaviour, the evidence here does not support this.

Chapter 6 Chalcopyrite Leaching in Alkaline Glycine Solutions

The fundamental electrochemical work in the preceding chapters has indicated that chalcopyrite leaching is not inhibited by passivation. An oxidant with a redox potential that overlaps the conduction band should allow dissolution. Stronger oxidants that overlap the valence band are likely to also react with glycine and inhibit its complexing properties. For this study, bottle roll tests were carried out with the relatively mild oxidants ferricyanide and triiodide. These have been previously identified as being reduced at a fast rate on the chalcopyrite surface in electrochemistry experiments, and so are likely to be effective oxidants (Parker et al., 1981).

6.1 Experimental

6.1.1 Sample details

A low grade chalcopyrite sample sized to $-106 \mu\text{m} + 75 \mu\text{m}$ was used in this study. This is a relatively coarse size compared to other studies in the literature and was chosen to eliminate any enhanced leaching effects from fine sizes. The elemental assay is shown in Table 6.1.

Table 6.1: Elemental assay sample used for leach tests

element	Abundance (%)
Cu	13.7
Ni	0.0
Fe	33.4
Si	2.7
Al	0.7
Ca	0.3
S	35.7
Zn	4.2
Pb	0.4
As	0.8

XRD showed this sample comprised chalcopyrite as the only copper mineral at 35%, with the main gangue being pyrite at about 30% and with 30% amorphous material likely to be silicates.

6.1.2 Leaching process

Bottle roll tests were carried out in 2 litre bottles rotated at 100 rpm. A heated cabinet was used for tests at 55°C, other tests were carried out at ambient temperature of 25°C. One gram of sample was added to the bottle with 500 mL of Perth tap water. The pH was adjusted by sodium hydroxide or sulfuric acid. Ferricyanide and triiodide were used as oxidants for the glycine leach, ferric sulfate was used for the acid leach. Samples were taken at regular intervals during the leach process. The triiodide ion is generated when iodine reacts with excess iodide (Guan and Han, 1997). For this work, potassium iodide was added at a ratio of ten to one with iodine. The equation for triiodide formation is shown in Equation 17. For leaching with grinding media, a single test with 50 g of 10 mm ceramic balls was used.



6.2 Results and discussion

6.2.1 Oxidant requirements

The molar requirements of oxidant were calculated based on Equation 11 and Equation 12 in section 2.6.6. For the sulfur in chalcopyrite to be oxidised to sulfate, 17 electrons need to be removed, for elemental sulfur it would require 5. The relatively high molecular weights of ferricyanide and iodine dictate that a high mass of oxidant is needed to oxidise the chalcopyrite in the sample. For this reason only 1 gram of chalcopyrite was used to keep the reagents at a manageable level.

Table 6.2: Oxidant requirements for 1 gram of chalcopyrite.

oxidant	E ⁰ V (vs SHE)	Molar mass (g/mol)	Mass to oxidise to S (g)	Mass to oxidise to SO ₄ ²⁻ (g)
K ₃ [Fe(CN) ₆]	0.35	329.2	3.5	12.1
I ₂ (for I ₃ ⁻ generation)	0.54	253.8	1.4	4.7
NaClO ₃	0.7	106.4	1.1	3.9

For the initial tests, the minimum stoichiometric weight requirements of oxidant were doubled to allow an excess to favour the oxidation of chalcopyrite. Staged oxidant additions were also trialled with further excess oxidant added for each step. For the acidic ferric sulfate test, a 0.15 M ferric concentration was used. It has been shown in other studies that increasing the ferric concentration up to 0.1 M increases the leach rate, with no influence using higher concentrations (Córdoba et al., 2008). Finally a test with a small amount of grinding media was carried out with a smaller staged addition of oxidant. A summary of the oxidant dosage scheme is presented in Table 6.3. Potassium iodide was added at 10 times the mass of iodine added at zero hours.

Table 6.3: Mass of oxidants added for each test

Oxidant	Time (h)						
	0	1	2	4	6	24	30
K ₃ Fe(CN) ₆ low (g)	8						
K ₃ Fe(CN) ₆ high (g)	25						
I ₂ low (g)	3						
I ₂ high (g)	9.5						
K ₃ Fe(CN) ₆ staged (g)	25		25		25	25	25
I ₂ staged (g)	9.5		9.5		9.5	9.5	9.5
NaClO ₃ (g)	15				15		
NaClO ₃ + K ₃ Fe(CN) ₆ (g)	15, 25				15, 0		
K ₃ Fe(CN) ₆ (g) + grind	25			25			

6.2.2 Effect of oxidant concentration

The results for the experiments with a single up front oxidant addition are shown in Figure 6.1. It can be seen that the copper extraction is far greater with the use of triiodide or ferricyanide compared to the acid leach with ferric ion. This is a fundamental change in leaching behaviour and supports the theory that chalcopyrite leaches as a semiconductor.

The standard potential for the ferric/ferrous ion couple is 0.77 V (vs SHE) which is within the band gap of chalcopyrite and so would not be expected to be effective as an oxidant. Ferricyanide overlaps the conduction band at 0.35 V (vs SHE) and yields the highest final recoveries for comparable oxidant concentrations. Triiodide also gives a good recovery, slightly less than ferricyanide. The standard potential for triiodide is 0.54 V (vs SHE), which is just inside the band gap for chalcopyrite. Unlike ferric acid systems, the leach rate increases with increasing oxidant concentration.

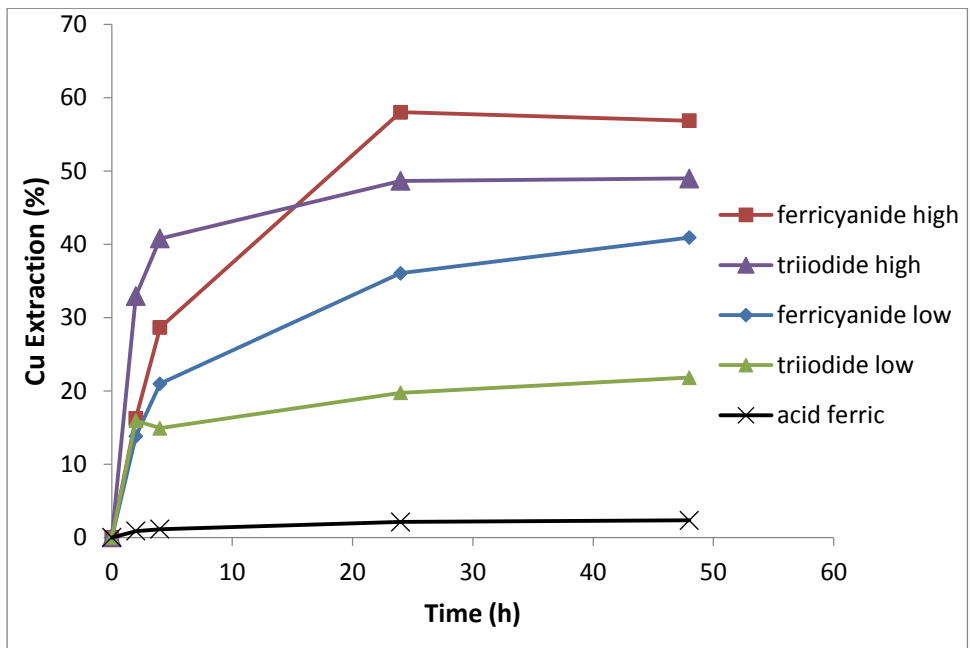


Figure 6.1: Comparison of alkaline glycine leaches at pH 10 with 0.3 M glycine and 0.15 M ferric leach. All were carried out at 55°C. Reagent dosages are specified in Table 6.3

The variations in solution potential and pH are shown in Figure 6.2. It can be seen that the pH is fairly constant, and was adjusted back to 10.0 where needed. The Eh was observed to drop constantly throughout the experiment, as the oxidant is consumed.

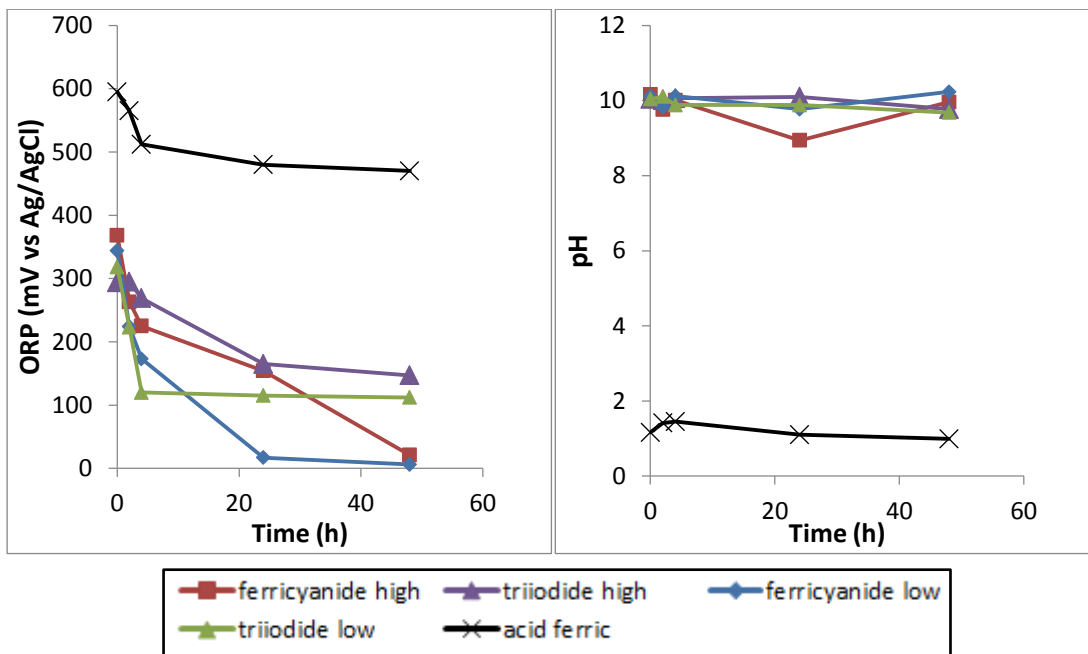


Figure 6.2: ORP and pH for the comparative leach tests in Figure 6.1

6.2.3 Effect of staged oxidant addition

The increase in leach recovery with increasing oxidant observed in Figure 6.1 suggests that a greater excess of oxidant is required to allow complete recovery of copper from chalcopyrite. A staged addition of chalcopyrite was carried out where an equivalent mass was added at 2, 6, 24 and 30 hours. The results of this staged addition are shown in Figure 6.3.

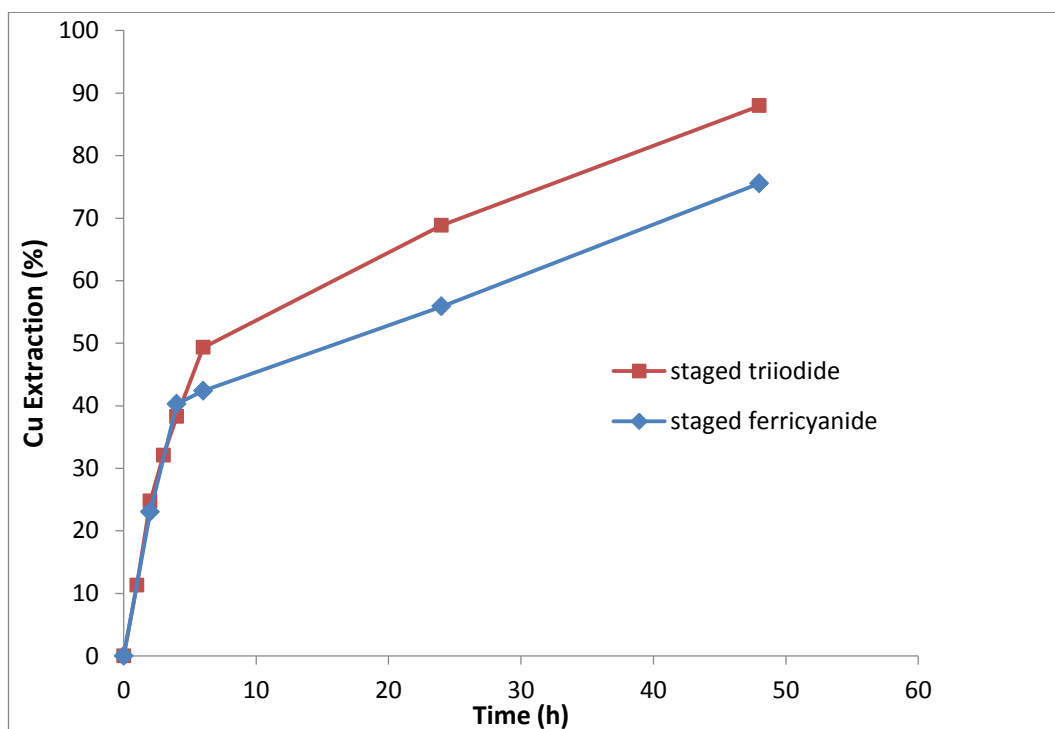


Figure 6.3: Effect of staged additions of ferricyanide and triiodide. All were carried out at 55°C

It can be seen that with a staged addition copper recovery is enhanced and continues increasing until the termination of the test. The leaching is clearly not inhibited by passivation, but by the availability of the oxidant. In this case triiodide allows a slightly faster leach rate compared to ferricyanide after 6 hours. The ORP and pH are shown in Figure 6.4 .

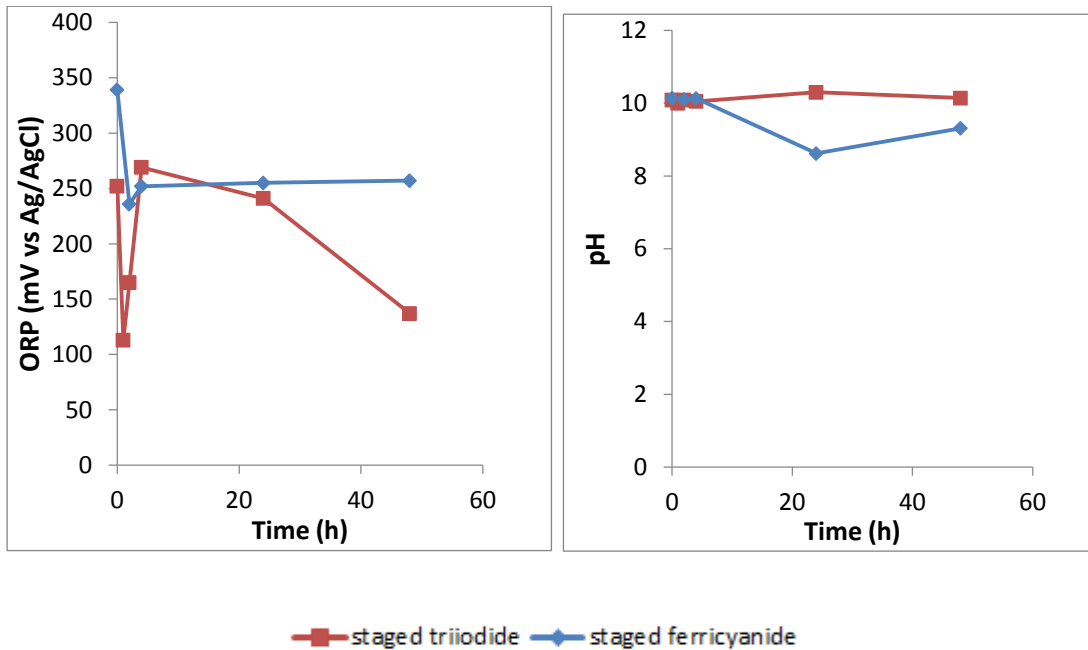


Figure 6.4: ORP and pH for the staged oxidant addition tests

6.2.4 Comparison with stronger oxidants

Chlorate is known to be an effective oxidant for chalcopyrite in acidic solutions with high recoveries in short times (Xian et al., 2012). The standard redox potential in acid solutions at pH 0 is 1.451 V (vs SHE) (Watling, 2013). However in alkaline solutions at pH 10 the potential is about 0.77 V (vs SHE), which is within the band gap of chalcopyrite and so should be less effective as an oxidant.

If the copper extraction with chlorate as the oxidant is low, it might be argued that chlorate is oxidising the glycine and therefore reducing its complexing ability. To eliminate this possibility, a blend of chlorate and ferricyanide was used for comparison. If chlorate was indeed oxidising the glycine, it would be shown by a poor copper recovery for the blend of the two oxidants too. The results for this test are shown in Figure 6.5.

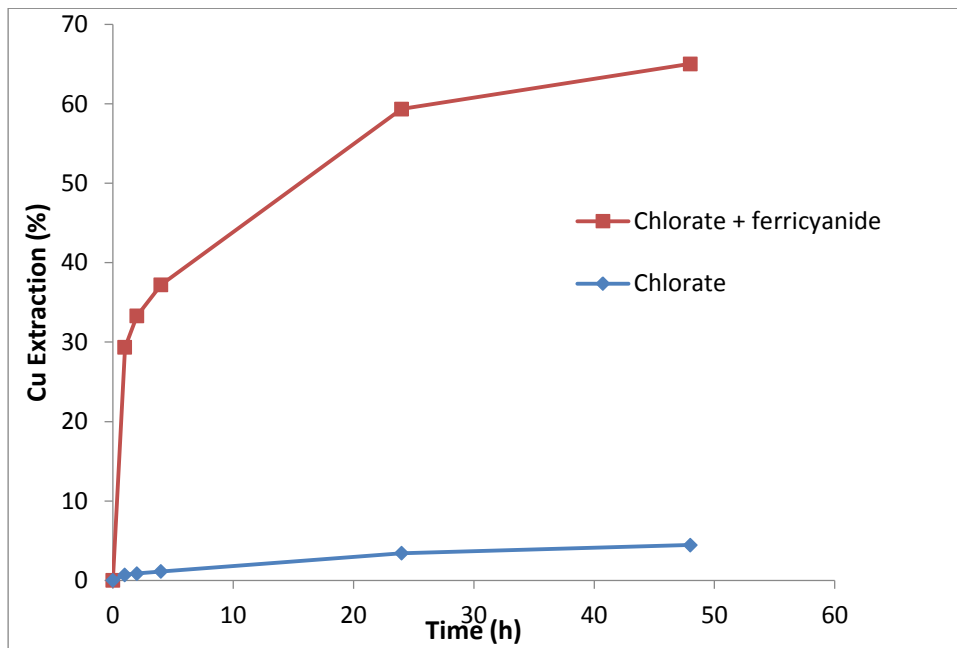


Figure 6.5: Comparison of chlorate leach to a ferricyanide and ferricyanide/chlorate blend in 0.3 M glycine at 25°C at pH 10

It can be seen that chlorate is not an effective oxidant. This was observed visually in the early stages of the experiment and the chlorate concentration was doubled at 4 hours in an attempt to improve the extraction. The blend of chlorate and ferricyanide gives a slightly better result than ferricyanide alone, indicating that glycine is not oxidised by chlorate in the time of the experiment. The result is slightly better than ferricyanide alone, perhaps because of a replenishment of ferricyanide to the +3 oxidation state by the chlorate. The ORP dropped rapidly in the chlorate system as can be seen in Figure 6.6

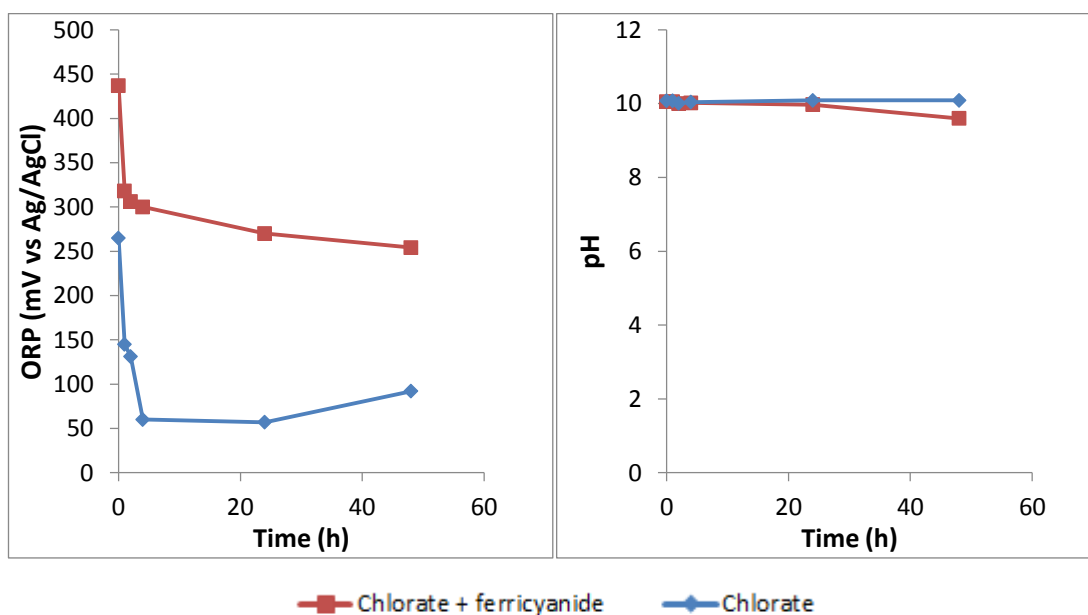


Figure 6.6: ORP and pH for chlorate and ferricyanide. pH 10, 0.3 M glycine.

The results here generally agree with what would be expected through semiconductor theory. That is, electron exchange occurs readily with the triiodide/iodide and ferric/ferro cyanide redox couples that have a standard potential that is near the conduction band edge of chalcopyrite, allowing electron exchange. Oxidants with a standard potential in the band gap such as ferric/ferrous and chlorate /chloride are ineffective, despite having higher standard potentials.

The electrochemical work in Chapter 4 showed that electron exchange could occur in the band gap through surface states. That did not seem to occur here for chlorate or for ferric ion in acid solution. The reason is speculative, but could be due to the different mechanism of electron extraction. In a chalcopyrite electrode, electrons are removed by a potential applied from a potentiostat through the conduction band. In leaching experiment it is through the species in solution.

Previous studies have been carried out on this on this sample using dissolved oxygen as an oxidant (Tanda, 2017). In this work, copper extraction reached about 20% in 48 hours with 15 ppm O₂ at 50 °C using 0.5 M glycine at pH 11.5. While lower than the extractions achieved here, this process may still be viable for applications such as heap leaching, provided that enough oxygen can be supplied to the system.

6.2.5 Leaching with Grinding Media

It has been shown that high levels of agitation are beneficial to leaching of chalcopyrite in alkaline ammonia solutions (Beckstead and Miller, 1977; Stanczyk and Rampacek, 1966). This has partly been attributed to the removal of iron oxides from the surface. In this work, 50 g of 10 mm ceramic balls were added to a bottle roll test to allow removal of lightly adhering oxide layers. The result is shown in Figure 6.7.

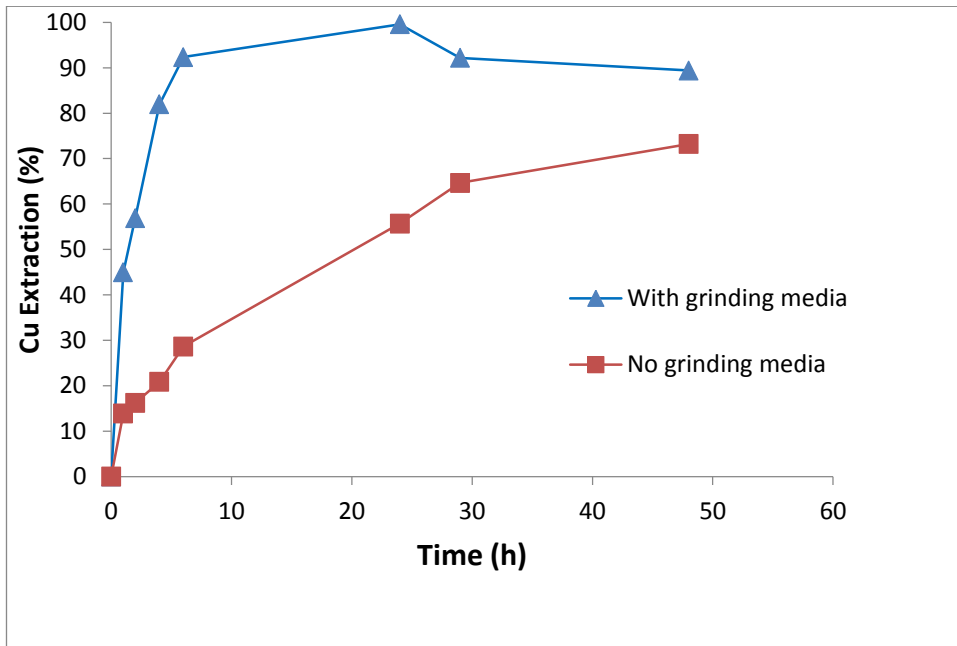


Figure 6.7: Leaching with grinding media at 25°C, pH 10, 0.3 M glycine. 25 g of ferricyanide added at 0 and 4 hours.

Almost 100% copper extraction was achieved in 24 hours, but some copper appears to have precipitated from solution after this time. The oxidant demand was not as high as it was for the tests with no grinding media present. A staged approach was taken with oxidant addition with an additional 25 g added at 4 hours. At this time the extraction was at 82%, compared to 21% where no media was used.

The high recovery obtained in this experiment may be due to a greater mineral surface area, or through improved liberation of fine chalcopyrite from gangue. Further work such as a mineral liberation study would reveal what the ultimate chalcopyrite grain size is for the +77 μm size fraction. This would clarify if the rate increase is due to enhanced liberation or increased surface area. The ORP and pH are shown in Figure 6.8

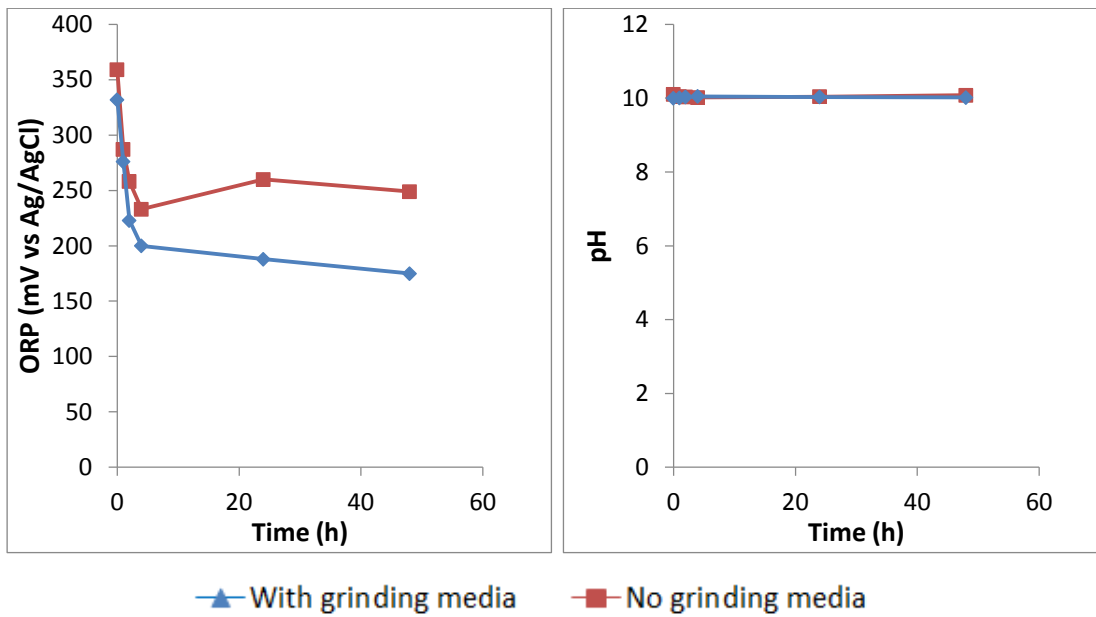


Figure 6.8: ORP and pH for tests with and without grinding media in the bottle.

6.2.6 Images of Leach Residue

Images of the leach residues were taken at 230x magnification using a Dino Capture 2.0 optical microscope. In Figure 6.9, the fresh chalcopyrite sample is shown on the left compared to the residues from 48 hours of ferric acid leaching on the right. There is little appreciable difference, except an absence of some fines that were present in the feed.

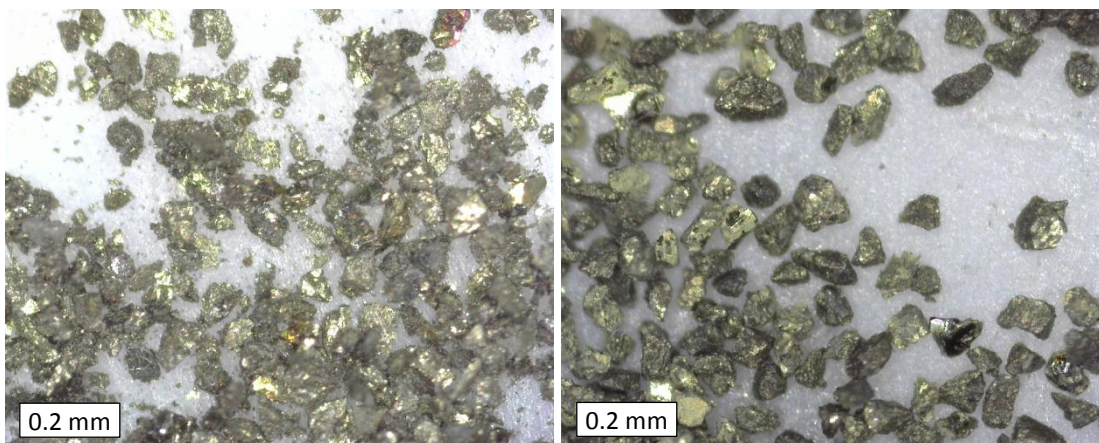


Figure 6.9: Fresh chalcopyrite (left) compared with acid leached residue (right)

Two partially leached samples from the alkaline glycine process are shown in Figure 6.10. On the left is the sample leached in ferricyanide, on the right is the sample leached in triiodide. These show a partial covering of iron oxides on the surface. For the sample leached in triiodide, the samples appear to also have a light violet colour which may be due to the iodine, as observed by others (Guan and Han, 1997).

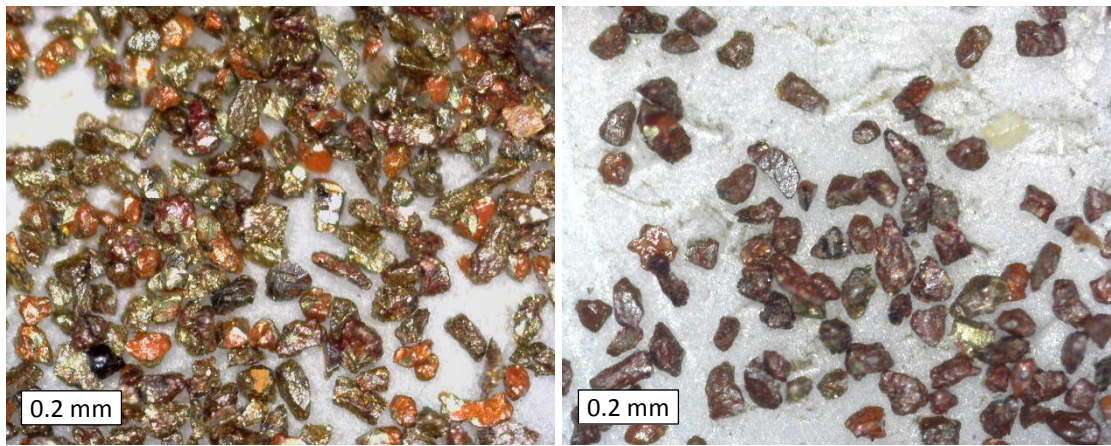


Figure 6.10: Chalcopyrite partially leached with low oxidant dosages. On the left is the ferricyanide leach, on the right is the triiodide leach

Two samples leached with higher doses of oxidant are shown in Figure 6.11. The sample leached in ferricyanide on the left appears to have less of an oxide coating than the previous sample. The sample leached in triiodide has a more extensive covering, possibly also with iodine species

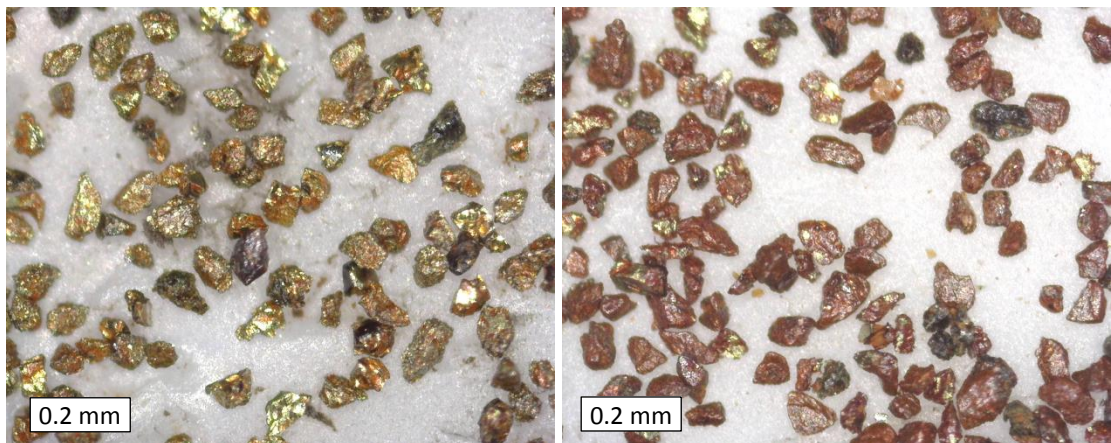


Figure 6.11: Chalcopyrite leached to about 50% to 55% copper extraction using high oxidant dosage. Ferricyanide (left); triiodide (right).

Samples that were leached with a staged addition of oxidants are shown in Figure 6.12. In these tests copper extraction was 73% for the ferricyanide experiment on the left and 85% for the triiodide experiment on the right. Remnant iron oxide particles are evident in both images, again with a different colour for the iodide leach.

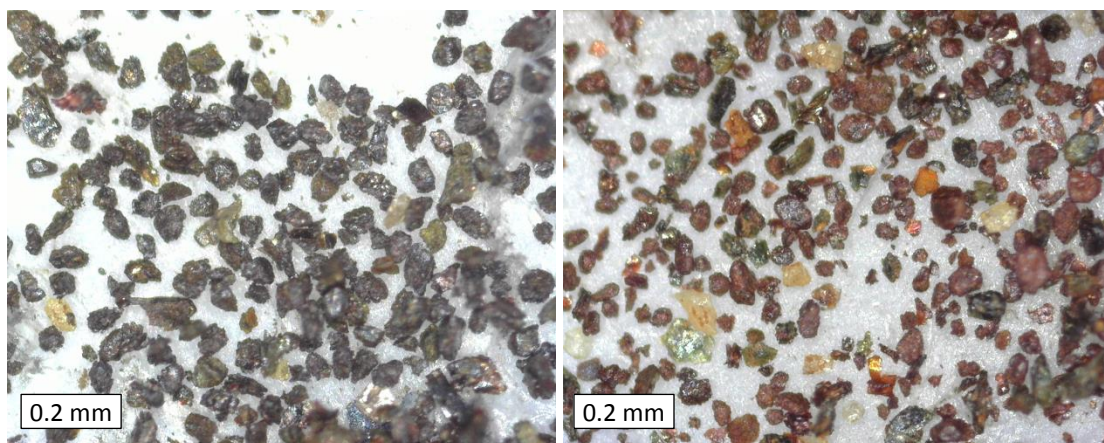


Figure 6.12 Chalcopyrite leached with a staged addition of a large excess of oxidant. Ferricyanide (left); triiodide (right).

6.2.7 Summary

Chalcopyrite can be leached with an appropriate oxidant in alkaline glycine solutions with no significant inhibition due to passivation. The extraction can be increased by increasing the concentration or by adding some grinding media to the bottle roll test. High quantities of oxidant are required to return high extractions, due to the need to extract 17 electrons per atom of copper. This is not suggested to be an economically feasible method for leaching chalcopyrite, but does demonstrate that passivation is not responsible for slow leach rates. Further research should be directed towards a cheaper oxidant, or a method for economically recycling the oxidants studied here.

Chapter 7 Conclusions and Recommendations

This study has shown that chalcopyrite behaves as expected for a non-ideal n-type semiconducting mineral in alkaline glycine solutions. It has no metal-like behaviour that would be expected if it were a degenerate semiconductor. This is evidenced by comparisons to metallic copper. Metallic copper displays typical behaviour of a metal showing passivation under conditions of low glycine concentration in quiescent solutions.

7.1 Metallic copper

Metallic copper shows electrochemical behaviour consistent with previous studies that can be extended to higher temperatures and glycine concentrations. It demonstrated genuine passivation at high pH values that could be of concern in a leaching operation. An optimal leaching pH was 10 at 60°C and 10.5 at 25°C. At higher temperatures, dissolution is enhanced further with increasing glycine concentration through an interaction effect.

The copper glycinate complex itself is an effective oxidant and can enhance dissolution through an autocatalytic process. The copper (II) is reduced to Cu(I) which can be readily oxidised back by dissolved oxygen. Increasing the copper concentration increased the corrosion current density considerably.

When a passive layer was generated it broke down upon removal of applied potential. Stirring prevented the formation of a layer, showing that solution conditions dictate the passivation effect. The passive layer showed capacitance behaviour consistent with that of a parallel plate capacitor.

7.2 Chalcopyrite

The literature on chalcopyrite electrochemistry and leaching is vast and inconsistent. There is some consensus that leaching is inhibited by a passive metal deficient sulfide layer but there are a growing number of researchers who disagree (Acero et al., 2007; Crundwell, 2015; Klauber, 2008; Mikhlin et al., 2004). The metal deficient passive layer has never been observed experimentally, unlike for example the well-known metal deficient covellite that forms on chalcocite during leaching (Burkin, 1969). The few studies that have investigated the surface layer in depth have based its existence solely on the presence of a disulfide peak in XPS. This is said to represent the metal deficient sulfide formed during the initial oxidation, but no explanation is given for its presence on unleached samples, or even samples held under reducing conditions.

In this study, the metal deficient sulfide species, inferred from a disulfide peak was also found on samples held at all potentials. This is consistent with what is seen in acid solutions by other researchers. These had no passivating effect on chalcopyrite. A porous iron oxyhydroxide layer impeded the dissolution at potentials where surface states played a role in electron transfer between 0.5 and 0.75 V (vs Ag/AgCl). This layer was not fully passivating and still allowed high rates of electron flow. At other potentials the layer had no significant effect on the dissolution rate. Even long step times of an hour showed this oxide layer did not prevent electron flow, with high current densities recorded. Leaching experiments also showed high extraction rates when the iron oxide layer was present.

The rotation of the chalcopyrite electrode had no appreciable effect on the current potential curve at any speed above 0 rpm. Slow rotation rates were enough to allow transport of reactants and products to and from the surface. An exception to this was at potentials above 0.9 V (vs Ag/AgCl) where the current density increased with rotation speed. This is likely due to increased transport of glycine to the surface and high dissolution rates. At low rotation rates glycine is depleted at the surface and alternative copper oxides are formed.

The trend of capacitance with potential did not follow the parallel plate model that is seen for metals with an oxide layer, and speculated for chalcopyrite in acid solutions. Instead, the capacitance decreases during the initial potential steps while the current increases. This reflects a complex contribution from the space charge layer, surface states and the mineral/solution double layer to the total capacitance. A change in slope of the capacitance at about 0.76 V (vs Ag/AgCl) coincides with the expected edge of the valence band and is consistent with a change from n-type to p-type conductivity.

XPS and Raman spectroscopy showed elemental sulfur and disulfides (suggesting a metal deficient sulfide) were present within the iron oxyhydroxide surface layer. These did not have any major inhibiting effect on the dissolution. These layers were present at all potentials, both in plateau regions and regions of increasing current.

Chronoamperometry showed a current decay pattern at most potentials. Stirring had no influence on this, unlike for copper metal which did not show a decay pattern with stirring. This suggests that the properties internal to the mineral, not the solution dictate this behaviour. An enhanced activation occurred if the sample was rested at the OCP for 30 s, but again unlike for the metal, current decay occurred even with stirring upon reapplication of potential.

Leaching experiments confirmed the results from electrochemistry, showing that relatively mild oxidants such as triiodide and ferricyanide were more effective than chlorate or ferric ion. These oxidants have a standard redox potential that corresponds to the energy of the conduction band edge. The extent of dissolution increased with increasing concentration of oxidant, and no passivation was observed in chemical leaching. Large quantities of oxidant were required to leach copper, due to the requirement for sulfide to be oxidised to sulfate.

7.3 Further study

The dissolution of chalcopyrite in alkaline glycine solutions is mostly dependent upon the availability of an appropriate oxidant that overlaps one of the populated energy bands. With 17 moles of electrons needed for each mole of copper, the challenge lies in finding a cheap oxidant or one which is easily regenerated. There might be some benefit from a blend of oxidants, with a primary oxidant that interacts with the conduction band of chalcopyrite and a secondary oxidant that regenerates the primary one as it is depleted. This effect has been seen in blends of ferric/cupric oxidants in acid solutions (Parker et al., 1981)

Further study with synthetic samples using known doping concentrations would settle the claim that natural chalcopyrite behaves as a degenerate semiconductor. Synthetic chalcopyrite samples have been widely studied for their semiconducting properties. Research resources should be directed away from attempting to study an unproven passive layer and into the characterisation of the electronic structure of chalcopyrite. There are promising fundamental characterisation studies underway with methods such as scanning tunnelling microscopy, low energy electron diffraction and ultra violet photoelectron spectroscopy (Rosso, 2001). Linking these with leaching and electrochemical behaviour might provide insights into finding an economic process for leaching chalcopyrite at an industrial scale.

References

- Acero, P., Cama, J. and Ayorya, C., 2007. Kinetics of chalcopyrite dissolution at pH 3. *European Journal of Mineralogy*, 19(2): 173-182.
- Adams, M.D., 2005. *Advances in gold ore processing* / edited by Mike D. Adams. Boston : Elsevier, Boston.
- Aksu, S. and Doyle, F.M., 2001. Electrochemistry of Copper in Aqueous Glycine Solutions. *Journal of The Electrochemical Society*, 148(1): B51-B57.
- Aksu, S. and Doyle, F.M., 2002. The Role of Glycine in the Chemical Mechanical Planarization of Copper. *Journal of The Electrochemical Society*, 149(6): G352-G361.
- Altundođan, H.S. and Tümen, F., 1997. Metal recovery from copper converter slag by roasting with ferric sulphate. *Hydrometallurgy*, 44(1-2): 261-267.
- Ammou-Chokroum, M., Cambazoglu, M. and Steinmetz, D., 1977. Oxidation Menagee de la Chalcopyrite en Solutionacide: Analyse CINETIQUE des Reactions: I. Modeles Chimiques. *Bull. Soc. Fr. Mineral. Cristallogr. / Bulletin de la Societe Française De Mineralogie Et De Cristallographie.*, 100: 16.
- Arbiter, N. and McNulty, T., 1999. Ammonia leaching of copper sulfide concentrates, *Copper 99-Cobre 99*, Vol. IV, *Hydrometallurgy of copper*. The Minerals, Metals & Materials Society, Warrendale, pp. 197-212.
- ASTM, 2014. *Standard Test Method for Conducting Potentiodynamic Polarization Resistance Measurements*. ASTM International, West Conshohocken, pp. 1-4.
- ASTM, 2016. *Standard Test Methods for Measuring Resistivity and Hall Coefficient and Determining Hall Mobility in Single-Crystal Semiconductors*. ASTM International, West Conshohocken, pp. 14.
- Ateya, B.G., Geh, G., Carim, A.H. and Pickering, H.W., 2002. Selective Dissolution below the Critical Potential and Back Alloying in Copper-Gold Alloy. *Journal of The Electrochemical Society*, 149(2): B27-B33.
- Azizkarimi, M., Tabaian, S.H. and Rezai, B., 2014. Electrochemical Investigation of Chalcopyrite Oxidation in Alkaline Solutions. *Separation Science and Technology*, 49(16): 2595-2601.
- Bard, A. and Faulkner, L., 2001. *Electrochemical Methods* 2nd ed 2001. John Wiley & Sons, New York.
- Beckstead, L.W. and Miller, J.D., 1977. Ammonia, oxidation leaching of chalcopyrite-surface deposit effects. *Metallurgical Transactions B (Process Metallurgy)*, 8B(1): 31-8.
- Benedict, C.H., 1917. Ammonia Leaching of Calumet Tailings. *Engineering and Mining Journal*, 104: 3.
- Biegler, T. and Horne, M.D., 1985. The Electrochemistry of Surface Oxidation of Chalcopyrite. *Journal of The Electrochemical Society*, 132(6): 1363-1369.
- Biegler, T. and Swift, D.A., 1979. Anodic electrochemistry of chalcopyrite. *J Appl Electrochem*, 9(5): 545-554.
- Braun, F., 1875. Ueber die Stromleitung durch Schwefelmetalle. *Annalen der Physik*, 229(12): 556-563.
- Brett, C. and Brett, A., 1993. *Electrochemistry Principles, methods, and Applications*. Oxford University Press, New York.
- Bryson, L.J. and Crundwell, F.K., 2014. The anodic dissolution of pyrite (FeS₂) in hydrochloric acid solutions. *Hydrometallurgy*, 143: 42-53.
- Bryson, L.J., van Aswegen, A., Knights, B. and Crundwell, F.K., 2016. Investigation of the Mechanism of Dissolution of Chalcopyrite using Photo-Effects. , *Hydrometallurgy Conference 2016: Sustainable Hydrometallurgical Extraction of Metals*. Southern African Institute of Mining and Metallurgy, Cape Town, pp. 173-184.

- Buckley, A. and Woods, R., 1984. An X-ray photoelectron spectroscopic study of the oxidation of chalcopyrite. *Australian Journal of Chemistry*, 37(12): 2403-2413.
- Burkin, A.R., 1969. Solid-State Transformations During Leaching. *Minerals science and engineering*, 1(1).
- Burstein, G.T. and Newman, R.C., 1981. Reactions of Scratched Copper Electrodes in Aqueous Solutions. *Journal of The Electrochemical Society*, 128(11): 2270-2276.
- Chen, G., Zen, J.M., Fan, F.R.F. and Bard, A.J., 1991. Electrochemical investigation of the energetics of irradiated FeS₂ (pyrite) particles. *The Journal of Physical Chemistry*, 95(9): 3682-3687.
- Córdoba, E.M., Muñoz, J.A., Blázquez, M.L., González, F. and Ballester, A., 2008. Leaching of chalcopyrite with ferric ion. Part I: General aspects. *Hydrometallurgy*, 93(3-4): 81-87.
- Crundwell, F.K., 1988. The influence of the electronic structure of solids on the anodic dissolution and leaching of semiconducting sulphide minerals. *Hydrometallurgy*, 21(2): 155-190.
- Crundwell, F.K., 2013. The dissolution and leaching of minerals: Mechanisms, myths and misunderstandings. *Hydrometallurgy*, 139: 132-148.
- Crundwell, F.K., 2015. The semiconductor mechanism of dissolution and the pseudo-passivation of chalcopyrite. *Canadian Metallurgical Quarterly*, 54(3): 279-288.
- Crundwell, F.K. et al., 2015. The effect of visible light on the dissolution of natural chalcopyrite (CuFeS₂) in sulphuric acid solutions. *Hydrometallurgy*, 158: 119-131.
- Cui, J. and Zhang, L., 2008. Metallurgical recovery of metals from electronic waste: A review. *Journal of Hazardous Materials*, 158(2-3): 228-256.
- Dai, X. and Breuer, P.L., 2013. Leaching and electrochemistry of gold, silver and gold-silver alloys in cyanide solutions: Effect of oxidant and lead(II) ions. *Hydrometallurgy*, 133: 139-148.
- De Chialvo, M.R.G., Marchiano, S.L. and Arví, A.J., 1984. The mechanism of oxidation of copper in alkaline solutions. *J Appl Electrochem*, 14(2): 165-175.
- Drissi-Daoudi, R., Irhzo, A. and Darchen, A., 2003. Electrochemical investigations of copper behaviour in different cupric complex solutions: Voltammetric study. *J Appl Electrochem*, 33(3): 339-343.
- Dutrizac, J., 1989a. Elemental Sulphur Formation During the Ferric Sulphate Leaching of Chalcopyrite. *Canadian Metallurgical Quarterly*, 28(4): 337-344.
- Dutrizac, J., McDonald, R.J.C. and Ingraham, T.R., 1969. The Kinetics of Dissolution of Synthetic Chalcopyrite in Aqueous Acidic Ferric Sulfate Solutions.
- Dutrizac, J.E., 1978. The kinetics of dissolution of chalcopyrite in ferric ion media. *MTB*, 9(3): 431-439.
- Dutrizac, J.E., 1981. Ammoniacal Percolation Leaching of Copper Ores. *Canadian Metallurgical Quarterly*, 20(3): 307-315.
- Dutrizac, J.E., 1982. Ferric ion leaching of chalcopyrites from different localities. *MTB*, 13(3): 303-309.
- Dutrizac, J.E., 1989b. Elemental sulphur formation during the ferric chloride leaching of chalcopyrite. *Hydrometallurgy*, 23(2-3): 153-176.
- Eksteen, J.J., Oraby, E.A. and Tanda, B.C., 2017. A conceptual process for copper extraction from chalcopyrite in alkaline glycinate solutions. *Minerals Engineering*, 108: 53-66.
- Free, M.L., 2013. *Hydrometallurgy : Fundamentals and Applications*. John Wiley & Sons, Somerset, NJ, USA.
- Fuerstenau, M., 2007. *Froth Flotation : A Century of Innovation*. Littleton : SME, Littleton.
- Geoscience Australia, 2012. *Copper*. In: K. Porritt (Ed.).
- Gerischer, H., 1969. On the role of electrons and holes in surface reactions on semiconductors. *Surface Science*, 13(1): 265-278.
- Ghahremaninezhad, A., Asselin, E. and Dixon, D.G., 2010. Electrochemical evaluation of the surface of chalcopyrite during dissolution in sulfuric acid solution. *Electrochimica Acta*, 55(18): 5041-5056.

- Ghahremaninezhad, A., Dixon, D.G. and Asselin, E., 2013. Electrochemical and XPS analysis of chalcopyrite (CuFeS₂) dissolution in sulfuric acid solution. *Electrochimica Acta*, 87(0): 97-112.
- Gomes, W.P. and Cardon, F., 1982. Electron energy levels in semiconductor electrochemistry. *Progress in Surface Science*, 12(2): 155-215.
- Gomes, W.P. and Vanmaekelbergh, D., 1996. Impedance spectroscopy at semiconductor electrodes: Review and recent developments. *Electrochimica Acta*, 41(7): 967-973.
- Grano, S.R., Sollaart, M., Skinner, W., Prestidge, C.A. and Ralston, J., 1997. Surface modifications in the chalcopyrite-sulphite ion system. I. collectorless flotation, XPS and dissolution study. *International Journal of Mineral Processing*, 50(1): 1-26.
- Grdeń, M., 2014. Interfacial capacitance of an oxidised copper electrode. *Journal of Electroanalytical Chemistry*, 713(Supplement C): 47-57.
- Greenawalt, W.E., 1912. *The Hydrometallurgy of Copper*. McGraw-Hill, New York.
- Guan, Y.C. and Han, K.N., 1997. The leaching kinetics of chalcopyrite (CuFeS₂) in ammonium iodide solutions with iodine. *Metall and Materi Trans B*, 28(6): 979-985.
- Habashi, F., 1965. Kinetics of corrosion of metals. *Journal of Chemical Education*, 42(6): 318.
- Habashi, F., 1978. *Chalcopyrite : its chemistry and metallurgy*. McGraw-Hill, New York.
- Hackl, R.P., Dreisinger, D.B., Peters, E. and King, J.A., 1995. Passivation of chalcopyrite during oxidative leaching in sulfate media. *Hydrometallurgy*, 39(1-3): 25-48.
- Halpern, J., Milants, H. and Wiles, D.R., 1959. Kinetics of the Dissolution of Copper in Oxygen-Containing Solutions of Various Chelating Agents. *Journal of The Electrochemical Society*, 106(8): 647-650.
- He, J.-B., Lu, D.-Y. and Jin, G.-P., 2006. Potential dependence of cuprous/cupric duplex film growth on copper electrode in alkaline media. *Applied Surface Science*, 253(2): 689-697.
- Heath, A.R. and Rumball, J.A., 1998. Optimising cyanide:oxygen ratios in gold cip/cil circuits. *Minerals Engineering*, 11(11): 999-1010.
- Holmes, P.R. and Crundwell, F.K., 2013. Polysulfides do not cause passivation: Results from the dissolution of pyrite and implications for other sulfide minerals. *Hydrometallurgy*, 139(0): 101-110.
- House, J.E., 2013. *Inorganic chemistry / James E. House. Inorganic Chemistry*. Waltham [Mass.] : Academic Press/Elsevier, Waltham [Mass.].
- Hua, X. et al., 2018. Leaching Mechanism and Electrochemical Oxidation on the Surface of Chalcopyrite in Ammonia-Ammonium Chloride Solution. *Journal of The Electrochemical Society*, 165(10): E466-E476.
- Huerta, F., Morallón, E., Vázquez, J.L., Pérez, J.M. and Aldaz, A., 1998. Electrochemical behaviour of amino acids on Pt(hkl). A voltammetric and in situ FTIR study.: Part III. Glycine on Pt(100) and Pt(110). *Journal of Electroanalytical Chemistry*, 445(1-2): 155-164.
- Hurley, B.L. and McCreery, R.L., 2003. Raman Spectroscopy of Monolayers Formed from Chromate Corrosion Inhibitor on Copper Surfaces. *Journal of The Electrochemical Society*, 150(8): B367-B373.
- Keenan, A., Webb, C., Kramer, D. and Compton, K., 1976. Polarization Resistance Study of the Effect of Alpha-Amino Acids on Cu Corrosion Kinetics. *Journal of the Electrochemical Society*, 123(2): 179-182.
- Keith, N.S., 1905. New methods in the metallurgical treatment of copper ores. *Journal of the Franklin Institute*, 160(2): 147-156.
- Kelly, R.G., 2002. *Electrochemical Techniques in Corrosion Science and Engineering*. Electrochemical techniques in corrosion science and engineering : Corrosion technology. Hoboken : Taylor and Francis, Hoboken.
- Klauber, C., 2003. Fracture-induced reconstruction of a chalcopyrite (CuFeS₂) surface. *Surface and Interface Analysis*, 35(5): 415-428.

- Klauber, C., 2008. A critical review of the surface chemistry of acidic ferric sulphate dissolution of chalcopyrite with regards to hindered dissolution. *International Journal of Mineral Processing*, 86(1–4): 1-17.
- Klauber, C., Parker, A., van Bronswijk, W. and Watling, H., 2001. Sulphur speciation of leached chalcopyrite surfaces as determined by X-ray photoelectron spectroscopy. *International Journal of Mineral Processing*, 62(1–4): 65-94.
- Konishi, Y., Katoh, M. and Asai, S., 1991. Leaching kinetics of copper from natural chalcocite in alkaline Na₄EDTA solutions. *MTB*, 22(3): 295-303.
- Kuhar, L.L., Breuer, P.L., Haque, N. and Robinson, D.J., 2018. Considerations and potential economic advantages for the in-situ recovery of gold from deep, hard-rock deposits. *Minerals Engineering*, 121: 14-22.
- Kunze, J., Maurice, V., Klein, L.H., Strehblow, H.-H. and Marcus, P., 2004. In situ STM study of the duplex passive films formed on Cu(1 1 1) and Cu(0 0 1) in 0.1 M NaOH. *Corrosion Science*, 46(1): 245-264.
- Laurent, J. and Landolt, D., 1991. Anodic dissolution of binary single phase alloys at subcritical potential. *Electrochimica Acta*, 36(1): 49-58.
- Lázaro, I. and Nicol, M., 2003. The Mechanism of the Dissolution and Passivation of Chalcopyrite. An Electrochemical Study., Hydrometallurgy TMS.
- Lefevre, R. et al., 2016. Thermoelectric properties of the chalcopyrite Cu_{1-x}M_xFeS_{2-y} series (M = Mn, Co, Ni). *RSC Advances*, 6(60): 55117-55124.
- Li, J., Tan, Q. and Li, J.-F., 2013. Synthesis and property evaluation of CuFeS_{2-x} as earth-abundant and environmentally-friendly thermoelectric materials. *Journal of Alloys and Compounds*, 551: 143-149.
- Li, Y. et al., 2014. Thermoelectric transport properties of diamond-like Cu_{1-x}Fe_{1+x}S₂ tetrahedral compounds. *Journal of Applied Physics*, 116(20): 203705.
- Linge, H.G., 1976. A study of chalcopyrite dissolution in acidic ferric nitrate by potentiometric titration. *Hydrometallurgy*, 2(1): 51-64.
- Lu, Z.Y., Jeffrey, M.I. and Lawson, F., 2000. An electrochemical study of the effect of chloride ions on the dissolution of chalcopyrite in acidic solutions. *Hydrometallurgy*, 56(2): 145-155.
- Lundström, M., Aromaa, J. and Forsén, O., 2009. Redox potential characteristics of cupric chloride solutions. *Hydrometallurgy*, 95(3): 285-289.
- Luo, Q., Babu, R.A., Mackay, S.V. and Babu, S.V., 1997. Copper Dissolution in Aqueous Ammonia-Containing Media during Chemical Mechanical Polishing. *Chemistry of Materials*, 9(10): 2101-2106.
- Luttrell, G.H. and Yoon, R.H., 1984. Surface studies of the collectorless flotation of chalcopyrite. *Colloids and Surfaces*, 12(C): 239-254.
- Marangoni, D.G., Smith, R.S. and Roscoe, S.G., 1989. Surface electrochemistry of the oxidation of glycine at Pt. *Canadian Journal of Chemistry*, 67(5): 921-926.
- Marsden, J.O., 2006. *Chemistry of Gold Extraction*. Chemistry of Gold Extraction. SME, Littleton.
- McCafferty, E., 2010. *Introduction to Corrosion Science* / by Edward McCafferty. New York, NY : Springer New York : Imprint: Springer, New York, NY.
- McCarron, J.J., Walker, G.W. and Buckley, A.N., 1990. An X-ray photoelectron spectroscopic investigation of chalcopyrite and pyrite surfaces after conditioning in sodium sulfide solutions. *International Journal of Mineral Processing*, 30(1-2): 1-16.
- McMillan, R.S., MacKinnon, D.J. and Dutrizac, J.E., 1982. Anodic dissolution of n-type and p-type chalcopyrite. *J Appl Electrochem*, 12(6): 743-757.
- Memming, R., 2007. *Semiconductor Electrochemistry*. Wiley-VCH Verlag GmbH, I-X pp.
- Mikhlin, Y.L. et al., 2004. Spectroscopic and electrochemical characterization of the surface layers of chalcopyrite (CuFeS₂) reacted in acidic solutions. *Applied Surface Science*, 225(1–4): 395-409.
- Mishra, K.K. and Osseo-Asare, K., 1992. Fermi Level Pinning at Pyrite (FeS₂)/Electrolyte Junctions. *Journal of the Electrochemical Society*, 139(3): 749-752.

- Moffat, T.P., Fan, F.R.F. and Bard, A.J., 1991. Electrochemical and Scanning Tunneling Microscopic Study of Dealloying of Cu₃Au. *Journal of The Electrochemical Society*, 138(11): 3224-3235.
- Montes, J.C., Hamdani, F., Creus, J., Touzain, S. and Correc, O., 2014. Impact of chlorinated disinfection on copper corrosion in hot water systems. *Applied Surface Science*, 314(Supplement C): 686-696.
- Morrison, S., R, 1980. *Electrochemistry at Semiconductor and Oxidized Metal Electrodes*.
- Morse, H. and Tobelmann, H., 1916. Leaching Tests at New Cornelia. *Trans. A.I.M.E.*, 55: 830.
- Moyo, T., Petersen, J., Franzidis, J.P. and Nicol, M., 2015. An electrochemical study of the dissolution of chalcopyrite in ammonia–ammonium sulphate solutions. *Canadian Metallurgical Quarterly*, 54(3): 269-278.
- Napier-Munn, T.J., 2014. *Statistical Methods for Mineral Engineers : How to Design Experiments and Analyse Data*. Julius Kruttschnitt Mineral Research Centre, Indooroopilly, Queensland.
- Nicol, M. and Zhang, S., 2017. The anodic behaviour of chalcopyrite in chloride solutions: Potentiostatic measurements. *Hydrometallurgy*, 167: 72-80.
- Nicol, M.J., 2016. Photocurrents at chalcopyrite and pyrite electrodes under leaching conditions. *Hydrometallurgy*, 163: 104-107.
- Nicol, M.J., 2017a. The anodic behaviour of chalcopyrite in chloride solutions: Overall features and comparison with sulfate solutions. *Hydrometallurgy*, 169: 321-329.
- Nicol, M.J., 2017b. A comparative assessment of the application of ammonium chloride and glycine as lixiviants in the heap leaching of chalcopyritic ores. *Hydrometallurgy*.
- Nicol, M.J., 2017c. The use of impedance measurements in the electrochemistry of the dissolution of sulfide minerals. *Hydrometallurgy*, 169: 99-102.
- Nicol, M.J., Tjandrawan, V. and Zhang, S., 2016. Cathodic reduction of iron(III) and copper(II) on various sulfide minerals in chloride solutions. *Hydrometallurgy*, 166(Supplement C): 113-122.
- O'Connor, G.M., Lepkova, K., Eksteen, J.J. and Oraby, E.A., 2018. Electrochemical behaviour of copper in alkaline glycine solutions. *Hydrometallurgy*, 181: 221-229.
- Oguchi, T., Sato, K. and Teranishi, T., 1980. Optical Reflectivity Spectrum of a CuFeS₂ Single Crystal. *Journal of the Physical Society of Japan*, 48(1): 123-128.
- Ogura, K., Kobayashi, M., Nakayama, M. and Miho, Y., 1998. Electrochemical and in situ FTIR studies on the adsorption and oxidation of glycine and lysine in alkaline medium. *Journal of Electroanalytical Chemistry*, 449(1–2): 101-109.
- Olvera, O.G., Rebolledo, M. and Asselin, E., 2016. Atmospheric ferric sulfate leaching of chalcopyrite: Thermodynamics, kinetics and electrochemistry. *Hydrometallurgy*, 165, Part 1: 148-158.
- Oraby, E.A. and Eksteen, J.J., 2014. The selective leaching of copper from a gold–copper concentrate in glycine solutions. *Hydrometallurgy*, 150(0): 14-19.
- Oraby, E.A. and Eksteen, J.J., 2015. Gold leaching in cyanide-starved copper solutions in the presence of glycine. *Hydrometallurgy*, 156: 81-88.
- Osseo-Asare, K., 1992. Semiconductor electrochemistry and hydrometallurgical dissolution processes. *Hydrometallurgy*, 29(1): 61-90.
- Panlasigui, R.A., 1970. Kinetics of copper dissolution.
- Parker, A.J., Paul, R. and Power, G., 1981. Electrochemical aspects of leaching copper from chalcopyrite in ferric and cupric salt solutions. *Australian Journal of Chemistry*, 34(1): 13-34.
- Parker, G.K., Woods, R. and Hope, G.A., 2008. Raman investigation of chalcopyrite oxidation. *Colloids and Surfaces A: Physicochemical and Engineering Aspects*, 318(1–3): 160-168.

- Patri, U.B., Aksu, S. and Babu, S.V., 2006. Role of the Functional Groups of Complexing Agents in Copper Slurries. *Journal of The Electrochemical Society*, 153(7): G650-G659.
- Paynter, J.C., 1973. REVIEW OF COPPER HYDROMETALLURGY. *Journal of The South African Institute of Mining and Metallurgy*, 74(4): 158-170.
- Pearlmutter, A.F. and Stuehr, J., 1968. Kinetics of copper(II)-glycine interactions in aqueous solution. *Journal of the American Chemical Society*, 90(4): 858-862.
- Perea, C.G. and Restrepo, O.J., 2018. Use of amino acids for gold dissolution. *Hydrometallurgy*, 177: 79-85.
- Pike, R.D., West, G.H., Steck, R., Cummings, R. and Little, B.P., 1930. Electrolytic Iron from Sulfide Ores *Trans. A.I.M.E.*, 90: 15.
- Prasanna Venkatesh, R. and Ramanathan, S., 2010. Electrochemical impedance spectroscopic studies of copper dissolution in glycine–hydrogen peroxide solutions. *J Solid State Electrochem*, 14(11): 2057-2064.
- Pridmore, D.F. and Shuey, R.T., 1976. The electrical resistivity of galena, pyrite, and chalcopyrite. *American Mineralogist*, 61(3): 248-259.
- Razzell, W.E. and Trussell, P.C., 1963. Microbiological Leaching of Metallic Sulfides. *Applied Microbiology*, 11(2): 105-110.
- Reilly, I.G. and Scott, D.S., 1977. The leaching of a chalcopyrite concentrate in ammonia. *Canadian Journal of Chemical Engineering*, 55(5): 527-533.
- Rios, J.F., Calderón, J. A. & Nogueira, R. P. , 2011. Electrochemical behavior of copper in drinking water: evaluation of dissolution process at low anodic overpotential. *J. Braz. Chem. Soc.*, 22(7): 9.
- Robertson, S., Jeffrey, M., Zhang, H. and Ho, E., 2005. An introductory electrochemical approach to studying hydrometallurgical reactions. *Metall and Materi Trans B*, 36(3): 313-325.
- Robinson, D. and Kuhar, L.L., 2018. In situ recovery – a move towards ‘keyhole mining’, *AusIMM Bulletin Aug 2018*. Citrus Media, pp. 54-56.
- Rosso, K.M., 2001. Structure and Reactivity of Semiconducting Mineral Surfaces: Convergence of Molecular Modeling and Experiment. *Reviews in Mineralogy and Geochemistry*, 42(1): 199-271.
- Sandoval, A.P., Orts, J.M., Rodes, A. and Feliu, J.M., 2013. DFT and In Situ Infrared Studies on Adsorption and Oxidation of Glycine, L-Alanine, and L-Serine on Gold Electrodes, *Vibrational Spectroscopy at Electrified Interfaces*. John Wiley & Sons, Inc., pp. 239-265.
- Sato, K. and Teranishi, T., 1976. Optical Absorption Spectrum of a Thin CuFeS₂ Film. *Journal of the Physical Society of Japan*, 40(1): 297-298.
- Schlesinger, M.E., King, M.J., Sole, K.C. and Davenport, W.G., 2011. *Extractive Metallurgy of Copper*. Elsevier, Amsterdam.
- Schmickler, W., 2010. *Interfacial Electrochemistry* / by Wolfgang Schmickler, Elizabeth Santos. Berlin, Heidelberg : Springer Berlin Heidelberg : Imprint: Springer, Berlin, Heidelberg.
- Seeger, K.a., 2004. *Semiconductor Physics : An Introduction* / by Karlheinz Seeger. Berlin, Heidelberg : Springer Berlin Heidelberg : Imprint: Springer.
- Shuey, R.T., 1975. *Semiconducting ore minerals*. Elsevier Scientific Pub. Co., Amsterdam.
- Siebentritt, S., 2006. *Wide-Gap Chalcopyrites* / edited by Susanne Siebentritt, Uwe Rau. Berlin, Heidelberg : Springer Berlin Heidelberg, Berlin, Heidelberg.
- Silverman, D.C., 2011. *Practical Corrosion Prediction Using Electrochemical Techniques*, Uhlig's Corrosion Handbook. John Wiley & Sons, Inc., pp. 1129-1166.
- Skrypnikova, E.A., Kaluzhina, S.A. and Orlova, E.V., 2011. Anode oxidation of copper in alkali media in the presence of glycine, α -alanine, and asparagine acid. *Russ J Electrochem*, 47(11): 1231-1235.
- Skrypnikova, E.A., Kaluzhina, S.A. and Popova, E.V., 2008. Peculiarities of copper anodic behavior in alkaline solutions with glycine additives. *ECS Transactions*, 13: 7-12.

- Smart, R.S.C., Skinner, W.M. and Gerson, A.R., 1999. XPS of sulphide mineral surfaces: metal-deficient, polysulphides, defects and elemental sulphur. *Surface and Interface Analysis*, 28(1): 101-105.
- Speckmann, H.D., Lohrengel, M.M., Schultze, J.W. and Strehblow, H.H., 1985. The Growth and Reduction of Duplex Oxide Films on Copper. *Berichte der Bunsengesellschaft für physikalische Chemie*, 89(4): 392-402.
- Springer, G., 1970. Observations on the Electrochemical Reactivity of Semiconducting Minerals *Transactions of the Institution of Mining and Metallurgy* Transactions of the Institution of Mining and Metallurgy, Section C, 79: 5.
- Stanczyk, M.H. and Rampacek, C., 1966. Oxidation leaching of copper sulfides in ammoniacal pulps at elevated temperatures and pressures. Report of investigations / United States. Bureau of Mines ;6808. U.S. Dept. of the Interior, Bureau of Mines, [Washington, D.C.], 13 p. pp.
- Strehblow, H.H., Maurice, V. and Marcus, P., 2001. Initial and later stages of anodic oxide formation on Cu, chemical aspects, structure and electronic properties. *Electrochimica Acta*, 46(24): 3755-3766.
- Streitwieser, A. and Heathcock, C.H., 1985. *Introduction to organic chemistry* New York : Macmillan, New York, 1 pp.
- Sullivan, J.D., 1933. Chemical and Physical Features of Copper Leaching. *Transactions Amer Inst Mining & Metallurgical Engrs*, 1.
- Tamilmani, S., Huang, W., Raghavan, S. and Small, R., 2002. Potential-pH Diagrams of Interest to Chemical Mechanical Planarization of Copper. *Journal of The Electrochemical Society*, 149(12): G638-G642.
- Tanda, B., Eksteen, J. and Oraby, E., 2017. An investigation into the leaching behaviour of copper oxide minerals in aqueous alkaline glycine solutions.
- Tanda, B.C., 2017. Glycine as a lixiviant for the leaching of low grade copper-gold ores, Curtin University.
- Teranishi, T., Sato, K. and Kondo, K.i., 1974. Optical Properties of a Magnetic Semiconductor: Chalcopyrite CuFeS_2 . I. Absorption Spectra of CuFeS_2 and Fe-Doped CuAlS_2 and CuGaS_2 . *Journal of the Physical Society of Japan*, 36(6): 1618-1624.
- Third, K.A., Cord-Ruwisch, R. and Watling, H.R., 2002. Control of the redox potential by oxygen limitation improves bacterial leaching of chalcopyrite. *Biotechnology and bioengineering*, 78(4): 433-41.
- Tkáčová, K. and Baláž, P., 1988. Structural and temperature sensitivity of leaching of chalcopyrite with iron(III) sulphate. *Hydrometallurgy*, 21(1): 103-112.
- Tossell, J.A., Urch, D.S., Vaughan, D.J. and Wiech, G., 1982. The electronic structure of CuFeS_2 , chalcopyrite, from x-ray emission and x-ray photoelectron spectroscopy and $X\alpha$ calculations. *The Journal of Chemical Physics*, 77(1): 77-82.
- Tributsch, H. and Bennett, J.C., 1981. Semiconductor-electrochemical aspects of bacterial leaching. I. Oxidation of metal sulphides with large energy gaps. *Journal of Chemical Technology and Biotechnology*, 31(1): 565-577.
- Tripathi, S., Doyle, F.M. and Dornfeld, D., 2009. Fundamental Mechanisms of Copper CMP – Passivation Kinetics of Copper in CMP Slurry Constituents.
- Vanmaekelbergh, D., 1997. Direct and surface state mediated electron transfer at semiconductor/electrolyte junctions—I. A comparison of steady-state results. *Electrochimica Acta*, 42(7): 1121-1134.
- Vaughan, D.J., 1978. *Mineral chemistry of metal sulfides*. Cambridge [Eng.] ; New York : Cambridge University Press

- Vaughan, D.J. and Tossell, J.A., 1983. Electronic structures of sulfide minerals — Theory and experiment. *Physics and Chemistry of Minerals*, 9(6): 253-262.
- Viramontes-Gamboa, G., Rivera-Vasquez, B.F. and Dixon, D.G., 2007. The Active-Passive Behavior of Chalcopyrite: Comparative Study Between Electrochemical and Leaching Responses. *Journal of The Electrochemical Society*, 154(6): C299-C311.
- Warren, G.W. and Wadsworth, M.E., 1984. The electrochemical oxidation of chalcopyrite in ammoniacal solutions. *MTB*, 15(2): 289-297.
- Warren, G.W., Wadsworth, M.E. and El-Raghy, S.M., 1982. Passive and transpassive anodic behavior of chalcopyrite in acid solutions. *MTB*, 13(4): 571-579.
- Watling, H.R., 2013. Chalcopyrite hydrometallurgy at atmospheric pressure: 1. Review of acidic sulfate, sulfate–chloride and sulfate–nitrate process options. *Hydrometallurgy*, 140(0): 163-180.
- Webb, R., 2012. Deep future: Will we run out of resources?, *New Scientist*.
- Weiss, I.-G., 1976. Leaching of a copper sulfide concentrate in an ammonia-oxygen system, University of Arizona, Arizona.
- Wills, B.A., 2015. *Wills' mineral processing technology : an introduction to the practical aspects of ore treatment and mineral recovery*. Mineral processing technology. Oxford : Butterworth-Heinemann.
- Xian, Y.J., Wen, S.M., Deng, J.S., Liu, J. and Nie, Q., 2012. Leaching chalcopyrite with sodium chlorate in hydrochloric acid solution. *Canadian Metallurgical Quarterly*, 51(2): 133-140.
- Xie, F., 2006. Catalytic leaching of silver with ferricyanide-cyanide solution, University of British Columbia.
- Xie, F. and Dreisinger, D.B., 2007. Leaching of silver sulfide with ferricyanide–cyanide solution. *Hydrometallurgy*, 88(1–4): 98-108.
- Xie, H. et al., 2016. The Role of Zn in Chalcopyrite CuFeS_2 : Enhanced Thermoelectric Properties of $\text{Cu}_{1-x}\text{Zn}_x\text{FeS}_2$ with In Situ Nanoprecipitates. *Advanced Energy Materials*: <xocs:firstpage xmlns:xocs="" />.
- Xu, Y. and Schoonen, M., 2000. The absolute energy positions of conduction and valence bands of selected semiconducting minerals, *Am. Miner.*, pp. 543-556.
- Yin, Q., Kelsall, G.H., Vaughan, D.J. and England, K.E.R., 1995. Atmospheric and electrochemical oxidation of the surface of chalcopyrite (CuFeS_2). *Geochimica et Cosmochimica Acta*, 59(6): 1091-1100.
- Yin, Q., Vaughan, D.J., England, K.E.R., Kelsall, G.H. and Brandon, N.P., 2000. Surface Oxidation of Chalcopyrite (CuFeS_2) in Alkaline Solutions. *Journal of The Electrochemical Society*, 147(8): 2945-2951.
- Zevgolis, E.N. and Cooke, S.R.B., 1975. Electrochemical Properties of the Semiconductor Mineral Chalcopyrite. In: m. Università di Cagliari. Istituto di arte (Ed.), *Proceedings : eleventh International Mineral Processing Congress*. Cagliari, Sardinia : Università, Istituto di arte mineraria e preparazione dei minerali, Cagliari, Sardinia.
- Zhao, H., Chang, J., Boika, A. and Bard, A.J., 2013. Electrochemistry of High Concentration Copper Chloride Complexes. *Analytical Chemistry*, 85(16): 7696-7703.
- Zhao, H. et al., 2017. Comparison of bioleaching and dissolution process of p-type and n-type chalcopyrite. *Minerals Engineering*, 109: 153-161.
- Zhou, S. et al., 2015. Catalytic effect of light illumination on bioleaching of chalcopyrite. *Bioresource Technology*, 182: 345-352.

Every reasonable effort has been made to acknowledge the owners of copyright material. I would be pleased to hear from any copyright owner who has been omitted or incorrectly acknowledged.

Appendix A Electrochemical measurements

There is a wide range of electrochemical measurements that have been used for studying the fundamentals of mineral and metal corrosion and dissolution. These methods are useful because of the accurate control of potential and measurement of current as an indicator of reaction rate. The methods used in this study are presented here, with a discussion of the benefits and risks with each.

A.1 Potentiodynamic polarisation.

Potentiodynamic polarisation is a commonly used technique in corrosion engineering as a rapid way to measure the corrosion rate. It is a standard procedure defined by ATSM method G59-97 and is described in detail in corrosion and electrochemistry texts (ASTM, 2014; Brett and Brett, 1993; Kelly, 2002). It is particularly useful for ranking different samples or samples under different conditions for their corrosion rate (Silverman, 2011). This technique exploits the linear relationship of current-potential curves for an electrode near the corrosion potential E_{corr} . This linear region can be in a potential range of 10 to 50 mV either side of the corrosion potential (McCafferty, 2010).

In this method an electrode is subjected to a small potential scan of about ± 10 mV at a slow scan rate of 0.1 mV/s and the resulting currents are recorded. The slope of the curve at the E_{corr} is the polarisation resistance, R_p . The corrosion current is related to the R_p by:

$$i_{\text{corr}} = \frac{\beta_a \cdot \beta_c}{2.303(\beta_a + \beta_c) R_p} \quad \text{Equation 18}$$

Where β_a and β_c are the anodic and cathodic Tafel slopes respectively. The values of the Tafel slopes often cannot be determined due to the non-linearity of the current potential curves. In such cases assumed Tafel slopes such as 0.12 V are sometimes used (Aksu and Doyle, 2002). This is based on a charge transfer coefficient of 0.5 for typical metal solution interfaces (Crundwell, 2013; Free, 2013). This approach has been shown to be useful for screening experiments to reveal trends in corrosion and extractive metallurgy (Silverman, 2011).

A hypothetical current potential plot is shown in Figure App A.1 shows the polarisation resistance data for different corroding systems (Kelly, 2002). The non-linearity is typical as shown by the solid lines, with a straight dashed line drawn from the asymptote drawn at a tangent at the E_{corr} . The slope of the tangent, and hence the resistance polarisation is independent of the degree of linearity.

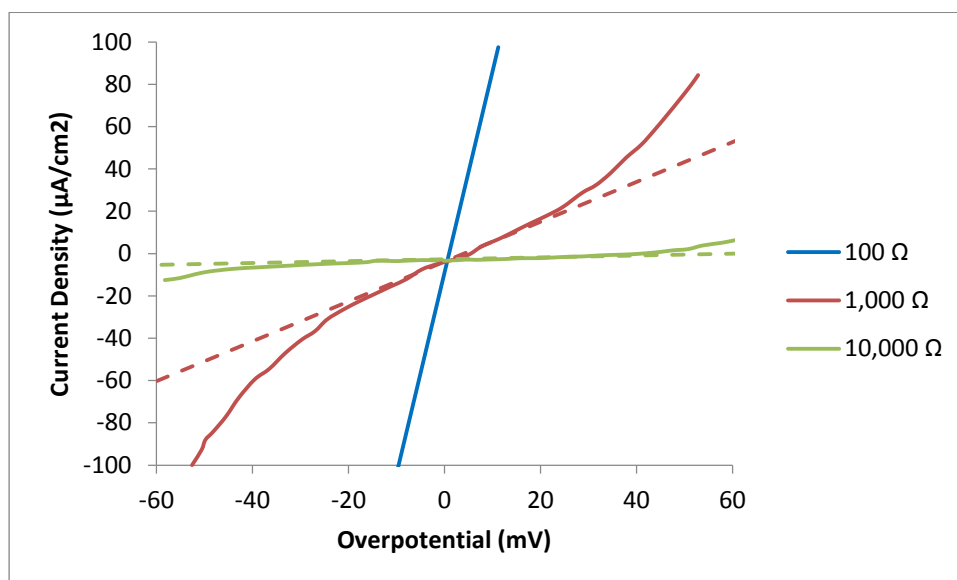


Figure App A.1. Typical current potential polarisation resistance plots for different corroding systems (Kelly, 2002) p 128

For the section on copper electrochemistry, this method was followed for a range of glycine concentrations, pH values and temperatures. All data were extracted using Biologic software. An example is shown in Figure App A.2.

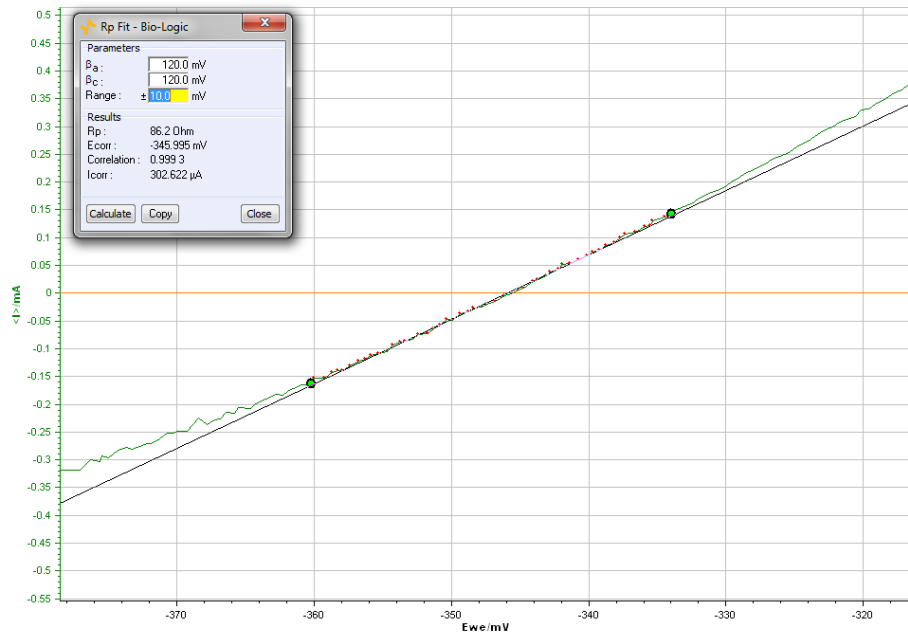


Figure App A.2: Example of Resistance polarisation calculation with Biologic software.

All potentiodynamic polarisation tests were performed in triplicate with results presented in Table App A-1

Table App A-1: Resistance polarisation and calculated i_{corr} values for copper metal

TEST	T (°C)	pH	Conc. (M)	OCP V (vs SHE)	R _p (Ω)	i_{corr} (mAcm ⁻²)
2LP10	22	9.0	0.1	-262	349	0.06
02LP18	22	9.0	0.1	-255	321	0.07
LP30	22	9.0	0.1	-266	350	0.06
02LP12	60	9.0	0.1	-290	134	0.17
02LP07	60	9.0	0.1	-294	122	0.18
LP34	60	9.0	0.1	-298	158	0.14
02LP03	22	10	0.1	-321	117	0.19
02LP19	22	10	0.1	-327	97.7	0.23
LP32	22	10	0.1	-328	92.9	0.24
02LP13	60	10	0.1	-337	42.4	0.53
02LP09	60	10	0.1	-340	46.8	0.48
LP36	60	10	0.1	-336	42.5	0.53
02LP05	22	9	0.3	-283	215	0.10
02LP01	22	9	0.3	-295	176	0.13
LP31	22	9	0.3	-285	200	0.11
02LP14	60	9	0.3	-326	65.4	0.34
02LP16	60	9	0.3	-327	53.5	0.42
LP35	60	9	0.3	-302	57.9	0.39
LP33	22	10	0.3	-359	77.3	0.29
02LP02	22	10	0.3	-347	80.9	0.28
02LP17	22	10	0.3	-355	68.9	0.33
02LP04	60	10	0.3	-386	21.2	1.06
LP37	60	10	0.3	-383	22.1	1.01
02LP06	60	10	0.3	-388	25.1	0.89
02LP11	41	9.5	0.2	-329	77.5	0.29
02LP08	41	9.5	0.2	-315	111	0.20
02LP15	41	9.5	0.2	-334	70.11	0.32
LP10	22	10.5	0.1	-343	81.1	0.28
LP12	22	10.5	0.1	-347	76.4	0.29
LP26	22	10.5	0.1	-348	86.2	0.26
LP02	60	10.5	0.1	-351	49.9	0.45
LP20	60	10.5	0.1	-345	61.4	0.37
LP19	60	10.5	0.1	-354	50.5	0.44
LP14	22	11.5	0.1	-319	103	0.22
LP13	22	11.5	0.1	-319	136	0.16
LP22	22	11.5	0.1	-318	111	0.20
LP23	60	11.5	0.1	-332	61.7	0.36
LP24	60	11.5	0.1	-327	51	0.44
LP15	60	11.5	0.1	-343	54.1	0.41

TEST	T (°C)	pH	Conc. (M)	OCP V (vs SHE)	Rp (Ω)	icorr (mAcm ⁻²)
LP01	22	10.5	0.3	-376	62.4	0.36
LP17	22	10.5	0.3	-378	56.7	0.40
LP21	22	10.5	0.3	-380	51.8	0.43
LP05	60	10.5	0.3	-393	46.8	0.48
LP03	60	10.5	0.3	-388	49.8	0.45
LP06	60	10.5	0.3	-394	53.1	0.42
LP27	22	11.5	0.3	-387	66.9	0.34
LP09	22	11.5	0.3	-387	57.4	0.39
LP07	22	11.5	0.3	-380	55.5	0.40
LP25	60	11.5	0.3	-388	45	0.50
LP18	60	11.5	0.3	-400	49	0.46
LP04	60	11.5	0.3	-396	63.1	0.36
LP16	41	11.0	0.2	-373	64	0.35
LP11	41	11.0	0.2	-372	55.8	0.40
LP08	41	11.0	0.2	-369	63.7	0.35

A.2 Linear sweep voltammetry and Evans diagrams

Linear sweep voltammetry is a common method used for the fundamental studies in hydrometallurgy. This is often used to study anodic and cathodic reactions independently of each other (Robertson et al., 2005). To study the anodic reaction the potential is slowly increased from the OCP to obtain a current potential curve. For a cathodic reaction the potential is slowly decreased. Often oxygen is removed from the system for the anodic sweep so that it does not contribute to the oxidation of the sample. If a complexing agent is used, such as cyanide for gold leaching, it is not added for a cathodic scan to prevent dissolution near the OCP.

The anodic and cathodic scans can be superimposed using the absolute current density. The point at which they intersect is the corrosion current. These diagrams can be useful for showing limitation by diffusion or chemical control and are widely used for gold/cyanide systems. A classic example is the influence of cyanide concentration and dissolved oxygen on gold dissolution as shown in Figure App A.3. This example is shown to compare with the copper glycine systems shown in Chapter 3.

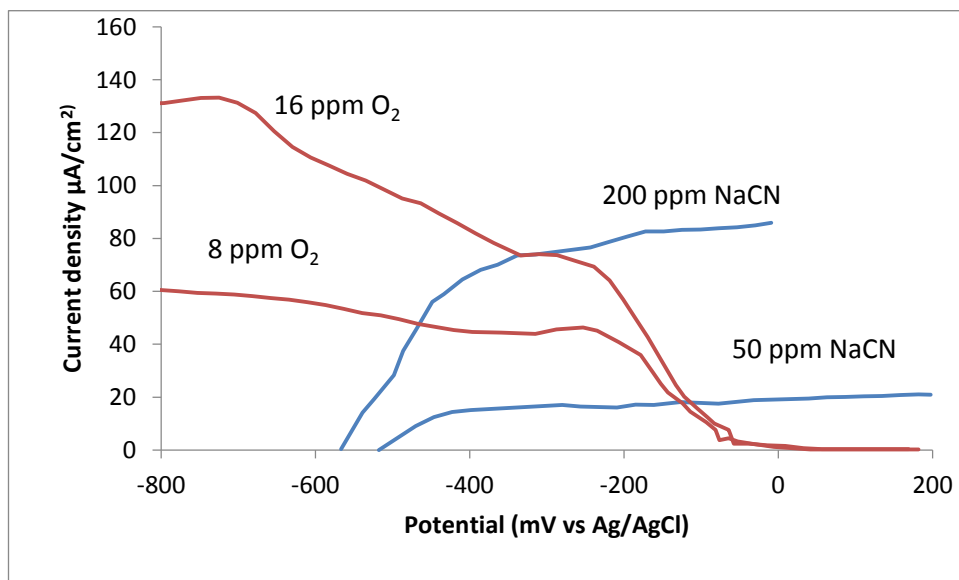
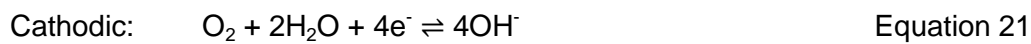
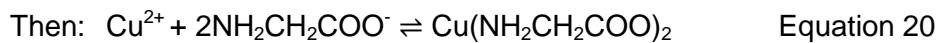


Figure App A.3. Example of how an Evans diagram for the commonly studied gold-cyanide system (Heath and Rumball, 1998)

It can be seen that the corrosion current can be controlled by diffusion of either oxygen or cyanide at everyday concentrations used in the gold industry. By comparison, the copper glycine system is controlled by the rate of the chemical reaction for realistic concentrations as shown in section 3.3.2. The Evans diagram methodology can however be misleading when the anodic and cathodic reactions are not independent of each other such as for systems of high purity gold and cyanide (Dai and Breuer, 2013).

The concentration of glycine where the reaction is limited by diffusion limitation can be calculated from first principles. The difference to gold/cyanide systems is that passivation may occur if local depletion of glycine occurs at the copper electrode. The bulk solution concentration where this occurs can be estimated by considering the diffusion characteristics of glycine and dissolved oxygen. First, the half reactions involved are (Aksu and Doyle 2001):



From Fick's second law where diffusion is the rate determining step the flux, j , is given by Equation 16 (Marsden 2006):

$$j = -D_i \cdot C_b / N \quad \text{Equation 22}$$

Where D_i is the diffusion coefficient of species i , C_b the concentration of the bulk solution and N is the Nernst diffusion layer thickness. Local depletion of glycine will occur if the flux of glycine is less than that of O_2 . Since four glycine molecules are required for each oxygen molecule, when the flux of anodic and cathodic reactants are equal,

$$D_{\text{Gly}} \cdot [\text{Gly}] = 4 \times D_{\text{O}_2} [\text{O}_2] \quad \text{Equation 23}$$

The ratio of glycine to dissolved oxygen is therefore:

$$[\text{Gly}] / [\text{O}_2] = 4 \times D_{\text{O}_2} / D_{\text{Gly}} \quad \text{Equation 24}$$

The diffusion coefficient of glycine is $1.0 \times 10^{-5} \text{ cm}^2/\text{s}$ and dissolved oxygen is $2.8 \times 10^{-5} \text{ cm}^2/\text{s}$ (Ma et al. 2005, Nakanishi et al. 1977, Marsden 2006). This gives the ratio:

$$[\text{Gly}] / [\text{O}_2] = 11.2 \quad \text{Equation 25}$$

Therefore, given a typical air saturated system at 8 ppm O₂, local glycine depletion may occur if the bulk concentration is less than 0.003 M. Clearly for the system studied at 0.1 M and 0.3 M, the local glycine concentration is unlikely to be depleted to a significant extent to allow complete passivation of the copper surface.

A.3 Chronoamperometry

Chronoamperometry involves the measurement of current held at a static potential for a given length of time. This can be particularly useful when combined with solution assays for determining information about the reaction mechanism (Moyo et al., 2015). By measuring the charge passed over a given time the number of electrons involved per atom of metal in solution can be determined. Other applications in hydrometallurgy include generating an oxidised mineral surface for analysis by spectroscopic means (Ghahremaninezhad et al., 2013; Holmes and Crundwell, 2013). Another application has been to measure the electrochemistry after the surface has been oxidised at a known potential. A well-known example of this is the reactivation of a supposedly passive surface (Parker et al., 1981).

A.4 Potential step-capacitance methods.

A potential step method is sometimes used instead of linear sweep voltammetry. It is well known that the scan rate used in linear sweep voltammetry can change the features observed in a current potential curve. This can be due to time dependent processes that are too slow for a fast sweep rate to measure. This has been shown for chalcopyrite in several studies where fast scan rates obscured the apparent passive region (Ghahremaninezhad et al., 2010; Viramontes-Gamboa et al., 2007).

Potential step methods are also used where capacitance measurements at different potentials are required. Changes in the capacitance of the interface have been used to help interpret the nature of the mineral solution boundary. The capacitance is determined by creating a small perturbation at the desired applied potential and measuring the impedance response. A common way of presenting this is the form of a Mott Schottky diagram, which gives information about the semiconducting nature of the electrode.

The capacitance of a semiconductor solution interface is related to the sum of the inverse of the space charge and Helmholtz layer capacitance. The space charge layer is internal to the semiconductor and dominates the total capacitance (Memming, 2007). Usually the parameters of interest in semiconductor physics are the conductivity type (n or p), density of charge carriers (N_b) and the “flat band potential”. The Mott Schottky relationship is shown follows (Ghahremaninezhad et al., 2010):

$$(1/C_{sc})^2 = (2/\epsilon \cdot \epsilon_0 \cdot e N_b) (E - E_{fb} - kT/e) \quad \text{Equation 26}$$

Where E is the applied potential, E_{fb} is the flatband potential, ϵ_0 is the permittivity of free space, ϵ is the dielectric constant of the semiconductor and C_{sc} is the space charge capacitance N_b is the carrier density.

While the Mott Schottky relationship has been used in other studies, for the work in this thesis a straight relationship of capacitance versus potential was used. The main reason is that the semiconducting parameters of interest from the Mott Schottky plot, that is the carrier density and the flat band potential, were not of interest for this study. Adding to this, it is said that the reliable determination of these values cannot be made when surface layers such as oxides are present (Memming, 2007). This results in a frequency dependent capacitance – potential curve with varying slopes.

For the chalcopyrite electrode an iron oxide layer formed and frequency dependent behaviour of capacitance with potential was observed. While this changes the calculated values of donor density and flat band potential it does not affect the sign of the slopes. As such, the change in n-type to p-type behaviour that was observed at around 0.75 V (vs Ag/AgCl) is still observed regardless of the value of the slope or its intercept with the x axis. The frequency dispersion was also observed in other studies where multiple frequencies were used (Ghahremaninezhad et al., 2010).

Appendix B XPS and Raman spectra interpretation.

B.1 XPS

XPS is often employed to show the oxidation state of surface elements. For studies of chalcopyrite surface species, the key peak of interest is sulfur. Sulfur can exist in a number of oxidation states from -2 to +6. These show up as components of a sulfur peak. For chalcopyrite, sulfur is ideally expected to be present in the form of S^{2-} as it appears in the lattice. However, all XPS studies have shown that the sulfur peak has at least two components, the lowest binding energy component is the monosulfide which typically occurs at 161.2 eV while a second component is present 1.8 eV higher that is interpreted as a disulfide, S_2^{2-} (Klauber, 2008). Of higher energy still may be elemental sulfur, polysulfide and sulfate.

The disulfide peak is sometimes attributed to the apparent metal deficient sulfide that is supposed to passivate chalcopyrite. This is a dimer with S-S bonding. It has been assigned to species such as $Cu_{0.8}S_2$, an uncharacterised metastable species CuS_2^* , or the more general $Cu_{1-x}Fe_{1-y}S_2$ (Buckley and Woods, 1984; Hackl et al., 1995; Yin et al., 1995). An alternative explanation is that the disulfide component is due to a partial pyritic layer on the surface with copper present as cuprite (Klauber, 2003).

Another component of the sulfur peak is sometimes attributed to a polysulfide. This has the general equation M_2S_n where n is between 2 and 6 (Klauber, 2008). The assignment of a component of the sulfur peak to polysulfide has been strongly criticised by Klauber (2008). Several errors have been made by some authors when interpreting previous studies such as mistakenly attributing an elemental sulfur peak as polysulfide. Earlier studies presented results for polysulfido complexes rather than polysulfides. An assignment of polysulfide would require a component for both terminal and central sulfur atoms, which are not always present (Klauber, 2008).

B.2 Raman Spectroscopy

Raman spectroscopy is used to measure the vibrational modes of a molecule. This includes modes such as stretching, bending and wagging of the bonds. These modes have characteristic vibrational frequencies that can allow identification of bond type and infer the identification of the molecule. This has been used to identify elemental sulfur and polysulfides on the chalcopyrite and pyrite surfaces (Holmes and Crundwell, 2013; Parker et al., 2008). For this study, the primary application was to compare spectra with a sulfur standard as a fingerprint. The purpose here was to confirm the presence of sulfur that was suspected from XPS sulfur peak deconvolution.

Appendix C Chalcopyrite Characterisation

C.1 Microprobe data

It is well known that chalcopyrite is an n-type semiconductor in nature. This is due to the non-stoichiometry of the mineral with an excess of metal over sulfur. This sample had the typical abundance of metals, and along with the thermoelectric current can be confidently said to be an n-type semiconductor.

SAMPLE	S (%)	Fe (%)	Cu (%)	Pb (%)	Ni (%)	Zn (%)	Co (%)	Ag (%)	Cd (%)
1	49.79390	25.19470	24.99670	0.00367	0.00000	0.00623	0.00278	0.00196	0.00000
2	49.81260	25.29410	24.88160	0.00512	0.00000	0.00637	0.00000	0.00021	0.00000
3	50.49550	24.52210	24.96610	0.00450	0.00000	0.01047	0.00137	0.00000	0.00000
4	49.82760	25.26420	24.89480	0.00365	0.00000	0.00664	0.00129	0.00191	0.00000
5	49.83700	25.20390	24.94830	0.00356	0.00000	0.00496	0.00000	0.00000	0.00228
6	49.86990	25.12090	24.99200	0.00427	0.00000	0.01019	0.00000	0.00000	0.00285
7	49.60930	25.35920	25.02020	0.00413	0.00195	0.00515	0.00000	0.00006	0.00000
8	49.70750	25.16000	25.11190	0.00239	0.00000	0.01422	0.00000	0.00239	0.00157
9	49.55730	25.40320	25.03220	0.00335	0.00000	0.00044	0.00012	0.00337	0.00000
10	49.91970	24.86160	25.19260	0.00189	0.00000	0.00640	0.00507	0.00788	0.00496
11	49.65070	25.18470	25.15370	0.00334	0.00000	0.00730	0.00027	0.00000	0.00000
12	49.63170	25.15410	25.19960	0.00152	0.00000	0.00849	0.00209	0.00000	0.00254
13	49.80370	25.09700	25.07820	0.00209	0.00405	0.00748	0.00000	0.00274	0.00475
14	49.72470	25.29580	24.97320	0.00237	0.00000	0.00244	0.00146	0.00000	0.00000
15	49.57400	25.30550	25.10620	0.00250	0.00030	0.01151	0.00000	0.00000	0.00000
16	49.57860	25.23760	25.17560	0.00466	0.00000	0.00350	0.00000	0.00000	0.00000
17	49.94800	25.05020	24.98260	0.00302	0.00000	0.00905	0.00000	0.00475	0.00239
18	49.67320	25.35410	24.95770	0.00201	0.00163	0.01136	0.00000	0.00000	0.00000
19	49.74020	25.22760	25.02180	0.00271	0.00108	0.00641	0.00000	0.00024	0.00000

SAMPLE	S (%)	Fe (%)	Cu (%)	Pb (%)	Ni (%)	Zn (%)	Co (%)	Ag (%)	Cd (%)
21	49.65910	25.34840	24.98120	0.00291	0.00000	0.00356	0.00000	0.00000	0.00490
22	49.61670	25.35800	25.02170	0.00124	0.00000	0.00236	0.00000	0.00000	0.00000
23	49.66090	25.18340	25.14720	0.00177	0.00000	0.00000	0.00131	0.00544	0.00000
24	49.70070	25.20090	25.08980	0.00145	0.00000	0.00235	0.00000	0.00480	0.00000
25	49.55150	25.52090	24.91350	0.00251	0.00000	0.00817	0.00186	0.00031	0.00131
26	49.71060	25.34640	24.93260	0.00232	0.00000	0.00788	0.00000	0.00021	0.00000
27	49.65420	25.38620	24.95340	0.00237	0.00000	0.00000	0.00385	0.00000	0.00000
28	49.58290	25.33110	25.07290	0.00190	0.00000	0.00653	0.00343	0.00127	0.00000
29	49.69520	25.23020	25.06180	0.00525	0.00000	0.00752	0.00000	0.00000	0.00000
30	49.64320	25.28090	25.07140	0.00102	0.00000	0.00353	0.00000	0.00000	0.00000
31	49.68010	25.26940	25.03810	0.00225	0.00000	0.01013	0.00000	0.00000	0.00000
32	49.53380	25.44080	25.01890	0.00210	0.00106	0.00212	0.00000	0.00000	0.00122
33	49.76060	25.17810	25.05120	0.00336	0.00000	0.00660	0.00000	0.00013	0.00000
34	49.75900	25.14280	25.08570	0.00119	0.00000	0.00615	0.00051	0.00000	0.00462
35	49.84080	24.92560	25.22400	0.00269	0.00000	0.00319	0.00000	0.00376	0.00000
36	49.88810	24.93260	25.16720	0.00187	0.00002	0.00185	0.00000	0.00620	0.00214
37	49.67720	25.21010	25.10910	0.00219	0.00000	0.00136	0.00000	0.00006	0.00000
38	49.50230	25.37830	25.11250	0.00343	0.00000	0.00347	0.00000	0.00000	0.00000
39	49.79490	25.16900	25.02560	0.00283	0.00000	0.00778	0.00000	0.00000	0.00000
41	49.76900	25.00730	25.21650	0.00169	0.00000	0.00562	0.00000	0.00000	0.00000
42	49.76640	25.06560	25.15200	0.00305	0.00014	0.01220	0.00000	0.00000	0.00065
43	50.00510	24.92540	25.06220	0.00159	0.00000	0.00525	0.00000	0.00049	0.00000
44	49.56740	25.32000	25.09830	0.00403	0.00000	0.01026	0.00000	0.00000	0.00000
45	49.65210	25.18540	25.15490	0.00278	0.00000	0.00482	0.00000	0.00000	0.00000
46	49.67600	25.10340	25.20630	0.00279	0.00000	0.00560	0.00370	0.00000	0.00223
47	49.61620	25.23120	25.14580	0.00175	0.00115	0.00393	0.00000	0.00000	0.00000
48	49.77650	25.15980	25.05240	0.00368	0.00185	0.00577	0.00000	0.00000	0.00000
49	49.74930	25.10190	25.13170	0.00354	0.00039	0.00878	0.00243	0.00191	0.00000
50	49.66820	25.15470	25.17060	0.00121	0.00000	0.00530	0.00000	0.00000	0.00000
51	49.57440	25.32190	25.09010	0.00304	0.00000	0.01055	0.00000	0.00000	0.00000
52	49.83280	24.96750	25.18500	0.00177	0.00075	0.00962	0.00046	0.00195	0.00018
53	49.69490	25.26910	25.02850	0.00300	0.00000	0.00336	0.00107	0.00000	0.00000
54	49.72050	25.11580	25.15310	0.00191	0.00000	0.00684	0.00000	0.00193	0.00000
55	49.98190	25.05060	24.94810	0.00354	0.00229	0.00672	0.00498	0.00000	0.00191
56	49.70790	25.18290	25.09990	0.00178	0.00000	0.00591	0.00160	0.00000	0.00000
57	49.83590	25.00910	25.14730	0.00324	0.00000	0.00105	0.00000	0.00160	0.00181
58	49.87470	24.88310	25.23310	0.00157	0.00000	0.00764	0.00000	0.00000	0.00000
59	49.92730	24.92730	25.13440	0.00070	0.00000	0.00896	0.00138	0.00000	0.00000
60	49.79470	25.08100	25.11210	0.00408	0.00092	0.00714	0.00000	0.00000	0.00000
61	49.75420	24.98200	25.25440	0.00336	0.00000	0.00056	0.00000	0.00311	0.00237
62	49.66860	25.02870	25.29040	0.00199	0.00000	0.00933	0.00092	0.00000	0.00000
63	49.72220	24.98980	25.27880	0.00204	0.00000	0.00617	0.00026	0.00073	0.00000
64	49.64820	25.01180	25.32590	0.00098	0.00000	0.01176	0.00139	0.00000	0.00000
65	49.75090	24.96300	25.27560	0.00241	0.00000	0.00807	0.00000	0.00000	0.00000
66	49.68050	25.03680	25.26380	0.00207	0.00002	0.00464	0.00460	0.00625	0.00136
67	49.83300	25.00830	25.15390	0.00301	0.00000	0.00053	0.00126	0.00000	0.00000

SAMPLE	S (%)	Fe (%)	Cu (%)	Pb (%)	Ni (%)	Zn (%)	Co (%)	Ag (%)	Cd (%)
68	49.81180	24.95620	25.21830	0.00261	0.00052	0.00964	0.00000	0.00007	0.00082
69	50.01160	24.91330	25.05480	0.00153	0.00000	0.00471	0.00000	0.00842	0.00569
70	49.89550	25.03210	25.06810	0.00252	0.00000	0.00000	0.00085	0.00092	0.00000
71	49.84930	25.16210	24.98010	0.00197	0.00000	0.00660	0.00000	0.00000	0.00000
72	50.04400	24.95050	24.98440	0.00385	0.00000	0.00744	0.00000	0.00601	0.00389
73	49.76720	24.96270	25.25650	0.00466	0.00000	0.00624	0.00184	0.00000	0.00095
74	49.88890	24.78710	25.31680	0.00211	0.00000	0.00139	0.00000	0.00101	0.00275
75	49.80190	24.86520	25.32080	0.00322	0.00000	0.00801	0.00000	0.00000	0.00093
76	49.66850	24.98520	25.33880	0.00063	0.00000	0.00066	0.00288	0.00052	0.00286
77	49.89380	24.87680	25.21170	0.00159	0.00046	0.01299	0.00267	0.00000	0.00000
78	49.98740	24.97650	25.02170	0.00164	0.00187	0.00569	0.00256	0.00267	0.00000
79	49.99270	24.90870	25.07890	0.00191	0.00000	0.00903	0.00000	0.00700	0.00184
80	49.95310	25.03300	25.00090	0.00211	0.00000	0.01088	0.00000	0.00000	0.00000
81	50.00030	24.89200	25.09100	0.00094	0.00000	0.00623	0.00034	0.00708	0.00207
82	49.89820	24.87330	25.21900	0.00571	0.00000	0.00000	0.00000	0.00000	0.00383
83	49.88260	24.94370	25.16620	0.00073	0.00000	0.00560	0.00112	0.00000	0.00000
84	50.10010	24.84460	25.05110	0.00356	0.00000	0.00000	0.00000	0.00000	0.00064
85	49.82860	25.10110	25.05260	0.00050	0.00000	0.01314	0.00102	0.00300	0.00000
86	49.73320	25.10510	25.14730	0.00442	0.00000	0.00797	0.00000	0.00000	0.00211
87	49.74880	25.02810	25.20010	0.00215	0.00000	0.01000	0.00000	0.00829	0.00256
89	49.89950	24.99940	25.09260	0.00415	0.00161	0.00276	0.00000	0.00000	0.00000
90	48.65100	25.61420	25.72620	0.00000	0.00000	0.00649	0.00206	0.00000	0.00000
91	49.77730	25.01550	25.19530	0.00393	0.00000	0.00465	0.00000	0.00000	0.00333
92	49.82290	25.06550	25.10330	0.00130	0.00000	0.00608	0.00097	0.00000	0.00000
93	49.84570	25.00650	25.13350	0.00129	0.00062	0.00841	0.00000	0.00000	0.00404
94	49.80920	25.04950	25.13530	0.00381	0.00000	0.00012	0.00000	0.00000	0.00212
95	49.90900	24.97840	25.10510	0.00335	0.00000	0.00122	0.00000	0.00292	0.00000
96	49.93660	24.99740	25.05610	0.00222	0.00000	0.00462	0.00000	0.00303	0.00002
97	49.66560	25.14840	25.17990	0.00193	0.00000	0.00422	0.00000	0.00000	0.00000
98	49.62740	25.14070	25.09110	0.00343	0.00000	0.13735	0.00000	0.00000	0.00000
99	49.66740	25.16830	25.14670	0.00301	0.00000	0.01325	0.00117	0.00021	0.00000
100	49.82810	25.04310	25.11790	0.00423	0.00037	0.00569	0.00000	0.00056	0.00000
101	49.64970	25.01160	25.33160	0.00303	0.00000	0.00000	0.00000	0.00387	0.00021
102	49.79210	24.86270	25.33920	0.00177	0.00000	0.00327	0.00000	0.00104	0.00000
103	49.64070	25.04650	25.30720	0.00159	0.00000	0.00411	0.00000	0.00000	0.00000
104	49.65590	25.03990	25.29180	0.00192	0.00038	0.00512	0.00000	0.00000	0.00501
105	49.69980	24.91690	25.37720	0.00200	0.00000	0.00181	0.00182	0.00051	0.00000
106	49.64160	24.96880	25.37820	0.00202	0.00000	0.00886	0.00054	0.00000	0.00000
107	49.77510	24.87590	25.34170	0.00136	0.00000	0.00601	0.00000	0.00000	0.00000
108	49.59860	25.05450	25.33200	0.00316	0.00000	0.00036	0.00086	0.00333	0.00720
109	49.77140	25.00020	25.21410	0.00170	0.00190	0.00235	0.00370	0.00254	0.00217
110	49.65120	25.02120	25.32080	0.00051	0.00000	0.00310	0.00000	0.00311	0.00000
111	49.68640	24.91410	25.39010	0.00283	0.00000	0.00488	0.00128	0.00043	0.00000
112	49.75260	24.94550	25.29260	0.00100	0.00000	0.00063	0.00128	0.00447	0.00186
113	49.79550	25.11120	25.08300	0.00178	0.00000	0.00720	0.00128	0.00000	0.00000
114	50.06700	24.73050	25.18860	0.00257	0.00000	0.00986	0.00000	0.00000	0.00140
115	49.85540	24.91440	25.21720	0.00287	0.00059	0.00948	0.00000	0.00000	0.00000

SAMPLE	S (%)	Fe (%)	Cu (%)	Pb (%)	Ni (%)	Zn (%)	Co (%)	Ag (%)	Cd (%)
116	49.81730	25.01190	25.15830	0.00098	0.00000	0.00751	0.00000	0.00401	0.00000
118	49.85740	24.99540	25.13320	0.00155	0.00000	0.01013	0.00000	0.00219	0.00012
119	49.77830	25.02990	25.18290	0.00000	0.00000	0.00000	0.00000	0.00725	0.00171
120	49.74460	25.08350	25.14940	0.00144	0.00000	0.01802	0.00000	0.00300	0.00000
121	49.68290	25.15320	25.14910	0.00000	0.00000	0.01269	0.00207	0.00000	0.00000
122	49.65240	24.99560	25.32630	0.00345	0.00000	0.01561	0.00000	0.00210	0.00465
123	49.69050	25.02940	25.26670	0.00115	0.00293	0.00544	0.00000	0.00000	0.00392
124	49.75840	24.87350	25.36200	0.00098	0.00000	0.00373	0.00000	0.00133	0.00000
125	49.64540	25.18030	25.16130	0.00005	0.00371	0.00819	0.00000	0.00105	0.00000
126	49.70690	25.08050	25.20110	0.00136	0.00183	0.00634	0.00000	0.00202	0.00000
127	49.84330	24.98160	25.16040	0.00007	0.00000	0.00781	0.00046	0.00443	0.00199
128	49.79960	25.08880	25.10150	0.00241	0.00000	0.00646	0.00023	0.00103	0.00000
129	49.81970	24.91610	25.24600	0.00076	0.00000	0.00940	0.00290	0.00511	0.00000
130	49.65680	24.92720	25.40670	0.00235	0.00000	0.00381	0.00000	0.00324	0.00002
131	49.74300	24.92780	25.32530	0.00000	0.00000	0.00000	0.00393	0.00000	0.00000
132	49.72240	24.91930	25.33960	0.00121	0.00151	0.01377	0.00000	0.00222	0.00000
133	49.58120	25.06440	25.33970	0.00155	0.00000	0.00736	0.00302	0.00076	0.00211
134	49.57080	25.03880	25.38440	0.00044	0.00000	0.00555	0.00000	0.00000	0.00000
136	49.45540	25.19080	25.34430	0.00000	0.00000	0.00482	0.00000	0.00470	0.00000
137	49.65330	24.95290	25.38330	0.00036	0.00000	0.00468	0.00000	0.00000	0.00552
138	49.58730	25.05990	25.34210	0.00253	0.00000	0.00612	0.00208	0.00000	0.00000
139	49.42490	25.10660	25.46690	0.00000	0.00000	0.00161	0.00000	0.00000	0.00000
140	49.45540	25.17110	25.36720	0.00000	0.00000	0.00624	0.00015	0.00000	0.00000

Appendix D Co-author Attribution Statement

To Whom It May Concern

I, Gregory Michael O'Connor contributed all laboratory work, data interpretation and writing to the papers/publication entitled:

- O'Connor, G.M., Lepkova, K., Eksteen, J.J. and Oraby, E.A., 2018. Electrochemical Behaviour of Copper in Alkaline glycine solutions. Hydrometallurgy, 181: 221-229
- O'Connor, G.M., Lepkova, K., Eksteen, J.J. and Oraby, E.A., 2018. Electrochemical Behaviour and Surface Analysis of Chalcopyrite in Alkaline Glycine Solutions. Hydrometallurgy, 182: 32-43.

The co-authors provided technical support with laboratory testing and experimental design, proof reading and corrections.

(Signature of Candidate)

I, as a Co-Author, endorse that this level of contribution by the candidate indicated above is appropriate.

Katerina Lepkova

(Full Name of Co-Author 1)

(Signature of Co-Author 1)

Jacques Eksteen

(Full Name of Co-Author 2)

(Signature of Co-Author 2)

Elsayed Oraby

(Full Name of Co-Author 3)

(Signature of Co-Author 3)